Interval Approach for Stability Analysis of a Nuclear Reactor with Appropriate Thermal-Hydraulic Model

Thesis submitted by

Shohan Banerjee

Doctor of Philosophy (Engineering)

School of Nuclear Studies and Applications,
Faculty Council of Engineering and Technology
Jadavpur University
Kolkata, India
2018

JADAVPUR UNIVERSITY

KOLKATA – 700032, INDIA

INDEX NO.: – 194/13/E

1. Title of the thesis:

Interval Approach for Stability Analysis of a Nuclear Reactor with Appropriate Thermal-Hydraulic Model

2. Name, Designation & Institution of the Supervisor/s:

Prof. Dr. Amitava Gupta, Professor, Department of Power Engineering, Jadavpur University, Kolkata and Director of School of Nuclear Studies and Applications, Jadavpur University, Kolkata.

Prof. Dr. Koushik Ghosh, Professor, Department of Mechanical Engineering, and School of Nuclear Studies and Applications, Jadavpur University, Kolkata.

3. List of Publications:

Peer reviewed Journals (as 1st author):

(i) S. Banerjee, K. Halder, S. Dasgupta, S. Mukhopadhyay, K. Ghosh, and A. Gupta, "An Interval Approach for Robust Control of a Large PHWR with PID Controllers", IEEE Transactions on Nuclear Science, 2015, vol. 62, no. 1, pp. 281-292.

(ii) S. Banerjee, D. Bose, A. Hazra, S. Chattopadhyay, K. Ghosh, and A. Gupta, "Controller Design for Operation of a 700MWe PHWR with Limited Voiding", Nuclear Engineering and Design, Elsevier, (under review).

Peer reviewed Journals (as co-author)

(i) S. Dasgupta, A. Routh, S. Banerjee, K. Agilageswari, R. Balasubramanian, S. G. Bhandarkar, S. Chattopadhyay, M. Kumar, and A. Gupta. "Networked control of a large pressurized heavy water reactor (PHWR) with discrete proportional-integral-derivative

(PID) controllers." IEEE Transactions on Nuclear Science 60, no. 5 (2013): 3879-3888.

(ii) S. Dasgupta, K. Halder, S. Banerjee and A. Gupta, "Stability of Networked Control System (NCS) with discrete time-driven PID controllers", Control Engineering Practice, September 2015, Vol. 42, pp. 41-49.

(iii) K. Halder, S. Das, S. Dasgupta, S. Banerjee, and A. Gupta, "Controller design for Networked Control Systems—An approach based on L2 induced norm", Nonlinear Analysis: Hybrid Systems, 2016, vol. 19, pp. 134-145.

(iv) D. Bose, S. Banerjee, M. Kumar, P. P. Marathe, S. Mukhopadhyay, and A. Gupta. "An Interval Approach to Nonlinear Controller Design for Load-Following Operation of a Small Modular Pressurized Water Reactor." IEEE Transactions on Nuclear Science 64, no. 9 (2017): 2474-2488.

4. List of Patents: NIL

5. List of Presentation in National/International Conferences:

(i) S. Banerjee, K. Halder, S. Dasgupta and A. Gupta, "LMI based Optimal PID Controller design for Bounded Parametric Uncertain Plant-An interval approach", in Electrical, Electronics, Signals, Communication and Optimization (EESCO), 2015 International Conference on, IEEE, Jan. 2015.

(ii) K. Halder, D. Bose, S. Banerjee and Amitava Gupta, "L2 induced norm based pole placement controller for networked control system", In Innovations in Electrical, Electronics, Instrumentation and Media Technology (ICEEIMT), 2017 International Conference on, pp. 32-37, IEEE, Feb. 2017.

(iii) S. Dasgupta, K. Halder, S. Banerjee, S. Chakraborty and A. Gupta, "Stability analysis and controller synthesis of networked control system (NCS) with arbitrary packet drop-outs," in Electronics and Communication Systems (ICECS), 2015 2nd International Conference on , pp.217-222, IEEE, Feb. 2015.

(iv) S. Dasgupta, K. Halder, S. Banerjee and A. Gupta, "Controller design of a NCS with guaranteed exponential stability- a trace

minimization approach", in Electrical, Electronics, Signals, Communication and Optimization (EESCO), 2015 International Conference on , pp.1-5, IEEE, Jan. 2015.

CERTIFICATE FROM THE SUPERVISOR

This is to certify that the thesis entitled "Interval Approach for Stability Analysis of a Nuclear Reactor with Appropriate Thermal-Hydraulic Model" submitted by Shri ***Shohan Banerjee****, who got his name registered on the* ***30th of Julyy 2013*** *for the award of the Ph.D. (Engg.) degree of Jadavpur University is absolutely based upon his own work under the supervision of* ***Prof. Dr. Amitava Gupta*** *and* ***Prof. Dr. Koushik Ghosh*** *and that neither his thesis nor any part of the thesis has been submitted for any degree/diploma or any other academic award anywhere before.*

_____

Signature of supervisor and date
with Office seal

_____

Signature of supervisor and date
with Office seal

Dedicated to my Late Grandma

Acknowledgement

I take this opportunity to express my sincere appreciation for my supervisors, Prof. Dr. Amitava Gupta and Prof. Dr. Koushik Ghosh for their patience and encouragement during the whole period of my PhD. During the work, they continuously provided me with enthusiasm, vision and wisdom. The guidance received from them cannot be acknowledged with few words. Their unconditional love, moral support and lucid illustrations of the technical matters have made my PhD journey memorable.

I am extremely thankful to all the members of the respected Doctoral Committee for the valuable internal reviews they provided regarding the work which was pivotal in giving a perfect blend to the thesis.

I am also grateful to the Director of School of Nuclear Studies and Applications (SNSA) and Head of the Power Engineering Department for providing the necessary departmental laboratory and library facilities during my course of work. I would like to extend my heartfelt gratitude to all faculty and non-teaching staffs of both the school and the department for their helpful attitude and constant encouragement.

The entire work of this dissertation has been supported and funded by the Technical Education Quality Improvement Programme (TEQIP Phase II) of Government of India and I acknowledge the support that was provided by them.

I would like to thank Mr. Sujit Chattopadhyay of Nuclear Power Corporation of India Limited and Dr. Siddhartha Mukhopadhyay of Bhabha Atomic Research Center for helping me with valuable technical details regarding my work.

I want to thank my parents, other family members, my fiancée and all my lab mates Kaushik, Debayan, Soumya and all other seniors and juniors who have helped me through this journey. The best part

of having such people in my lab has been that they have always made me feel insecure with their outstanding research capabilities and thus I was compelled to push myself further so that I could achieve my goal.

Finally I would like to thank God and the role of millions of countrymen who do not have much to eat or wear and who could have been fed and clothed with the money used for supporting my research and many others like mine.

Shohan Banerjee

Jadavpur University

Preface

This dissertation is the final documentation of my doctoral study at the School of Nuclear Studies and Applications, Jadavpur University. This dissertation is guided by my thesis advisors Prof. Dr. Amitava Gupta of the Department of Power Engineering and School of Nuclear Studies and Applications and Prof. Dr. Koushik Ghosh of the Department of Mechanical Engineering and School of Nuclear Studies and Applications, Jadavpur University and no part of the thesis belong to any other dissertation. This dissertation consists of five broad chapters which are mentioned as below:

Chapter 1 *introduces the dissertation by discussing in details the basic components of the Pressurized Heavy Water Reactors (PHWRs). It is then followed by detailed discussion of the major issues and approaches towards the stability and control of PHWRs that has been addressed by the researchers till date. Finally this chapter also put forwards the motivations, major contributions and outline of this dissertation.*

Chapter 2 *addresses the formulation of developing an interval model of a 540MWe PHWR with bounded parametric uncertainties during power maneuvering. This is then followed by the stability analysis of the interval. Further, for stable operation of the reactor, the methodology of designing a single robust optimal Proportional-Integral-Derivative (PID) controller has also been discussed.*

Chapter 3 *deals with the stability analysis and control of a 700MWe PHWR with limited coolant voiding. Modeling of void fraction in transient time has been discussed in details. The methodologies of designing robust PID controller for power maneuvering control and optimal PI controllers for Pressurizer pressure control to keep voiding within prescribed limit, has been discussed in details.*

Chapter 4 compiles the simulation and results of the reactor models and their associated controllers. The results have been validated on real-time platform using Hardware-in-Loop (HiL). The corresponding results have been published in the end to corroborate the credibility of the aforesaid approaches on practical systems.

Chapter 5 summarizes salient concluding points of the dissertation and discusses in details the future scope of research.

Shohan Banerjee

Jadavpur University

Nomenclature

PHWR	Pressurized Heavy Water Reactor
NPPs	Nuclear Power Plants
PDHRS	Passive Decay Heat Removal System
ROPS	Regional Overpower Protection System
CSS	Containment Spray System
PHT	Primary Heat Transport
PCP	Primary Circulating Pumps
LOCA	Loss of Coolant Accident
LZCS	Liquid Zone Control System
ZCC	Zonal Control Compartment
RRS	Reactor Regulatory System
SDS	Shutdown System
BWR	Boiling Water Reactor
PWR	Pressurized Water Reactors
NDI	Nonlinear Dynamic Inversion
SFC	State Feedback Control
SFAC	State Feedback Assisted Control
FO	Fractional Order
FOPID	Fractional Order PID
SMC	Sliding Mode Control
OISMC	Optimal Integral Sliding Mode Control
FLC	Fuzzy Logic Control
NCS	Networked Control System
PID	Proportional-Integral-Derivative
LQR	Linear Quadratic Regulator
ARE	Algebraic Ricatti Equation
FP	Full Power
GA	Genetic Algorithm
SISO	Single Input Single Output
MISO	Multiple Input Single Output
MIMO	Multiple Input Multiple Output
ITAE	Integrated Time Absolute Error
SBC	Simulated Binary Crossover
HiL	Hardware-in-Loop

List of Symbols

$\mathbf{A}$	Interval system matrix
$\mathbf{B}$	Interval input matrix
$\mathbf{A}_{80}$	Nominal system matrix corresponding to 80%FP
$\mathbf{B}_{80}$	Nominal input matrix corresponding to 80%FP
$\mathbf{N} \in \left[\underline{\mathbf{N}}, \overline{\mathbf{N}}\right]$	Interval matrix
$\mathbf{Q}$	A positive semi definite matrix
$\mathbf{R}$	A positive definite matrix
$\mathbf{U}_{60}^{100}$	Controllability matrix in interval

A	Active heat transfer area
C	Delayed neutron precursor concentration
c_{p_c}	Specific heat of the coolant
c_{p_f}	Specific heat of the fuel
e	Specific internal energy
f	Objective function for GA
h_{fc}	Fuel to coolant heat transfer co-efficient
h	Total specific enthalpy
h_i	Input enthalpy of the coolant channel
h_l	Specific enthalpy of liquid
h_o	Output enthalpy of the coolant channel
h_v	Specific enthalpy of vapor
$h_{P_R l}$	Specific enthalpy of saturated water
$h_{P_R v}$	Specific enthalpy saturated steam
$h_{P_R x1}$	Specific enthalpy of fluctuation water
I	Iodine concentrations for a particular zone
J	Cost function
K_p, K_i and K_d	PID controller gains
k_p and k_i	PI controller gains
l	Total length of coolant channel
$\dot{m}$	the mass flow rate of the coolant
m_c	Mass of the coolant in the core

m_f	Mass of the fuel in the core
$\dot{m}_l$	Mass flow rate of liquid phase in coolant channel
$m_{P_R l}$	Mass of coolant of the pressurizer
$m_{P_R g}$	Mass of steam of the pressurizer
$\dot{m}_v$	Mass flow rate of vapor phase in coolant channel
$N \in \left[\underline{N},\ \overline{N} \right]$	Interval variable
$\underline{N}$	*Infimum* of the interval variable
$\overline{N}$	*Supremum* of the interval variable
p	Pressure of coolant in the coolant channel
P_R	Output pressure of the pressurizer
P_{Rref}	Pressure reference of the pressurizer
P_{th}	Zonal reactor thermal power
$\dot{q}$	Linear heat rate
Q_h	electrical heater power of the pressurizer
S	Slip ratio
T_c	Average coolant temperature
$T_{c_{input}}$	Inlet coolant temperatures
$T_{c_{outlet}}$	Outlet coolant temperatures
$T_{c_{ss}}$	Initial (equilibrium) values of average coolant temperatures
T_f	Average fuel temperature
$T_{f_{ss}}$	Initial (equilibrium) values of average fuel temperatures
u_l	Velocity of the liquid in the coolant channel
u_v	Velocity of the vapor in the coolant channel
V	Volume of coolant
V_{P_R}	Total volume of pressurizer
$v_{P_R l}$	Specific volume of the water inside the pressurizer tube
$v_{P_R v}$	Specific volume of the steam inside the pressurizer tube
W_{sa}	The mass flow-rate of the safety valve flow
W_{sp}	Flow-rate of water droplet jet through the spray valve
W_{su}	Surge flow of the coolant into the pressurizer
x	Flow quality
X	Xenon concentrations for a particular zone

α_c	Temperature coefficients of reactivity of the coolant
α_f	Temperature coefficients of reactivity of the fuel
α_v	Reactivity coefficients for the void
β	Delayed neutron fractional yield

γ_I	Iodine yield per fission
γ_X	Xenon yield per fission
δ_v	Void fraction
ζ	Closed loop damping
λ	Decay constant
λ_I	Iodine decay constants
λ_X	Xenon decay constants
$\Delta\rho$	Reactivity defect
ρ_{ext}	Reactivity introduced in the zone due to LZC
ρ_l	Density of liquid in two-phase flow
ρ_{net}	The net reactivity input
ρ_v	Density of vapor in two-phase flow
σ	Closed loop real pole
σ_I	Microscopic thermal neutron absorption cross sections of iodine
σ_X	Microscopic thermal neutron absorption cross sections of xenon
ω	Closed loop frequency
$\sum_a$	Macroscopic thermal neutron absorption
$\sum_f$	Fission cross sections

Abstract

A nuclear reactor exhibits changing behavior with variation in reactor power. Further, uncertainties in the measurement of the actual power produced by the reactor, the heat transfer from the fuel to the coolant and the reactivity change due to the change in the fuel and coolant temperatures and condition of the core, make it necessary to adopt a robust control approach for design of control systems for such plants. In this dissertation, a 540MWe Indian PHWR consisting of 14 zones has been modeled using inexact models incorporating bounded parametric variations in power, heat transfer from the fuel to the coolant and temperature coefficients of reactivity of fuel and coolant. The stability analysis of the inexact models suggests that though the system is marginally stable in nature, the system is controllable. Therefore for stable operation, these inexact models are then used to obtain a robust and optimal PID controller gains for controlling the reactor power with specified time response under parametric variations, using an interval approach. The methodology is established with credible real-time and offline simulations as and where applicable.

Enhancement of available power output from a 540MWe Pressurized Heavy Water Reactor (PHWR) with limited coolant voiding has been attempted in the recent past. Coolant voiding in such a core usually occurs in the high power regime and introduce positive reactivity in the core which makes a reactor increasingly unstable. This dissertation presents a scheme for a 700MWe PHWR, which is capable of controlling the reactor from 60%to 93.2% of its Full Power (FP) using the Liquid Zone Control System (LZCS) and the again from 93.2% to 100%FP in conjunction with a pressurizer which is activated to change the pressure

in the coolant channel by a small amount, thus keeping the void fraction constraint. The dissertation presents a dynamic model for estimation of void fraction in the 700MWe PHWR core as a function of reactor power in transient time and then proposes an optimal controller for pressurizer control. The pressurizer pressure controller has been designed using Genetic Algorithm (GA) to keep void fraction limited. The controller performance has been validated using credible Hardware-in-Loop (HiL) simulation.

List of Figures

List of Tables

Contents

Chapter 1

Introduction

1.1 Introduction to Pressurized Heavy Water Reactor (PHWR)

With the increasing demand of electrical power, the world energy market is shifting its focus towards increased utilization of vast nuclear resources to meet its demand. For Nuclear Power Plants (NPPs), the fixed cost (primarily reflects the cost of building the power plant) far exceeds the variable cost (primarily reflects the cost of fuel, operation and maintenance) [1]. In fact, the development of NPPs was in part driven by its ability to use much cheaper fuel (natural Uranium and heavy water) than coal, oil or natural gas. However, for fossil fuel based thermal power plants, the fixed cost is lower but the variable cost is higher than that of the NPPs [1]. Therefore it can be inferred that in a long-run, the NPPs are more economical than that of the fossil fuel based thermal power plants in terms of fuel utilization, operation and maintenance.

In context of Indian NPPs, out of the 22 operational nuclear reactors in 7 NPPs with a total installed capacity of 6780MW, 20 reactors are Pressurized Heavy Water Reactors (PHWRs) in nature [2]. PHWRs exhibit excellent neutron economy by using Heavy Water (D_2O) as a moderator and coolant which facilitates the use of natural Uranium fuel. Natural Uranium being un-enriched in nature, it counterbalances the additional cost of Heavy Water which is much more

expensive than light water. In 1980, a 220MWe PHWR was first synchronized to feed electrical power directly to the national grid [3]. After the successful installation and operation of 220MWe plant, the focus was to develop a PHWR of larger power generation capacity and hence 540MWe reactors were introduced which are operational since 2004 [4]. At the present stage, the focus is to develop PHWRs of 700MWe capacity and they are in the advanced stage of construction. A schematic figure of PHWR based electrical power generation plant is shown in figure 1.1.

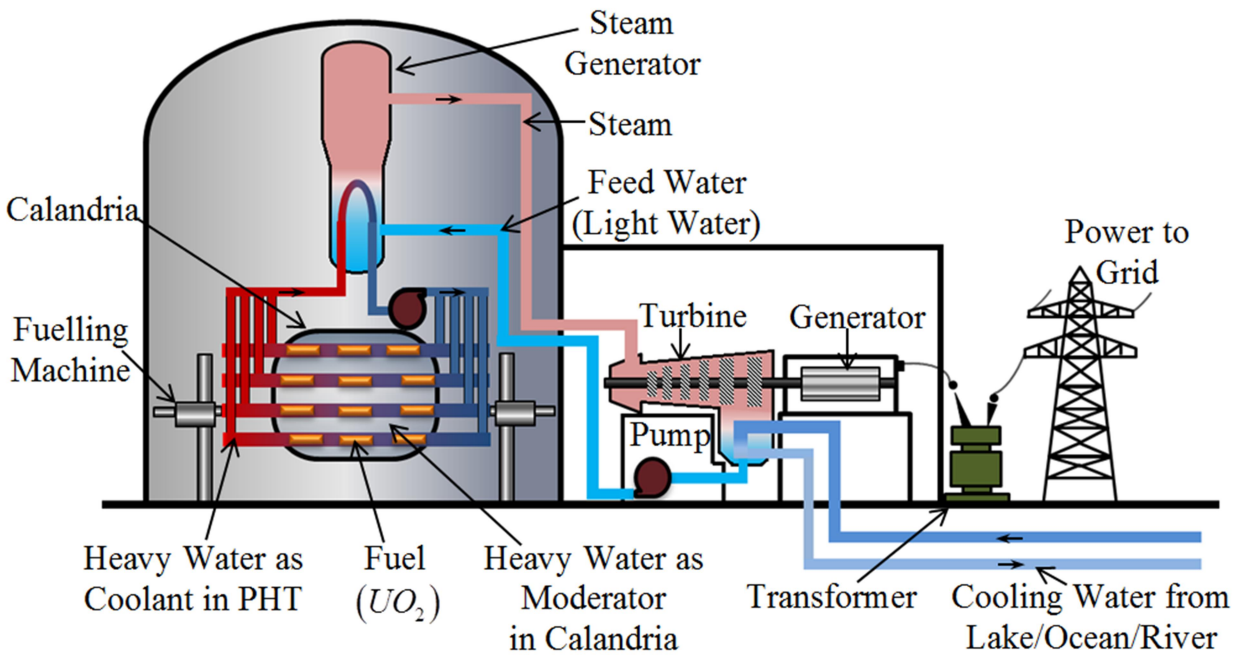

Fig. 1.1 Schematic diagram of PHWR based electric power generation plant [5]

The core design, operations and control of 220MWe PHWRs are different from the 540MWe because large power reactors possesses large sized, loosely neutronically coupled core [4]. However, the core design, operation and control, shutdown systems and cooling systems of the 700MWe PHWRs are similar to that of 540MWe PHWRs except for the fact that 700MWe PHWRs have some additional improved features such as Passive Decay Heat Removal System

(PDHRS), Regional Overpower Protection System (ROPS), Containment Spray System (CSS), and steel liners on the inner surface of the containment building, over 540MWe PHWRs [4]. Such enhancements allow extraction of more power per channel in the 700MWe reactors by allowing a limited coolant voiding toward the end of the channels. Brief descriptions of salient reactor components of the 540MWe and/or 700MWe PHWR reactors are provided in the following sub-sections.

1.1.1 Fuel and Core Design

The Reactor core for a 700Mwe PHWR is a two-end shielded integral assembly consisting of fuel bundles and calandria tubes. For both 540MWe and 700MWe PHWRs, 37 natural uranium dioxide fuel pellets of each 0.5m length form a fuel pin and 12 such fuel pins form a fuel bundle, is contained inside a pressure tube made of Zr-2.5%Nb (Zirconium-Niobium) alloy [6]. Each fuel bundle is spatially separated from the rest of the bundles and is welded into a bearing at both end of the tube [6] [7]. Likewise there are 392 pressure tubes arranged in square lattice structure, spatially distributed throughout the core and each pressure tube is of 49.5cm length [6]. Both ends of the pressure tubes are wrapped by modified stainless steel fittings which penetrate through the core shields and provide provision for online fuel refueling [7]. The schematic of a pressure tube is given below in Fig. 1.2.

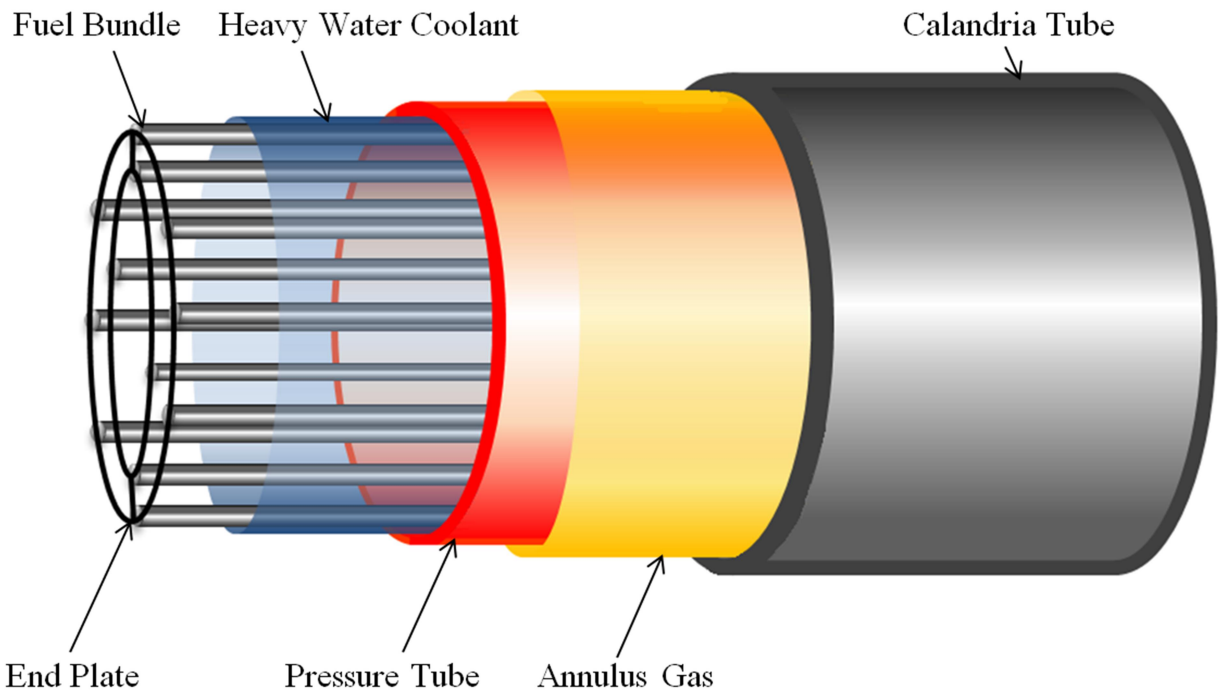

Fig. 1.2 Schematic of pressure tube [8]

Primary coolant consisting of heavy water at low temperature runs through the pressure tubes for the purpose of extracting heat from the fuel generated due to fission reaction, thereby forming an altogether of 392 coolant channels in the core. Each pressure tube is surrounded by a concentric calandria tube and the annular space between the calandria tube and the pressure tube is filled with carbon dioxide gas [7]. The carbon dioxide gas provides thermal insulation in between the high temperature primary coolant inside the pressure tube and low temperature moderator outside the calandria tube as shown in Fig. 1.3.

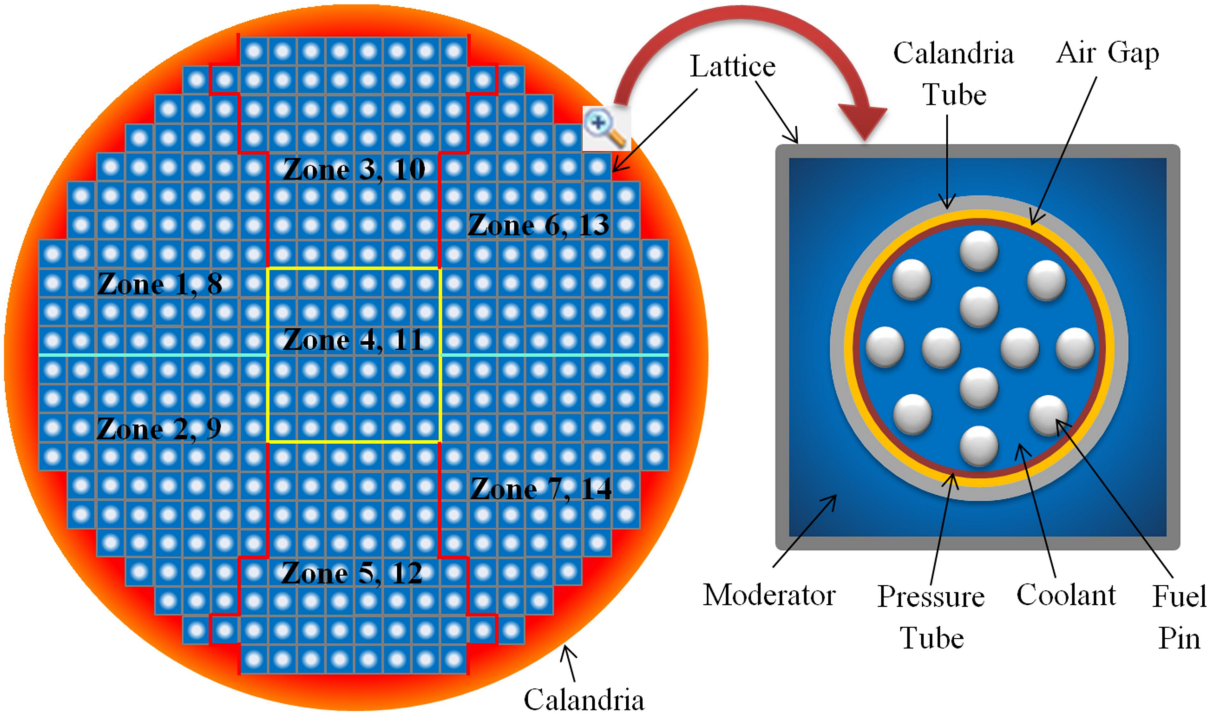

Fig.1.3 Schematic of cross section of Calandria [6]

For the purpose of spatial control, the entire core is considered to be divided into 14 zonal compartments. The power level corresponding to each zone for both 540MWe and 700MWe PHWRs are given below in Table 1.1 [9].

Table 1.1

Thermal power level of 14 zones of 540MWe and 700MWe PHWRs

Reactor type (in MWe)	Equivalent thermal power (MWth) distribution of each zones						
	(1, 8)	(2, 9)	(3, 10)	(4, 11)	(5, 12)	(6, 13)	(7, 14)
540	132.75	135.99	123.30	98.55	123.30	132.75	135.99
700	159.75	163.64	148.01	118.59	148.01	159.75	163.64

1.1.2 Primary Heat Transport (PHT) System

The primary objective of the PHT system is to extract the heat generated in the reactor core due to fission reaction. The schematic of the coolant loop in the reactor core is shown in Fig. 1.4.

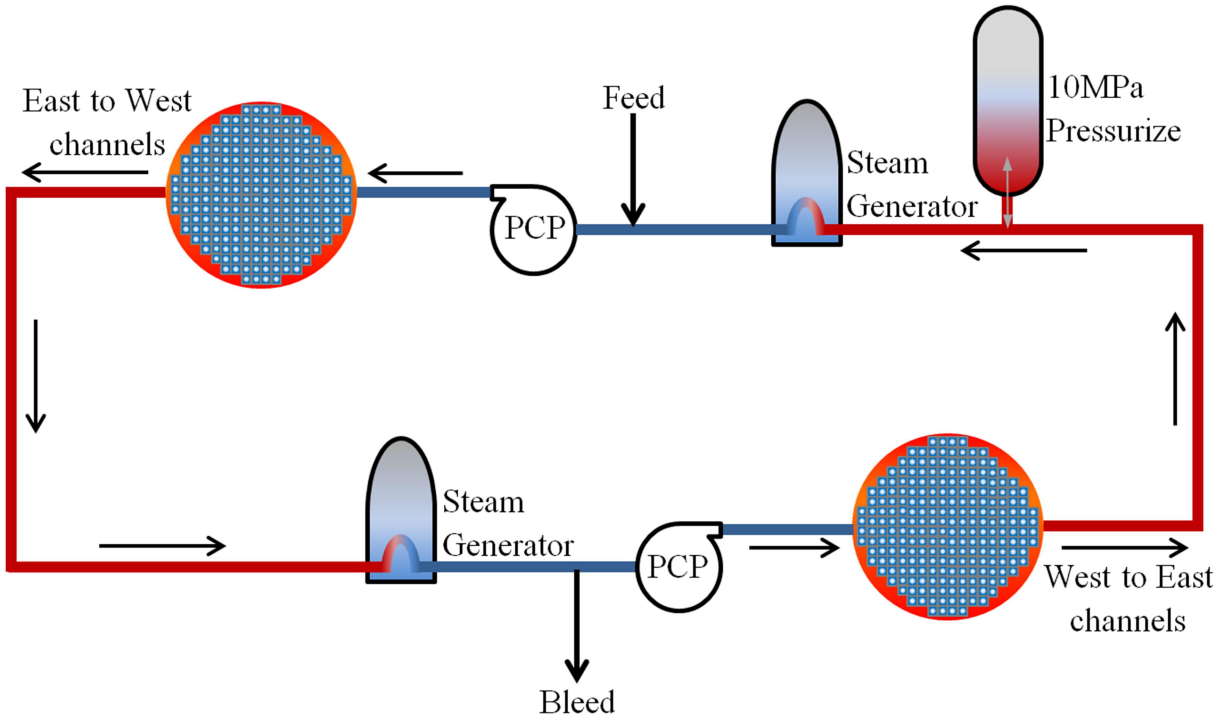

Fig. 1.4 Schematic diagram of primary coolant loop [10]

As per the schematic, there are two inlet headers connected on each side of the reactor and coolant channels are directed through 196 inlet feeders attached to a single inlet feeder [6] [10]. Coolant is directed to flow through these inlet feeders by two Primary Circulating Pumps (PCPs) attached on both the side of the reactor. Likewise there are two outlet headers on each side of the reactor each containing 196 outlet feeders through which the coolant flow out of the reactor [6]. Thus there are two primary coolant loops in the core operating in interleaved fashion i.e. in one loop the coolant flows from east-to-west direction and in other loop the coolant flow from west-to-east direction [6]. It is to be noted that two-loop coolant flow system is advantageous as it

automatically isolates the loop where a Loss of Coolant Accident (LOCA) condition has occurred [6]. Coolant flowing out of the reactor is carried into a heat exchanger where it transfers the accumulated heat to the secondary side coolant generating steam.

For 540MWe PHWRs, the nominal temperature rise of coolant inside the core is 36^0C i.e., from 267^0C at inlet to 303^0C at the outlet [11]. Similarly for 700MWe PHWRs, the nominal temperature rise is about 44^0C i.e., from 266^0C at inlet to 310^0C at the outlet [12]. The pressurizer component of PHT maintains the primary side pressure of 9MPa and 9.8MPa for 540MWe and 700MWe PHWRs respectively [11], [12]. Another important component of the PHT is the pressure relief valve attached to the pressurizer providing safety to the PHT from over-pressurization.

1.1.3 Reactivity Control and Shutdown System

The control system in a nuclear reactor generates the inputs which modulate the reactivity control devices to alter the reactivity input to the reactor. An increased reactivity increases the neutron flux and hence burn-up of fissile material while a reduction in reactivity input reduces the burn-up of fissile material. The Reactor Regulatory System (RRS) is the inherent control system of the reactor which facilitates control of reactor power of a large PHWR during power maneuvering and shutdown. The basic components of the RRS consist of the following:

1.1.3.1 Liquid Zone Control System (LZCS)

As already discussed, the reactor core is divided into 14 zones and each of these 14 zones has a Zonal Control Compartment (ZCC) filled with light water which acts as neutron absorber. The light water level in each of these compartments is varied in accordance with the demand power for the purpose of bulk power control [13]. The LZCS uses a complex hydro-pneumatic

system to control the light water level in each of the compartments as a function of pressure difference between the gas outlet header and the delay tank [13], [14]. The light water level alteration ultimately affects the reactivity variation of the core thereby providing a fine continuous control of reactor power level and power distribution for each zone. It consists of six cylindrical vertically oriented tubes running interstitially between the calandria tubes from the top to the bottom of the core as shown in figure 1.5.

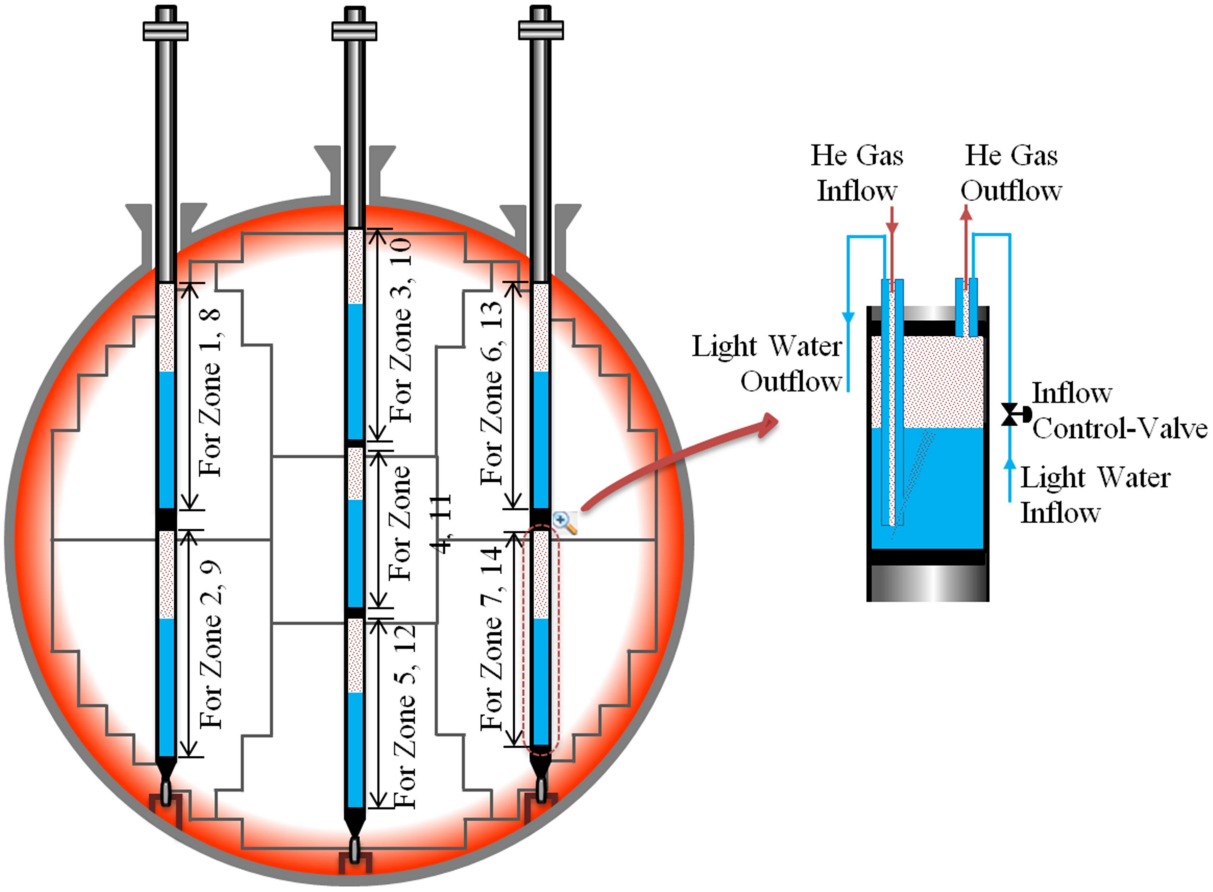

Figure 1.5 Schematic diagram of LZCS inside the Calendria [14]

The two tubes located at the center are divided into three compartments each where the compartments are separated by bulkheads. Similarly the four tubes located on the outer side are

divided into two compartments each. Altogether there are 14 individual compartments for 14 zones. The LZC compartment is located approximately at the center of each zone and partially filled with the light water and the water inlet into each LZC compartment is taken through a control valve which can be used to vary the water inflow rate while the outflow from the compartment is maintained at a constant rate. The water level in the compartment may be changed in the desired manner by properly manipulating the signal to the control valve. The reactivity variation is directly related to the water level in the LZC compartment. The top part of the LZC is filled with Helium gas instead of air which not only reduces neutron activation but also reduces the corrosion rates of the zirco-alloy structures. It is evident that when an LZCS is emptied, the reactor tends to become super-critical due to the reduction of light-water level which acts as neutron absorbent. It is to be noted that when an LZCS goes from full state to an empty state, the net reactivity change of worth 5mK occurs in the reactor core.

1.1.3.2 Control Rods

Through the movement of the external control rods, it is possible to add and remove reactivity quickly in the reactor core thereby providing the provision of regulation of reactor power level and spatial control of axial flux tilting in the reactor core. There are 21 adjustable control rods among which 17 rods are made of Cobalt and sandwiched by stainless steel to provide Xenon override control and rest 4 rods are made of Cadmium and sandwiched by stainless steel, which are used for rapid power reduction [6].

1.1.3.3 Shutdown System (SDS)

In addition to two systems mentioned above, two Shutdown Systems (SDSs) are also provided, which are used for maintaining the long term sub-criticality margin and also used for

handling fast transient reactivity during power maneuvering and accidental scenario [6]. During the scenario of reactor shutdown, the SSD-1 which consists of 28 mechanical rods made by cadmium and sandwiched by stainless steel material, is first activated [6]. The SSD-2 on the other hand is used to inject liquid poison inside the calandria tubes which mixes with the moderator and help to reduce the reactivity.

1.2 Approaches for Controlling Nuclear Reactors

The LZCS, control rods and the SDS discussed above are actuating devices actuated by the control signal generated by the controller. The controller design technique requires ample attention and is a highly challenging task because of many reasons. The first and foremost of these is the inherent non-linear and time-variant nature of the system which depends on the operating power of the reactor [15]. Further, the *reactivity defect* (i.e. the change in reactivity) caused by the change in reactor power varies with fuel condition of the core (fresh or equilibrium core) and adds to uncertainties in reactivity feedback. Uncertainties also exist in the estimation of the heat-transfer coefficient and heat transfer area. Owing to these difficulties, the domain of nuclear reactor control has always attracted the attention of the contemporary researchers since its inception and some of the significant contributions made in this regard are discussed below in brief.

1.2.1 Classical robust control approaches

Methods based on classical robust control approaches like H_∞ based controller design methodology and μ synthesis have been attempted by some researchers [16] [17] [18] both with non-linear and linearized models. It is to be noted that casting a reactor model in a H-infinity

template is indeed very difficult and as pointed out in [17] a guaranteed solution may not exist. In addition to this, classical robust control methodologies like H_∞ and μ synthesis are known to produce higher order controllers which are difficult to realize in practice and often require order reduction [18].

1.2.2 Parametric Variation Based Robust Control Approach

Robust control methodologies dealing with control of nuclear reactors to tackle parametric variation and uncertainties have been attempted by contemporary researchers using various techniques e.g. a technique for Boiling Water Reactors (BWRs) proposed by Shyu *et al*. in [19] which is based on co-ordinated control of manipulated variation. Similarly, the approach by Edwards *et al*. in [20], is based on a design that uses sensitivity of the system's dominant Eigen values due to parametric variation, which has been applied for Pressurized Water Reactors (PWRs).

In the recent past, development of new tools for dealing with interval mathematics has led to application of interval techniques for control systems design which have been used for a wide variety of applications e.g. [21], [22], [23] but these have not been extended to nuclear reactors so far. The Kharitonov's Polynomial Theorem forms the fundamental basis of applicability of interval mathematics to controller design for linear systems and the treatment has been presented in [24]. Some contemporary researchers, for example, Lee *et al.* [25] have used the Kharitonov theorem to design a robust controller for a nuclear reactor. The methodology presented in [25] starts with an inexact transfer function model of a nuclear reactor. The Kharitonov theorems [25] are then used to derive a controller that can take care of typical parametric uncertainties in measured reactor power, reactivity defect and heat-transfer coefficient when used in a

Pressurized Water Reactor (PWR). A robust control approach for a Boiling Water Reactor (BWR) to achieve integrated control of turbine power, water level and throttle pressure has been proposed by Shyu *et al.* in [19]. This approach, however, requires co-ordinated control of changing manipulated variables.

1.2.3 Nonlinear Dynamic Inversion (NDI) based Control Approach

A recent trend in power level control of nuclear reactors involves the use of NDI approach towards nonlinear controller design. In Bose *et al.* [26], NDI technique merged with Interval Approach has been used to design load-following controller for small modular PWR. The designed controller can not only guarantee efficient load-following operation over entire power regime but also ensure meeting of system constraints. In another work by Yadav *et al.* [27], the NDI technique merged with constrained optimization has been used to design load-following controller for large PWRs with Xenon induced oscillation. The designed controller eliminates the Xenon induced oscillations, guarantees load-following operation and ensures satisfaction of operating constraints. However, it is to be noted that the NDI technique used in these works does not guarantees optimality in terms of achieving desired system performance with minimum control rod movements.

1.2.4 State Feedback Control (SFC) Approach

Tiwari *et al.* in [28] have explored the use of singular perturbation theory towards the modeling of large PHWRs considering additional Xenon and Iodine dynamics. For controller design, a linear optimal state feedback regulator has been considered where the designed controller is only near-optimal. Edwards *et al.* in [20] propose an approach based on State Feedback Assisted Control (SFAC) which is based on sensitivity of a system's dominant eigen

values to variations in plant parameters. Here the state feedback controller is assisted by the embedded classical controller where the state feedback controller generates the demand signal for the embedded classical controller. Together they guarantee optimal performance, improve performance and stability robustness. The method has been applied to control of a PWR.

1.2.5 Fractional Order (FO) Control Approach

Robust control of PHWRs has also been attempted by Saha *et al.* in [15] using a Fractional Order (FO) phase shaper in conjunction with a PID controller and Das *et al.* in [29] using Fractional Order PID (FOPID) controllers, mainly to take care of variation in system gain with varying operating power of the reactor. However, these methodologies require implementation of a FO element which is not easy to realize and the models considered in [15], [29] do not consider the uncertainties in the reactor model though they have been shown to produce satisfactory response at different power levels.

1.2.6 Sliding Mode Control (SMC) Approach

Sliding Mode Control (SMC), is another popular technique because of its capability of robustly controlling both linear and nonlinear plants [30] [31], and efficiently handling system uncertainties. Ansarifar *et al*. in [32] have proposed a second order sliding mode controller for handling Xenon induced feedback oscillation. Reddy *et al*. in [33] have also proposed sliding mode multi-rate output feedback controller for controlling Xenon induced spatial oscillations on large PHWRs. However, these SMC based controllers exhibit the chattering in transient state which may effects the stability of the systems. In [34], robust Optimal Integral Sliding Mode Control (OISMC) has been proposed which eliminates the chattering by using a boundary layer technique where a continuous approximation is used instead of signum function. However, it has

been clearly stated in [34] that the optimality of this controller decreases with increasing of uncertainty.

1.2.7 Periodic Output Feedback Control Approach

Talange *et al.* in [9] proposed a de-centralized controller for a 540MWe Indian PHWR by varying the level of light water in the corresponding ZCC. The methodology is based on periodic output feedback. The controller design methodology considers the thermal-hydraulic effects and parametric uncertainties caused by a changing reactor power and produces acceptable response in presence of these. However, this methodology requires a fast sampler, as the input needs to be changed more number of times within an output sample interval, which may be difficult to achieve.

1.2.8 Fuzzy Logic Control (FLC) Approach

Fuzzy Logic Controllers (FLCs) are known for their uncertainty handling capabilities and some researchers [14] [35] have also proposed use of FLCs for control of PHWRs. Bhatt *et al.* in [14] proposed a FLC based control methodology for maintaining constant pressure difference between the gas outlet header and delay tank of the LZCS of a large PHWR by controlling the feed and bleed valves. In [35] Liu *et al.* proposed a technique to control the spatial power of a large PHWR by using Decentralized Fuzzy Model Predictive Control (DFMPC) where a fuzzy modeling has been used to approximate the nonlinear process. To reduce the conservatism, a fuzzy Lyapunov function and quasi-min-max methodology has been applied. However, the use of such controllers for control of nuclear reactors needs rigorous validation from stability point of view and is likely to cause regulatory concerns.

1.2.9 Networked Control System Approach

From the perspective of the control system design, the focus is shifting towards the objective of de-centralized controller design where the controller and the system are connected over a network. Such networked control system reduces cost of wiring, installation and maintenance. Networked control system has also been extended towards the control of PHWRs as evident from [36] and [37]. In [36], the designed controller is Linear Quadratic Regulator (LQR) based state feedback controller, whereas in [37], the designed controller is memory-less Proportional-Integral-Derivative (PID) controller. However, it is to be noted that these works focus mainly on handling network induced uncertainties like packet drop and/or jitter.

1.3 Motivation of the dissertation

From the discussions of various control approaches for the nuclear reactors, it is evident that the design of robust optimal controller is necessary for controlling a large reactor like 540MWe, 700MWe PHWRs during power maneuvering. Nuclear reactors are subject to various bounded uncertainties and parametric variations. The nature of the nuclear reactor is inherently non-linear and time-varying depending primarily on the operating power of the reactor [15] [16]. Also the variation of reactivity (i.e. reactivity defect) caused by the change in reactor power variation, depends on the fuel condition i.e. whether the core is fresh core or equilibrium core and adds to uncertainties in reactivity feedback. The estimation of the various thermal hydraulic parameters like heat-transfer coefficient for fuel and coolant, heat transfer area etc., also results in bounded uncertainties to the system. It is to be noted that for 700MWe PHWRs, limited voiding is allowed in coolant channels which leads to bounded uncertainty in void fraction estimation ultimately affecting the feedback reactivity. Therefore it is evident that the designed

controller must be capable of handling system with bounded uncertainties and parametric variations caused due to reactor power maneuvering.

Apart from the controller being capable of handling bounded uncertainties and parametric variations, it is always preferable that the controller must ensure maximum burn-up of fissile material with minimum control effort for PHWRs. Maximum burn-up of fissile material is essential because PHWRs use natural uranium as fuel material and accomplishing this with minimum control effort is the subject of interest. Minimizing control effort drastically reduces the cost of control and this signifies achieving desired performance using minimum movement of actuators (control rod banks, valves of LZCS) which ultimately minimizes the reactivity requirement of the reactor.

Therefore, from the above discussion it can be inferred that the major objectives of the designed controller are:

a. *Controller must be a Robust Controller capable of handling bounded uncertainties and parametric variations.*
b. *Controller must be an Optimal Controller capable of ensuring maximum burn-up of fissile material with minimum control effort.*

Motivated by this necessity, the objective here is to design a single robust optimal controller capable of ensuring desired system performance over a wide operating regime of power variation. The designed single robust optimal controller will in turn guarantee the stability of the system.

1.4 Major Contribution and Outline of this thesis

As discussed before, various techniques for designing robust optimal controller exists, for e.g. H_∞ controller, modified sliding mode controller design, etc. However, these controllers are not PID controllers. In practice, 90% of the controllers used for industrial control are PID controllers [38], known for their excellent ability to achieve tracking, robustness, disturbance rejection and noise immunity. Therefore, the design of single robust optimal PID controller is one of the major contributions of the dissertation. He *et al.* in [39], has designed Linear Quadratic Regulator (LQR) based optimal PID controller capable of placing the closed loop poles of the system within a specified region in the s-plane thereby ensuring stability of the system. However, it is a well-known fact that LQR based optimal controller is derived from the Algebraic Ricatti Equation (ARE) that can never guarantee controller robustness to parametric variations and uncertainties. Over the recent years, advances in interval mathematics and development of tools like Real Paver [40] and INTLAB [41] have opened the possibility of analyzing systems with bounded parametric uncertainties as interval systems that paved the way to the application of modern control techniques for control systems design with inexact models. Therefore, in this dissertation, the ARE is modified to be written as an Interval System and the PID controller gains are derived accordingly such that the designed single PID controller gains satisfies the interval ARE equation. The merger of ARE with Interval Arithmetic ensures that not only the designed single PID controller is robust due to the use of Interval Arithmetic, but also guarantees optimality due to the use of ARE and this can be counted as one of the major contribution of this dissertation which has been discussed in details in *Chapter 2*.

In this context, a 540MWe Indian PHWR plant is first modeled as an Interval System and then model-order reduced into an interval second-order integrator template which is also a major

contribution of this dissertation illustrated in *Chapter 2*. The uncertainty bounds are derived from the uncertainty bounds of physical parameters like the reactor zonal powers, reactivity coefficients, parameters related to heat transfer from the fuel to the coolant etc., corresponding to the power maneuvering from 60% of its Full Power (FP) to 100%FP. Stability analysis of the interval model over the interval of power variation suggests that the system is controllable within the interval considered even though the system may be unstable in nature. Therefore, for stable operation of the reactor, there arises the need for design of a robust controller. With a robust, optimal PID controller designed for the nominal plant corresponding to 80%FP, controllers are designed for each zone and it is shown that the same controller can be used for controlling the reactor power varying between 60%FP and 100%FP. The controller remains optimal with a bounded change in cost of control [42] on the parameters of the system. The approach allows the designer to associate appropriate weight to the reactivity input to the reactor, thus controlling the fissile material burn-up. On the other hand, the advantages of a PID controller are also preserved.

The next objective is to extend the same controller design methodology towards the control of a 700MWe Indian PHWR where there is a provision of limited voiding in a coolant channel in the higher (92.3%FP) power regime. The occurrence of voiding in a coolant channel poses a major challenge towards operation and control engineers of a 700MWe PHWR operating at 100%FP. Voiding in the coolant channel, if left uncontrolled, may result in a severe accident due to positive reactivity defect. Many contemporary researchers like [43] and [44] have established the characteristic of voiding and attempted to estimate the void fraction in a two phase flow in the coolant channels. However, in both cases it is difficult for a control engineer to choose a proper control strategy as these estimations are computationally intensive. Moreover, these methods do not provide any information in the transient time, i.e. during power maneuvering.

Literature survey [43], [44] reveals that the operational analysis of a nuclear power plant in transient time during the occurrence of voiding in a coolant channel is limited. Also, majority of the existing literature related to void analysis, do not provide void modeling in the transient time though this is an important analysis that is required to be carried out for 700MWe PHWRs and is essential for design of controllers. Motivated by the need to bridge this gap, this dissertation puts forward the details of void fraction modeling in transient time as a function of demand power maneuvering, in *Chapter 3*. Operation of a 700MWe PHWR, therefore proposes to tackle two major challenges viz. the first challenge to design single robust optimal controller for power maneuvering control from 60%FP to 100%FP and the second major challenge is to keep void fraction limited during such power maneuver. Voiding leads to non-polytopic variation of reactor parameters with respect to the reactor power variation and therefore the controller design methodology for a 540MWe PHWR is incapable of ensuring robustness, performance and stability when applied to a 700MWe PHWR. Therefore, the controller design methodology for 540MWe PHWR is modified to handle bounded non-polytopic parametric uncertainty and this can be regarded as one of the major contribution of the dissertation illustrated in *Chapter 3*. The next objective is to keep the void fraction within its specified limit and for this purpose the pressurizer pressure of the PHT is altered in a very tight interval as soon as the voiding starts. The pressurizer pressure control is accomplished by optimally controlling the spray flow and heating element of the pressurizer. The optimal PI controller for pressurizer has been designed using Genetic Algorithm (GA) [45], [46]. The presence of two sets of optimal controller-one for controlling the power level designed using LQR approach and interval arithmetic and another for controlling the pressurizer pressure designed using GA, can together achieve efficient power tracking of 700MWe Indian PHWR keeping the coolant channel void fraction within its

prescribed limit and this can be counted as the final-most major contribution of this dissertation discussed in details in *Chapter 3*. Thus, modeling of void fraction from principles of reactor thermal-hydraulics and its use in the design of a power controller for the 700MWe PHWR with limited controlled void formation is another major contribution of this dissertation and this is presented in detail in *Chapter 3.*

The methodologies illustrated in *Chapters 2* and *3* are validated using simulation based studies and the corresponding results are presented in *Chapter 4*. *Chapter 5* summarizes the salient conclusions from the dissertation and finally presents the scope for future work.

This page is intentionally left blank

This page is intentionally left blank

Chapter 2

A 540MWe PHWR in Open-loop and Controller Design for its Stable Operation

2.1 Introduction

This chapter discusses in details the dynamics of a 540MWe PHWR under variable reactor power and proposes a methodology to design a single robust optimal controller that can be used for control of the reactor within a specified bound of reactor power variation. The controller can also take care of bounded parametric variations in the reactor's parameters arising out of uncertainties in modeling. For this purpose, The PHWR is modeled as an interval system and the nature of its open-loop behavior is first studied. It is obvious that modeling an uncertain system as an interval system would extensively require the knowledge of the Interval Arithmetic and therefore the requisite mathematical formulae of Interval Arithmetic are discussed in brief at the very beginning of this chapter. This is then followed by a detailed methodology of modeling a plant with bounded parametric uncertainties and uncertainties in measurements (reactor system) as an interval system in general and as applied to the modeling of a 540MWe PHWR plant specifically. Finally this chapter concludes with the details of designing a single robust optimal PID controller to control the power in a 540MWe PHWR under changing

reactor power in the presence of uncertainties in measured reactor power, reactivity defect and heat transfer estimates.

2.2 Basic Interval Mathematics

An interval system with bounded parametric uncertainties can be described using the following general transfer function representation defined as

$$\left.\begin{aligned} G(s,\mathbf{p}) &= \frac{f_0 + f_1 s^m + \ldots + f_m s^m}{g_0 + g_1 s + \ldots + g_n s^n} \\ \mathbf{p} &= [f_0, f_1, \ldots, f_m; g_0, g_1, \ldots, g_n]; \end{aligned}\right\} \tag{2.1}$$

The set $\mathbf{p}$ is the set of all parameters with admissible uncertainties and is represented by the set of all interval variables in $G(s,\mathbf{p})$. In (2.1) and throughout the rest of this dissertation a bounded interval variable Z is defined as $Z \in \mathbb{R} \,|\, \underline{Z} \le Z \le \overline{Z}$ where $\underline{Z}$ represents *infimum* of Z and $\overline{Z}$ its *supremum* and $\left[\underline{Z},\ \overline{Z}\right]$ represents the interval of Z. The definition of interval holds for a vector or a matrix as well. Further, if $N \in \left[\underline{N},\ \overline{N}\right]$ be another interval variable, then the following hold [47]:

$$\left.\begin{aligned} &\left[\underline{Z},\ \overline{Z}\right] + \left[\underline{N},\ \overline{N}\right] = \left[\left(\underline{Z} + \underline{N}\right), \left(\overline{Z} + \overline{N}\right)\right] \\ &\left[\underline{Z},\ \overline{Z}\right]\left[\underline{N},\ \overline{N}\right] - \left[\underline{V},\ \overline{V}\right] = \left[\left(\underline{Z} - \overline{N}\right),\ \left(\overline{Z} - \underline{N}\right)\right] \\ &\left[\underline{Z},\ \overline{Z}\right] \times \left[\underline{N},\ \overline{N}\right] = \begin{bmatrix} \min\left(\underline{Z}\underline{N}, \underline{Z}\overline{N}, \overline{Z}\underline{N}, \overline{Z}\overline{N}\right), \\ \max\left(\underline{Z}\underline{N}, \underline{Z}\overline{N}, \overline{Z}\underline{N}, \overline{Z}\overline{N}\right) \end{bmatrix} \\ &\frac{\left[\underline{Z},\ \overline{Z}\right]}{\left[\underline{N},\ \overline{N}\right]} = \left[\underline{Z},\ \overline{Z}\right] \times \left[\frac{1}{\overline{N}}, \frac{1}{\underline{N}}\right] \end{aligned}\right\} \tag{2.2}$$

It is to be noted that equation (2.2) is only valid for the scalar variable.

For matrices, the interval operations are different from the ones defined in (2.2) [48]. If $\mathbf{N}$ is termed an interval matrix then $\mathbf{N}$ can be defined as:

$$\mathbf{N} = \begin{bmatrix} n_{11} & n_{12} & \cdots & n_{1n} \\ n_{21} & n_{22} & \cdots & n_{2n} \\ \vdots & \vdots & \ddots & \vdots \\ n_{n1} & n_{n2} & \cdots & n_{nn} \end{bmatrix} \tag{2.3}$$

where, any element $n_{ij} \in \mathbf{N}$ is an *interval variable* defined as $n_{ij} = \left[\underline{n}_{ij}, \overline{n}_{ij}\right]$. Correspondingly, the matrix $\underline{\mathbf{N}}$ denoted as the *infimum* of $\mathbf{N}$ and the matrix $\overline{\mathbf{N}}$ denoted as the *supremum* of $\mathbf{N}$, may be defined as

$$\underline{\mathbf{N}} = \begin{bmatrix} \underline{n}_{11} & \underline{n}_{12} & \cdots & \underline{n}_{1n} \\ \underline{n}_{21} & \underline{n}_{22} & \cdots & \underline{n}_{2n} \\ \vdots & \vdots & \ddots & \vdots \\ \underline{n}_{n1} & \underline{n}_{n2} & \cdots & \underline{n}_{nn} \end{bmatrix} \tag{2.4}$$

and

$$\overline{\mathbf{N}} = \begin{bmatrix} \overline{n}_{11} & \overline{n}_{12} & \cdots & \overline{n}_{1n} \\ \overline{n}_{21} & \overline{n}_{22} & \cdots & \overline{n}_{2n} \\ \vdots & \vdots & \ddots & \vdots \\ \overline{n}_{n1} & \overline{n}_{n2} & \cdots & \overline{n}_{nn} \end{bmatrix} \tag{2.5}$$

respectively. Again, the matrix $\mathbf{N}$ can be alternatively expressed as

$$\mathbf{N} = \mathbf{N}_c + \mathbf{N}_r \tag{2.6}$$

where *'c'* as a suffix represents nominal matrix and *'r'* as a suffix represents the variation of the *infimum* and/or *supremum* from the nominal matrix. Therefore,

$$\mathbf{N}_c = \frac{1}{2}\left(\underline{\mathbf{N}} + \overline{\mathbf{N}}\right) \tag{2.7}$$

$$\mathbf{N}_r = \mathbf{N}_c - \underline{\mathbf{N}} \tag{2.8}$$

Now if $\mathbf{Z} \in [\underline{\mathbf{Z}}, \overline{\mathbf{Z}}]$ be another interval matrix, then using the results presented in Rump *et al.* [48], for the product $\mathbf{W} = \mathbf{NZ}$, the following hold:

$$\mathbf{W}_r = \left(|\mathbf{N}_c|.\mathbf{Z}_r\right) + \mathbf{N}_r\left(|\mathbf{Z}_c| + \mathbf{Z}_r\right) \tag{2.9}$$

$$\mathbf{W}_c = \mathbf{N}_c\mathbf{Z}_c \tag{2.10}$$

$$\overline{\mathbf{W}} = \mathbf{N}_c.\mathbf{Z}_c + \mathbf{W}_r \tag{2.11}$$

$$\underline{\mathbf{W}} = \mathbf{N}_c.\mathbf{Z}_c - \mathbf{W}_r \tag{2.12}$$

If $\mathbf{N}$ is a *point matrix* as opposed to an interval matrix, then $\mathbf{N}_c = \mathbf{N}$ and $\mathbf{N}_r = 0$. For such cases, the following hold for the product $\mathbf{W} = \mathbf{NZ}$

$$\mathbf{W}_r = \left(|\mathbf{N}|.\mathbf{Z}_r\right) \tag{2.13}$$

$$\overline{\mathbf{W}} = \left(\mathbf{N}.\mathbf{Z}_c + \mathbf{W}_r\right) \tag{2.14}$$

$$\underline{\mathbf{W}} = \left(\mathbf{N}.\mathbf{Z}_c - \mathbf{W}_r\right) \tag{2.15}$$

Again for a set of interval variables $\mathbf{w} = [w_1, w_2, ...w_N]$ a convex box of $\mathbf{w}$ means the Cartesian product of the intervals $[\underline{w}_1, \overline{w}_1] \times [\underline{w}_2, \overline{w}_2] \times \cdots \times [\underline{w}_N, \overline{w}_N]$.

In equation (2.1) the transfer function $G(s, \mathbf{p})$ represents a ratio of two polynomials in s, the coefficients of each being interval variables represented by real numbers which lie within specific bounds $[\underline{g}_i, \overline{g}_i]$ $\forall i \in [0, m]$ and $[\underline{f}_j, \overline{f}_j]$ $\forall j \in [0, n]$. If the denominator of the interval plant is expressed as

$$q(s, \mathbf{p}) = g_0 + g_1 s + g_2 s^2 + \ldots + g_n s^n \tag{2.16}$$

then the interval plant $G(s,\mathbf{p})$ will be Hurwittz stable if the set of following four polynomials known as Kharitonov Polynomials [24] are Hurwitz stable:

$$\left.\begin{aligned} q_1(s) &= \underline{g}_0 + \underline{g}_1 s + \overline{g}_2 s^2 + \overline{g}_3 s^3 + \underline{g}_4 s^4 + \underline{g}_5 s^5 \ldots \\ q_2(s) &= \overline{g}_0 + \overline{g}_1 s + \underline{g}_2 s^2 + \underline{g}_3 s^3 + \overline{g}_4 s^4 + \overline{g}_5 s^5 \ldots \\ q_3(s) &= \underline{g}_0 + \overline{g}_1 s + \overline{g}_2 s^2 + \underline{g}_3 s^3 + \underline{g}_4 s^4 + \overline{g}_5 s^5 \ldots \\ q_4(s) &= \overline{g}_0 + \underline{g}_1 s + \underline{g}_2 s^2 + \overline{g}_3 s^3 + \overline{g}_4 s^4 + \overline{g}_5 s^5 \ldots \end{aligned}\right\} \quad (2.17)$$

Hurwitz stability of Kharitonov Polynomials serve as the necessary and sufficient condition for robust stability of the interval plant $G(s,\mathbf{p})$.

2.3 Realizing reactor system as an interval system and analysis of its open-loop behavior

In this sub-section, it is first attempted to represent the relationship between demand power error (i.e. the difference between the demand power and the actual power produced) and power output of the reactor in the form of a transfer function representing a standard interval plant with bounded parametric uncertainties [25] described as

$$\left.\begin{aligned} G(s,\mathbf{p}) &= \frac{L}{s^2 + as + b} \\ \mathbf{p} &= [L,\ a,\ b] \\ L &\in [\underline{L},\ \overline{L}];\ a \in [\underline{a},\ \overline{a}];\ b \in [\underline{b},\ \overline{b}] \end{aligned}\right\} \quad (2.18)$$

It has been shown in [15], [25] that under varying power condition (2.18) holds for a reactor system. The results reported by Lee *et al.* are based on a similar assumption but a higher order template. In this chapter, the uncertainty bounds in (2.6) are derived from the uncertainty

bounds of physical parameters like the reactor zonal powers, reactivity coefficients and parameters related to heat transfer from the fuel to the coolant. The plant

$$G_0(s) = \frac{L_0}{s^2 + a_0 s + b_0} \tag{2.19}$$

is termed as the *nominal plant* and referred to as such throughout the rest of the dissertation interchangeably with the term *nominal system*.

2.3.1 Development of Interval Model of a 540MWe PHWR

As mentioned in *Chapter 1* a 540MWe PHWR consists of 14 zones each of which can be controlled by varying the height of the water column in its ZCC by a LZCS. The water level in each ZCC is controlled by modulating control valves to fill or drain the compartments with light water, thus controlling the reactivity input. There exist significant coupling between the different zones. A comprehensive description of the LZCS has been given in *Chapter 1* and in this chapter the data presented in [9] and [49] has been used for model development.

In this section, it is attempted to develop an inexact transfer function model for each PHWR zone of the general form $G(s,\mathbf{p})$ defined by (2.18). A lumped parameter point kinetic model of a PHWR zone neglecting inter zone coupling can be represented by the following set of equations.

$$\frac{dP_{th}}{dt} = -\frac{\beta}{l}P_{th} - \frac{\sigma_x X}{\Sigma_a}\frac{P_{th}}{l} + \lambda C + \rho_{net}\frac{P_{th}}{l} \tag{2.20}$$

$$\frac{dC}{dt} = \beta\frac{P_{th}}{l} - \lambda C \tag{2.21}$$

$$\frac{dI}{dt} = -(\lambda_I + \sigma_I P_{th})I + \gamma_I \Sigma_f P_{th} \tag{2.22}$$

$$\frac{dX}{dt} = -\left(\lambda_X + \bar{\sigma}_X P_{th}\right) X + \lambda_I I + \gamma_x \sum_f P_{th} \tag{2.23}$$

$$\frac{dT_f}{dt} = \frac{1}{m_f c_{p_f}} \left\{ P_{th} - Ah\left(T_f - T_c\right) \right\} \tag{2.24}$$

$$\frac{dT_c}{dt} = \frac{1}{m_c c_{p_c}} \left\{ \left[\dot{m} c_{p_c} T_{c_{input}} - \dot{m} c_{p_c} T_{c_{exit}} \right] + Ah_{fc}\left(T_f - T_c\right) \right\} \tag{2.25}$$

where P_{th} is the zonal reactor thermal power (W), ρ_{net} is the net reactivity input, incorporating reactivity defect due to change in fuel and coolant temperatures, C denotes delayed neutron precursor concentration and I and X represent the iodine and xenon concentrations respectively for a particular zone (m^{-3}). Similarly, β denotes for delayed neutron fractional yield, λ denotes decay constant (sec^{-1}) while σ_X and σ_I represent the microscopic thermal neutron absorption cross sections of xenon and iodine respectively (m^2). Similarly, γ_X and γ_I denote xenon and iodine yield per fission, λ_X and λ_I denote corresponding decay constants (sec^{-1}) and $\sum_a$ and $\sum_f$ represent thermal neutron absorption and fission cross sections (m^{-1}). Further in the same set of equations, m_f and m_c denote mass of the fuel and mass of the coolant in the core (kg), c_{p_f} and c_{p_c} represent specific heat of the fuel and specific heat of the coolant respectively at constant pressure ($J/kg.^0C$) while A is the active heat transfer area (m^2) and h_{fc} is the fuel to coolant heat transfer co-efficient ($W/m^2.^0C$). The symbol $\dot{m}$ denotes the mass flow rate of the coolant (kg/sec), T_f (^0C) denotes the average fuel temperature and T_c denotes the average coolant temperature (^0C) defined as

$$T_c = \frac{T_{c_{inlet}} + T_{c_{outlet}}}{2} \tag{2.26}$$

where $T_{c_{input}}$ and $T_{c_{outlet}}$ are the inlet and outlet coolant temperatures respectively in ^{0}C. In the formulation (2.20)-(2.25) $T_{c_{inlet}}$ is assumed to be constant.

The net reactivity input to a zone ρ_{net} may be expressed

$$\rho_{net} = \rho_{ext} + \alpha_f \left(\mathrm{T}_f - \mathrm{T}_{f_{ss}}\right) + \alpha_c \left(\mathrm{T}_c - \mathrm{T}_{c_{ss}}\right) \tag{2.27}$$

where ρ_{ext} denotes the reactivity introduced in the zone due to control rod movement and change in ZCC level, $T_{f_{ss}}$ and $T_{c_{ss}}$ represent the initial (equilibrium) values of average fuel and coolant temperatures and α_c, α_f represent the temperature coefficients of reactivity of the coolant and fuel respectively (^{0}C^{-1}).

The equation set (2.20) - (2.27) is used to develop an incremental state-vector model for the PHWR zone of the form

$$\dot{\tilde{\mathbf{x}}} = \mathbf{A}\tilde{\mathbf{x}} + \mathbf{B}\tilde{\mathbf{u}} \text{ and } \tilde{\mathbf{y}} = \mathbf{C}\tilde{\mathbf{x}} \tag{2.28}$$

where $\tilde{\mathbf{x}} = \begin{bmatrix} \tilde{P}_{th} & \tilde{C} & \tilde{I} & \tilde{X} & \tilde{T}_f & \tilde{T}_c \end{bmatrix}^{\mathrm{T}}$ denotes the set of incremental state variables around an equilibrium state $\begin{bmatrix} P_{ss} & C_{ss} & I_{ss} & X_{ss} & T_{ss} & T_{ss} \end{bmatrix}^{\mathrm{T}}$ and $\tilde{\mathbf{u}}$ denotes the incremental change in net reactivity and is equal to ρ_{net}. Similarly set by $\mathbf{C} = \begin{bmatrix} 1 & 0 & 0 & 0 & 0 & 0 \end{bmatrix}$ and $\tilde{\mathbf{y}}$ denotes the incremental reactor zonal power $\tilde{P}_{th}$ calculated around P_{ss}. Substituting $\Omega = Ah_{fc}$, $M_c = \dot{m}c_{p_c}$, $\mu_f = m_f c_{p_{cf}}$ and $\mu_c = m_c c_{p_c}$ in (2.20)-(2.25), the matrices $\mathbf{A}$, $\mathbf{B}$ are computed as

$$\mathbf{A}=\begin{bmatrix} -\left(\beta+\frac{\sigma_X X_{ss}}{\Sigma_a}\right)\frac{1}{l} & \lambda & 0 & -\frac{\sigma_X X_{ss}}{\Sigma_a l} & \alpha_f\frac{P_{ss}}{l} & \alpha_c\frac{P_{ss}}{l} \\ \frac{\beta}{l} & -\lambda & 0 & 0 & 0 & 0 \\ -\sigma_I I_{ss}+\gamma_I\Sigma_f & 0 & -\left(\lambda_I+\sigma_I P_{ss}\right) & 0 & 0 & 0 \\ \left(\gamma_X\Sigma_f-\sigma_X X_{ss}\right) & 0 & \lambda_I & -\left(\lambda_X+\sigma_X P_{ss}\right) & 0 & 0 \\ \frac{1}{\mu_f} & 0 & 0 & 0 & -\frac{\Omega}{\mu_f} & \frac{\Omega}{\mu_f} \\ 0 & 0 & 0 & 0 & \frac{2\Omega}{\mu_c} & -\left\{\frac{2\dot{m}c_{p_c}+\Omega}{\mu_c}\right\} \end{bmatrix} \tag{2.29}$$

$$\mathbf{B}=\begin{bmatrix}\frac{P_{ss}}{l} & 0 & 0 & 0 & 0 & 0\end{bmatrix}^{\mathrm{T}} \tag{2.30}$$

Equation (2.29) and (2.30) represent a 6th order interval system with the uncertainty vector

$$\left.\begin{aligned}&\mathbf{p}=\left[P_{ss},\,\alpha_c,\,\alpha_f,\,\Omega\right]\\&P_{ss}\in\left[\underline{P}_{ss},\overline{P}_{ss}\right];\ \alpha_f\in\left[\underline{\alpha}_f,\,\overline{\alpha}_f\right];\ \alpha_c\in\left[\underline{\alpha}_c,\,\overline{\alpha}_c\right];\ \Omega\in\left[\underline{\Omega},\overline{\Omega}\right]\end{aligned}\right\} \tag{2.31}$$

2.3.2 Analysis of stability and controllability of the non-linear plant in the power regime 60%FP to 100%FP

The matrix $\mathbf{A}$ in (2.29) obtained after linearization, is actually an interval matrix and for an interval of $\mathbf{A}_{80}$ $[60\%\text{FP},100\%\text{FP}]$ associated with the reactor power P_{ss} produce an interval matrix $\mathbf{A}_{60}^{100}$ represented as:

$$\mathbf{A}_{60}^{100}=\begin{bmatrix} [-12.39,-11.74] & 0.608 & 0 & [-63.8,-34.7] & [-4.845,-3.3083]\times10^{6} & [-10.526,-5.574]\times10^{7} \\ [9.4936708,9.4936709] & -0.608 & 0 & 0 & 0 & 0 \\ [5.808,5.809]\times10^{-4} & 0 & [-2.88,-2.79]\times10^{-5} & 0 & 0 & 0 \\ [-5.6,-5.4]\times10^{-5} & 0 & 2.812\times10^{-5} & [-2.1,-2.101]\times10^{-5} & 0 & 0 \\ [4.01,4.05]\times10^{-8} & 0 & 0 & 0 & [-0.1946,-0.1751] & [0.1946,0.1751] \\ 0 & 0 & 0 & 0 & [0.1142,0.1307] & [-2.1161,-2.106] \end{bmatrix} \tag{2.32}$$

It is assumed that $\mathbf{A}_{60}$ represents the value of $\mathbf{A}$ at 60%FP, $\mathbf{A}_{80}$ represents its value at 80%FP and $\mathbf{A}_{100}$ represents the value of $\mathbf{A}$ at 100%FP. Since, the demand power variation is considered in the range 60%FP to 100%FP, the design methodology presented in this chapter uses 80%FP as the design basis and the corresponding value of the matrix $\mathbf{A}$ at 80%FP becomes

$$\mathbf{A}_{80} = \begin{bmatrix} -12.3 & 0.608 & 0 & -43.83 & -4.25\times10^{6} & -7.42\times10^{7} \\ 9.49367088 & -0.608 & 0 & 0 & 0 & 0 \\ 5.8087\times10^{-4} & 0 & -2.83\times10^{-5} & 0 & 0 & 0 \\ -5.53\times10^{-5} & 0 & 2.812\times10^{-5} & -2.1\times10^{-5} & 0 & 0 \\ 4.033\times10^{-8} & 0 & 0 & 0 & -0.188 & 0.188 \\ 0 & 0 & 0 & 0 & 0.122 & -2.101 \end{bmatrix} \quad (2.33)$$

The Eigen values of the matrix $\mathbf{A}_{80}$ are enumerated in Table 2.1 as:

Table 2.1
Eigen values at different power level

Sl. No	Eigen values of $\mathbf{A}_{80}$
1	-10.088597
2	-2.091980
3	-0.104790+ 0.114542i
4	-0.104790-0.114542i
5	-0.00000000125
6	0.000000

From Table 2.1 it is seen that the real-part of all Eigen values of the matrix $\mathbf{A}_{80}$ are not all negative and hence the open-loop linearized non-linear plant is not stable at 80%FP. It is then attempted to study the establish the bounds of Eigen values of the interval matrix $\mathbf{A}_{60}^{100}$.

The bounds of the Eigen Values of the interval matrix (2.32) can be calculated as in [50] by defining

$$\left.\begin{aligned}\mathbf{A}_c &= \frac{1}{2}\left(\underline{\mathbf{A}}_{60}^{100} + \overline{\mathbf{A}}_{60}^{100}\right)\\ \mathbf{A}_\Delta &= \frac{1}{2}\left(\overline{\mathbf{A}}_{60}^{100} - \underline{\mathbf{A}}_{60}^{100}\right)\end{aligned}\right\} \tag{2.34}$$

and further

$$\left.\begin{aligned}\mathbf{S}_c &= \frac{1}{2}\left(\mathbf{A}_c + \mathbf{A}_c^{\mathrm{T}}\right)\\ \mathbf{S}_\Delta &= \frac{1}{2}\left(\mathbf{A}_\Delta + \mathbf{A}_\Delta^{\mathrm{T}}\right)\end{aligned}\right\} \tag{2.35}$$

it can be proved that if $\mathbf{\Lambda}$ denotes the set of all real Eigen values of $\mathbf{A}_{60}^{100}$ then the following interval bound holds

$$\Lambda \subseteq \boldsymbol{\lambda}^0 := \left[\underline{\lambda}^0,\ \overline{\lambda}^0\right] \tag{2.36}$$

where,

$$\left.\begin{aligned}\underline{\lambda}^0 &= \lambda_{\min}\left(\mathbf{S}_c\right) - \rho\left(\mathbf{S}_\Delta\right)\\ \overline{\lambda}^0 &= \lambda_{\max}\left(\mathbf{S}_c\right) + \rho\left(\mathbf{S}_\Delta\right)\end{aligned}\right\} \tag{2.37}$$

It is to be noted that for a symmetric matrix $\mathbf{\Lambda}$ represents the set of *all* Eigen values where tighter bounds are possible.

Thus bounds for the real Eigen values of $\mathbf{A}_{60}^{100}$ are computed and expressed in Table 2.2

Table 2.2

Bounds of the real Eigen values of $\mathbf{A}_{60}^{100}$

$\left[\underline{\lambda}^0,\ \overline{\lambda}^0\right]$	**Interval Bounds of the real part of Eigen values**
$\underline{\lambda}^0$	-5.2688×10^{7}
$\overline{\lambda}^0$	5.2688×10^{7}

From Table 2.2 it is seen that the real part of all the Eigen values of the interval matrix lie bounded in the interval $\left[-5.2688\times10^{7},\ 5.2688\times10^{7}\right]$. Therefore, it can be concluded that the non-linear plant represented by the equation set (2.20)-(2.25) is not guaranteed open-loop stable in the power regime [60%FP,100%FP] [50], [48] as there could be one or more real Eigen values of the interval matrix $\mathbf{A}_{60}^{100}$ on the origin or the positive half of the real axis..

Next, it is attempted to study the controllability of the non-linear plant in the power regime selected i.e. $\left[60\%\text{FP},100\%\text{FP}\right]$ and to do that the corresponding interval of the matrix $\mathbf{B}$ expressed as $\mathbf{B}_{60}^{100} := \left[\mathbf{B}_{60},\ \mathbf{B}_{100}\right]$ is computed as yields

$$\mathbf{B}_{60}^{100} = \left[\left[1.3671,\ 2.2785\right]\times10^{6} \quad 0 \quad 0 \quad 0 \quad 0 \quad 0\right]^{\mathrm{T}} \tag{2.38}$$

From (2.32) and (2.38), the interval controllability matrix may be written as

$$\mathbf{U}_{60}^{100} = \left[\mathbf{B}_{60}^{100} \quad \mathbf{A}_{60}^{100}\mathbf{B}_{60}^{100} \quad \ldots \quad \left(\mathbf{A}_{60}^{100}\right)^{5}\mathbf{B}_{60}^{100}\right] \tag{2.39}$$

which produces

$$\mathbf{U}_{60}^{100} = \begin{bmatrix} [1.36,2.27]\times10^{7} & [-2.16-1.29]\times10^{7} & [1.30,2.18]\times10^{8} & [-2.19,-1.32]\times10^{9} & [1.33,2.21]\times10^{10} & [-2.23,-1.345]\times10^{11} \\ 0 & [1.29,2.13]\times10^{7} & [-2.185,-1.31]\times10^{8} & [1.33,2.20]\times10^{9} & [-2.22,-1.34]\times10^{10} & [1.346,2.24]\times10^{11} \\ 0 & [833.5,1389.1] & [-13.18-7.91]\times10^{3} & [7.98,13.29]\times10^{4} & [-13.4,-8.05]\times10^{6} & [8.12,13.52]\times10^{6} \\ 0 & [-128.5,-77.103] & [73.2,112.3] & [-9.86,-7.38]\times10^{3} & [7.45,12.4]\times10^{6} & [-12.51,-7.532]\times10^{5} \\ 0 & [6.19,10.13]\times10^{-2} & [-0.97,-0.59] & [6.04,9.81] & [-99.4,-60.9] & [6.154,10.03]\times10^{3} \\ 0 & 0 & [8.1,11.7]\times10^{-4} & [-0.95,-0.13] & [0.99,1.41] & [-1.43,-1.007] \end{bmatrix} \tag{2.40}$$

For any interval matrix, it is always possible to determine whether a given interval matrix contains a matrix of a given rank r [51], however a study of the interval matrix $\mathbf{U}_{60}^{100}$ reveals the following:

(i) The elements of the matrix $\mathbf{U}_{60}^{100}$ lie within bounded intervals which do not include 0

(ii) The intervals are such that no row can be expressed as a multiple of another

The observations (i) and (ii) indicate that the rank of the matrix $\mathbf{U}_{60}^{100}$ remains same as that of the controllability matrix $\mathbf{U}_{80}$ corresponding to 80%FP which is equal to 5 and same as that of the system matrices $\mathbf{A}_{60}, \mathbf{A}_{80}$ and $\mathbf{A}_{100}$. This implies that the non-linear system remains controllable in the entire regime of power variation considered in this paper which is [60%FP,100%FP] .

A standard controllability approach based on linearization has been adopted in this chapter rather than a conventional reachability analysis for a non-linear system based on the lie-bracket approach [52] as the controller design methodology employed uses an LQR approach which is extended for interval systems, which requires the system $(\mathbf{A}_{60}^{100}, \mathbf{B}_{60}^{100})$ to be stabilizable. The steps involved in controller design are detailed in the following sections.

2.3.3 Deriving the 2nd order interval plant

This 6th order system is reduced to derive the interval plant of the general template (2.18) using a two-step approach. First, the aggregation method detailed in [53] is used to derive a reduced order plant which yields

$$L = \frac{P_{ss}\lambda_X\left(2M_c + 2\Omega\right)k_{LZC}}{\left(2M_cP_{ss} + \beta + \frac{\sigma_X X}{\Sigma_a} - 2M_c\beta - \Omega\alpha_cP_{ss} + 2M_c + \Omega\alpha_fP_{ss}\right)} \tag{2.41}$$

$$a = \frac{\frac{\Omega}{\mu_f} + \frac{2M_c + \Omega}{\mu_c} + \lambda + \frac{\left(\beta + \frac{\sigma_X X}{\Sigma_a}\right)}{l}}{\frac{\Omega\lambda}{\mu_f\mu_c l}\left(2M_cP_{ss} + \beta + \frac{\sigma_X X}{\Sigma_a} - 2M_c\beta - \Omega a_cP_{ss} + 2M_c + \Omega a_fP_{ss}\right)} \tag{2.42}$$

and

$$b = 0 \tag{2.43}$$

with the assumption that the control rods are stationary and power is controlled by the LZCS alone such that $\rho_{ext} = k_{LZC}.\Delta P_d$, where ΔP_d denotes the power error and the gain term k_{LZC} has been assumed to be equal to 2.5×10^{-6} based on the data presented in [9]. The relevant Matlab code involving symbolic manipulation is detailed in Apendix-I.

It is seen that the RHS of equations (2.41) and (2.42) involve interval variables $P_{ss} \in \left[\underline{P}_{ss}, \overline{P}_{ss}\right]$, $\alpha_f \in \left[\underline{\alpha}_f, \overline{\alpha}_f\right], \alpha_c \in \left[\underline{\alpha}_c, \overline{\alpha}_c\right]$, $\Omega \in \left[\underline{\Omega}, \overline{\Omega}\right]$ which result due to uncertainties in measurement or due to variations in reactor power or both and can be used to derive the interval variables $L = L_0 \pm \Delta L, a = a_0 \pm \Delta a, b = 0$ around their nominal values $[L_0, a_0]$ to obtain interval plants described by (2.19) . The nominal system can be obtained by substituting $L = L_0, a = a_0$ and $b = 0$ in (2.19).

Table 2.3 enumerates the representative values of the Thermal-Hydraulic parameters used in equations (2.42)-(2.43) as reported by contemporary researchers [9], [49]. The values of the parameters reported in Table 2.3 and those of α_c and α_f correspond to 80%FP and the values of these parameters at other power levels used in this dissertation are as reported in [49]. In Table 2.3 P_{ss_0} and Ω_0 denote the nominal values of the interval variables P_{ss} and Ω respectively. Table 2.3 does not include the values of the neutronic parameters (i.e. β, σ_X, σ_I, l, λ, λ_X, λ_I, γ_X, γ_I, Σ_a and Σ_f) for the sake of brevity and they have been taken as reported in [9]. The nominal values of α_c and α_f are taken as $-5.59\times10^{-4}\ ^0C^{-1}$ and $-3.2\times10^{-5}\ ^0C^{-1}$ respectively for all 14 zones assuming an equilibrium core.

Table 2.3

Thermal-Hydraulic Parameters for Nominal System at 80%FP

Zone	P_{ss_0}	Ω_0	μ_f	μ_c	M_c
1,8	108.48×10^6	3.128×10^5	1.661×10^6	5.113×10^6	5.181×10^6
2,9	110.88×10^6	3.203×10^5	1.701×10^6	5.236×10^6	5.305×10^6
3,10	100.66×10^6	2.907×10^5	1.54×10^6	4.753×10^6	4.816×10^6
4,11	80.35×10^6	2.321×10^5	1.23×10^6	3.794×10^6	3.844×10^6
5,12	100.66×10^6	2.907×10^5	1.54×10^6	4.753×10^6	4.816×10^6
6,13	108.48×10^6	3.128×10^5	1.661×10^6	5.113×10^6	5.181×10^6
7,14	110.88×10^6	3.203×10^5	1.701×10^6	5.236×10^6	5.305×10^6

Table 2.4 represents the intervals of P_{ss} and Ω and the corresponding intervals $\left[\underline{L}, \overline{L}\right]$ and $\left[\underline{a}, \overline{a}\right]$ for each zone computed using rule-set (2.2) and equations (2.41)-(2.43) with a $\pm10\%$ of uncertainty bound for each interval variable P_{ss}, α_c, α_f and Ω, at 80%FP. The intervals $\left[-6.149, -5.031\right]\times10^{-4}\ {}^0\mathrm{C}^{-1}$ and $\left[-3.52, -2.88\right]\times10^{-5}\ {}^0\mathrm{C}^{-1}$ associated with α_c and α_f respectively, remain same for all zones and are not presented in Table 2.4.

Table 2.4

Interval Parameters with $\pm 10\%$ Uncertainties at 80%FP

Zone	$[\underline{P_{ss}}, \overline{P_{ss}}]$	$[\underline{\Omega}, \overline{\Omega}]$	$[\underline{L}, \overline{L}]$	$[\underline{a}, \overline{a}]$
1,8	$[97.57, 119.26]\times10^6$	$[2.81, 3.44]\times10^5$	$[0.0055, 0.0074]$	$[1.3287, 1.7793]$
2,9	$[99.79, 121.96]\times10^6$	$[2.88, 3.52]\times10^5$	$[0.0054, 0.0072]$	$[1.3235, 1.7725]$
3,10	$[90.58, 121.96]\times10^6$	$[2.61, 3.19]\times10^5$	$[0.0061, 0.0082]$	$[1.3030, 1.7450]$
4,11	$[72.31, 88.38]\times10^6$	$[1.98, 2.43]\times10^5$	$[0.0075, 0.0101]$	$[1.3247, 1.7740]$
5,12	$[90.58, 121.96]\times10^6$	$[2.61, 3.19]\times10^5$	$[0.0061, 0.0082]$	$[1.3030, 1.7450]$
6,13	$[97.57, 119.26]\times10^6$	$[2.81, 3.44]\times10^5$	$[0.0055, 0.0074]$	$[1.3287, 1.7793]$
7,14	$[99.79, 121.96]\times10^6$	$[2.88, 3.52]\times10^5$	$[0.0054, 0.0072]$	$[1.3235, 1.7725]$

Next, the equations (2.41)-(2.43) are also used to derive the values of the variables L_0, a_0 at 80%FP, 100%FP and at 60%FP and the values are represented in Table 2.5. For each power level corresponding values of $[\alpha_c, \alpha_f, \Omega]$ that have been used in the computation of L, a are as reported in [49].

Table 2.5

Nominal Values of L, a at 100%FP, 80%FP and 60%FP

Zone	100%FP		80%FP		60%FP	
	L_0	a_0	L_0	a_0	L_0	a_0
1,8	0.0051034	1.55889	0.0064626	1.55496	0.0084124	1.533248
2,9	0.0050102	1.56477	0.0062857	1.54870	0.00825668	1.540570
3,10	0.0052687	1.53291	0.0071854	1.524855	0.0093849	1.510010
4,11	0.0068255	1.55388	0.0088249	1.549330	0.01149299	1.533319
5,12	0.0052685	1.53291	0.0071854	1.524855	0.0093849	1.510017
6,13	0.0051034	1.55889	0.0064626	1.554968	0.00841247	1.533248
7,14	0.0050102	1.56477	0.0062856	1.54870	0.0082566	1.540575

The data set corresponding to 80%FP in Table 2.4 is used to derive the nominal plant transfer functions for each of the 14 zones of the PHWR of the form (2.19). Since the parameter $b = 0$ for all zones, each plant represents an integrator plant with a real pole which moves closer to the origin with reducing power P_{ss} as evident from a study of the parameter a for each zone of the PHWR corresponding to different power levels in Table 2.5. This general nature of a reactor with thermal-hydraulic feedback has been reported in [49] also.

The set of equations (2.20)-(2.25) does not take into consideration the effect of coupling between the different zones of a PHWR. The coupling between the different zones of a 540MWe PHWR exists and this has been reported by contemporary researchers [36], [54]. It is therefore necessary to compare the models obtained using (2.41)-(2.43) with the results obtained through system identification using practical plant data. Table 2.6 presents the nominal plant parameters

L_0, a_0 (data corresponding to 80%FP) obtained by system identification using practical plant data which takes into consideration both thermal-hydraulic effects and coupling between the zones.

Table 2.6

Identified Model at 80%FP

Zone	L_0	a_0
1,8	0.0064890	1.56021
2,9	0.0063465	1.55056
3,10	0.0072003	1.53406
4,11	0.0089023	1.55043
5,12	0.0072003	1.53406
6,13	0.0064890	1.56021
7,14	0.0063465	1.55056

It is seen from Table 2.5 and Table 2.6 that for each zone the difference between the nominal system parameters reported in Table 2.5 and Table 2.6 lies within the intervals $\left[\underline{L}, \overline{L}\right]$ and $\left[\underline{a}, \overline{a}\right]$ reported in Table 2.5 implying that a robust controller designed with parametric uncertainty bounds defined in Table 2.5 will be able to handle uncertainties induced due to coupling.

2.3.4 Analysis of open-loop poles behavior for the reduced order system

The interval of $a = \left[\underline{a}, \overline{a}\right]$ depicted in Table 2.4 signifies the interval variation of open-loop poles location for different zones of a 540MWe PHWR with 10% bounded parametric

uncertainties. Also, from Table 2.5, it is evident that the pole location of the nominal plant varies in an interval with the variation of the demand power in the interval of $[60\%FP, 100\%FP]$. From Table 2.4 and Table 2.5 it is evident that $[\underline{a}_0, \overline{a}_0] \subseteq [\underline{a}, \overline{a}]$. Figure 2.1-2.4 depicts the interval variation of open-loop pole location for corresponding zone.

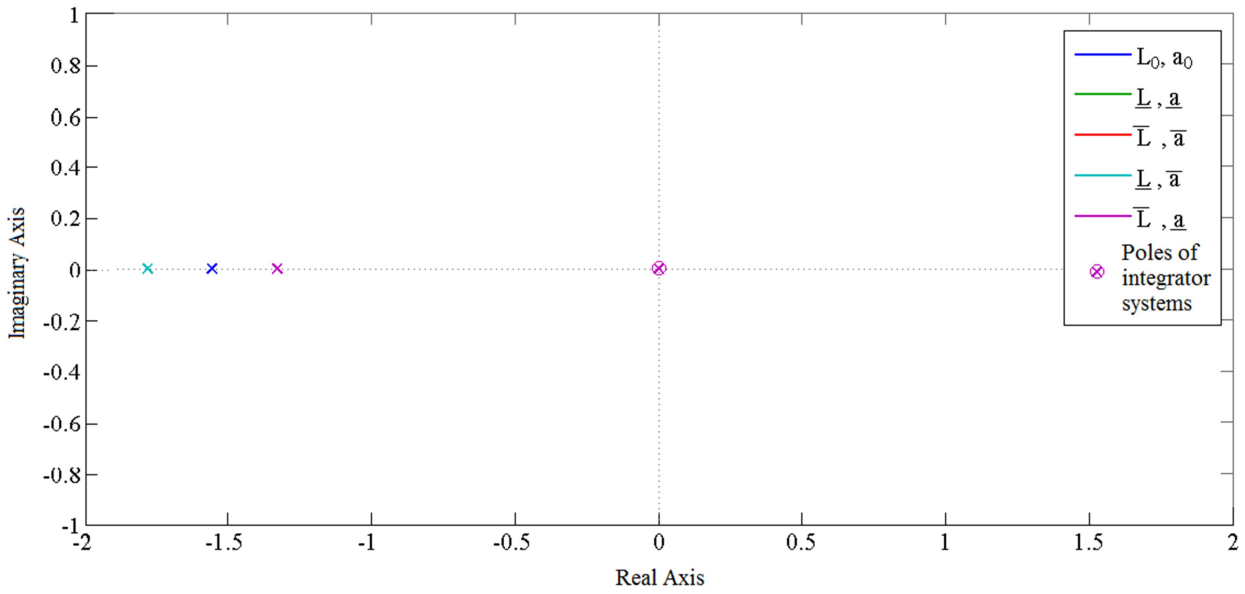

Fig. 2.1 open loop poles for interval system of zone 1, 8, 6 and 13

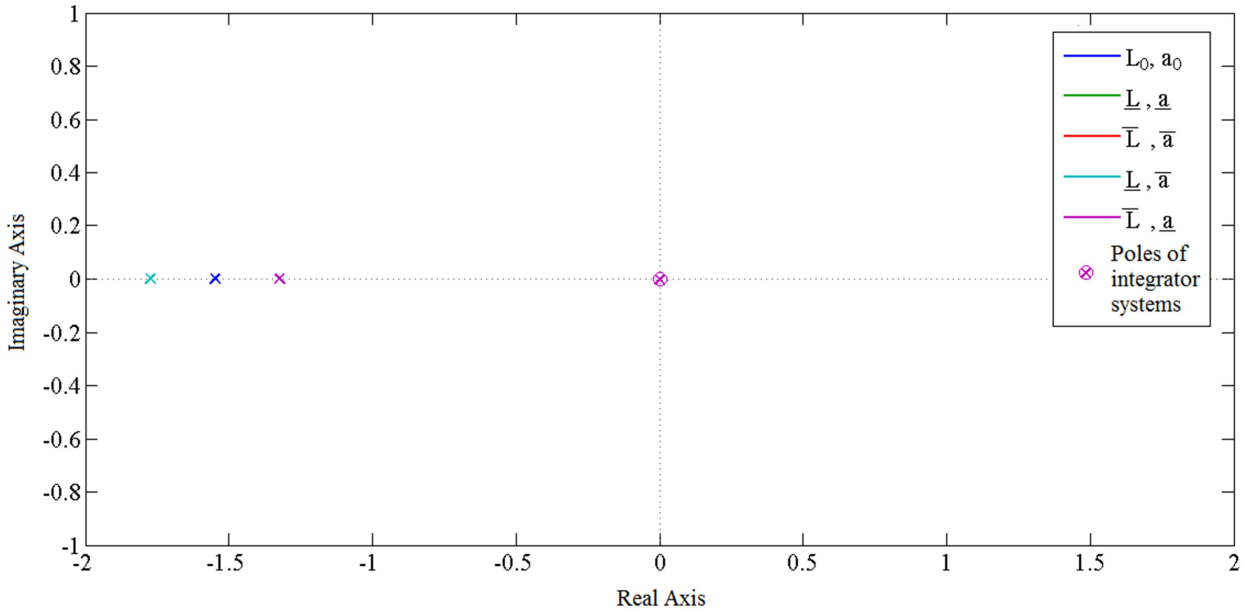

Fig. 2.2 open loop poles for interval system of zone 2, 9, 7 and 14

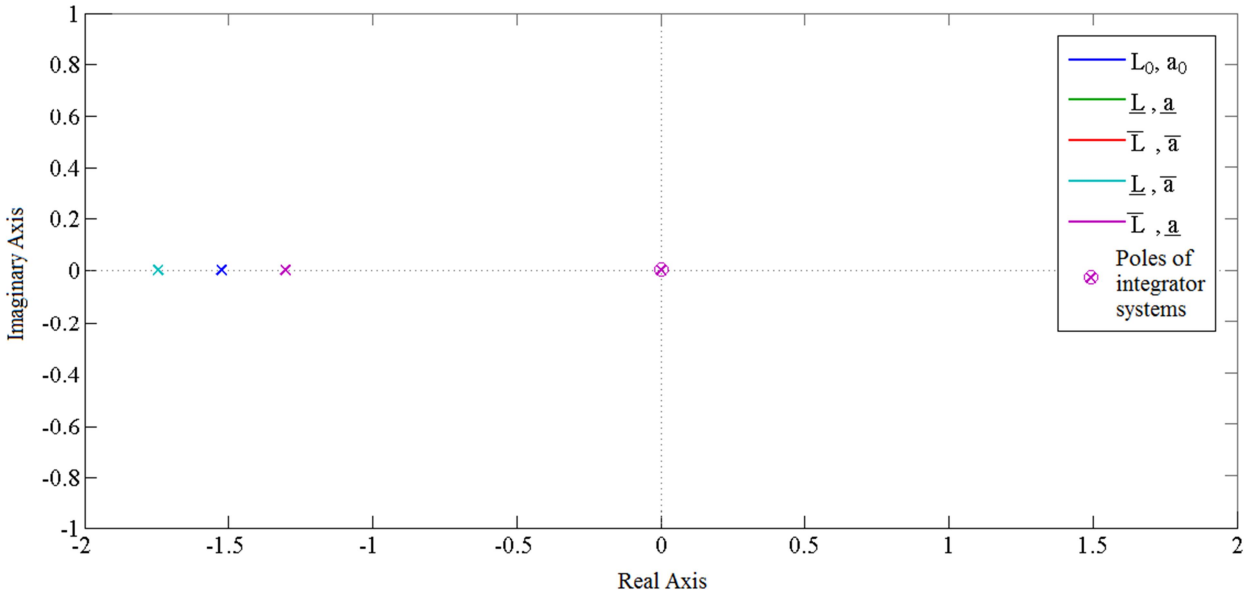

Fig. 2.3 open loop poles for interval system of zone 3, 10, 5 and 12

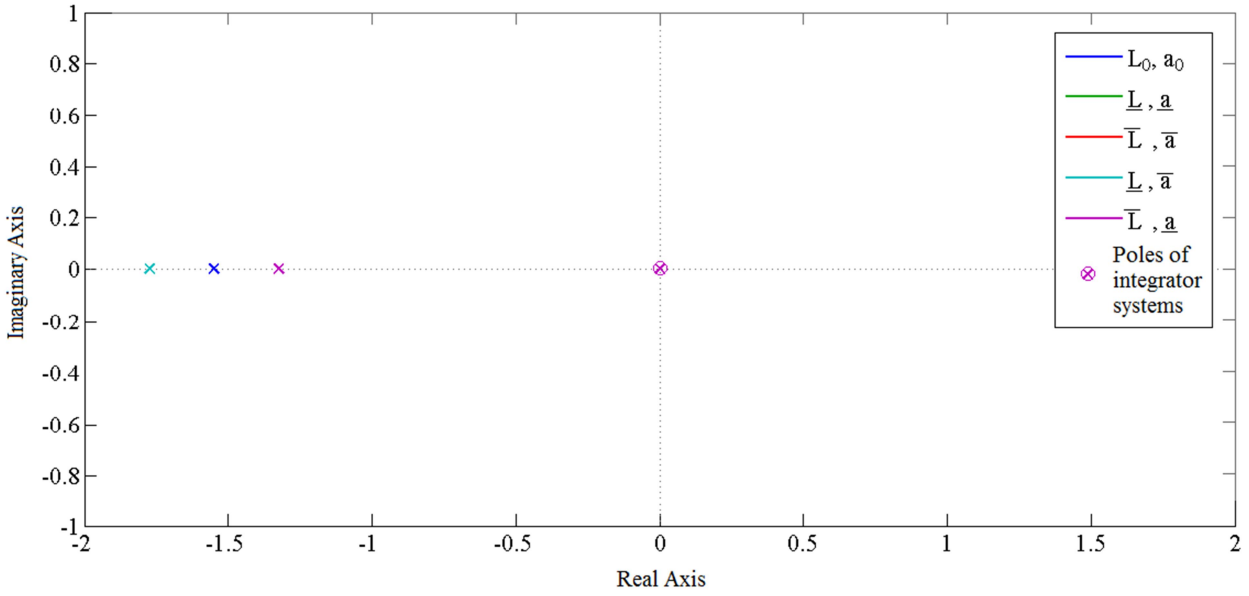

Fig. 2.4 open loop poles for interval system of zone 4 and 11

It is interesting to note that the system considered here corresponds to a template defined by (2.18) representing an integrating system, since $b = 0 \; \forall \left[L, a \right]$. Therefore one open-loop pole must lie at the origin and this is clearly depicted in Fig. 2.1-2.4. Thus, the system is a marginally stable system. An examination of Fig. 2.1-2.4 suggests that the location of the pole of the

nominal plant which corresponds to 80%FP shifts away from the origin as and when power is increased from 80%FP to 100%FP and shifts towards the origin when power is reduced from 80%FP to 60%FP. Therefore it can be inferred that with the increase of demand power for 540MWe PHWR, the reactor system tends towards more stable region and vice-versa. This phenomenon has also been reported in [49].

2.4 Controller Design Approach

In this section it is first attempted to design a PID controller

$$H(s) = K_p + \frac{K_i}{s} + K_d s \tag{2.44}$$

for the nominal plant (2.18) with $b = 0$ to yield a nominal closed-loop system of the form

$$\left.\begin{aligned} G_{c0}(s) &= \frac{\dfrac{L_0}{s(s+a_0)}\left(K_p + \dfrac{K_i}{s} + K_d s\right)}{1 + \dfrac{L_0}{s(s+a_0)}\left(K_p + \dfrac{K_i}{s} + K_d s\right)} \\ &= \frac{L_0\left(K_p s + K_i + K_d s^2\right)}{s^2(s+a_0) + L_0\left(K_p s + K_i + K_d s^2\right)} \\ &= \frac{L_0\left(K_p s + K_i + K_d s^2\right)}{(s+\sigma_0)\left(s^2 + 2\zeta_0\omega_0 s + \omega_0^2\right)} \end{aligned}\right\} \tag{2.45}$$

with specified values of closed-loop damping ζ_0, closed-loop frequency ω_0 and closed-loop real pole $-\sigma_0$, using the LQR approach presented in [39]. Specification of σ_0, ζ_0 and ω_0 indirectly specifies the position of closed-loop poles. A large value of σ_0 ensures that the closed-loop time response of $G_{c0}(s)$ is governed by its complex roots.

The PID controller methodology adopted in this dissertation follows an LQR approach presented in [39] and is particularly significant for a PHWR which uses natural Uranium fuel containing only 0.7% of fissile material. The approach allows the designer to associate appropriate weight to the reactivity input to the reactor, thus controlling the fissile material burn-up. On the other hand, the advantages of a PID controller are preserved. It has been shown in [39] that the controller (2.44) follows from a unique solution $\mathbf{P} = \mathbf{P}^{\mathrm{T}} > \mathbf{0}$ of an ARE which is formulated with definitions of σ_0, ζ_0 and ω_0 incorporated within the elements of the weight matrices. The resultant PID controller is thus an optimal controller for (2.19) which guarantees a specified closed-loop response for the nominal plant and is termed *nominal* PID controller in this dissertation.

The methodology presented in [39] then formulates the design of a PID controller (2.44) as an optimal Full State Feedback Controller (FSFC)

$$\mathbf{K} = -\begin{bmatrix} K_i & K_p & K_d \end{bmatrix} \tag{2.46}$$

and if $y(s)$ be output of the plant $G_0(s)$, the state vector of the system (2.19) is first augmented as

$$\mathbf{x}(t) = \begin{bmatrix} \int y(t) & y(t) & \dot{y}(t) \end{bmatrix} \tag{2.47}$$

It is clear that any controller $\mathrm{H}(s)$ defined by (2.44) and designed for $G_0(s)$ does not guarantee the desired placement of closed-loop poles for $G(s,\mathbf{p})$, or optimality of such a controller either. Marsh *et al.* in [42] propose a method to establish a robustness bound for systems with bounded parametric uncertainties, controlled by an optimal FSFC. It is established in [42] that if J_0 be the cost of control when the nominal controller is used with the nominal

system $G_0(s)$ and J be the cost when the same controller is used with the interval system $G(s,\mathbf{p})$, then there exists a scalar bound for robustness μ, such that $J \le \mu J_0$ holds. The method assumes that both the interval plant and the nominal plant are represented in appropriate state-variable form incorporating norm-bounded time-varying parametric uncertainties [42] and the robustness bound μ is computed as a function of this norm. While this ensures that the uncertainties in output response remain bounded under bounded uncertainties in the plant, this methodology does not allow specification of closed-loop pole positions, which is necessary for meeting time response requirements.

In this chapter, the basic LQR approach of PID controller design presented in [39] is extended to an interval plant (2.18). A simple criterion based on interval approach is proposed in this chapter, which ensures that if $H(s)$, designed for nominal plant $G_o(s)$, produces the closed-loop system $G_{c0}(s)$ defined by (2.45), then it produces a closed-loop interval system

$$\left.\begin{aligned} G_c(s,\mathbf{q}) &= \frac{L\left(K_p s + K_i + K_d s^2\right)}{(s+\sigma)\left(s^2 + 2\zeta\omega s + \omega^2\right)} \\ \mathbf{q} &= [L,\ \sigma,\ \zeta,\ \omega] \\ L &\in [\underline{L},\ \overline{L}];\ \sigma \in [\underline{\sigma},\ \overline{\sigma}];\ \zeta \in [\underline{\zeta},\ \overline{\zeta}];\ \omega \in [\underline{\omega},\ \overline{\omega}] \end{aligned}\right\} \qquad (2.48)$$

$H(s)$ still remains an optimal PID controller even when it is used with the interval plant $G(s,\mathbf{p})$. The control cost however changes and it is shown that as in [42], the incremental cost of control can be expressed in terms of uncertainty bounds in $G(s,\mathbf{p})$.

In another alternate approach for robust PID controller design, Khadraoui *et al.* [55] propose a novel method by which intervals $[\underline{K}_p, \overline{K}_p], [\underline{K}_i, \overline{K}_i], [\underline{K}_d, \overline{K}_d]$ for the

proportional, integral and derivative gains of a PID controller can be obtained for an interval plant (2.18) by defining a *reference plant* of the form (2.45) first and then using set inversion. The intervals $\left[\underline{K}_p, \overline{K}_p\right], \left[\underline{K}_i, \overline{K}_i\right], \left[\underline{K}_d, \overline{K}_d\right]$ are such that controllers with gains in these intervals, used in conjunction with an interval plant (2.18) produce closed loop plants whose time and frequency response are *bounded* by those of (2.45) [56]. Though set inversion has exponential complexity, for a low order interval plant e.g. (2.18) this approach seems to be pragmatic. However, the approach by Khadraoui *et al.* is not adopted in this chapter as the approach in [55] provides no control over system input, as opposed to a LQR approach adopted in this chapter with an obvious advantage when applied to control of a PHWR as mentioned before.

The detailed optimal PID controller design methodology for an interval plant is presented in the next section.

2.5 Design of an optimal PID controller for a second order plant with bounded parametric uncertainties

In this section a methodology for design of an optimal PID controller for a second order SISO interval plant (2.18) is presented. He *et al.* in [39] have proposed a methodology by which a PID controller can be designed for a standard second order plant described, for example, by $G_0(s)$ of the form (2.19) using a LQR approach, the basic approach of which has been introduced in the previous section.

Following the methodology presented in [39], it is possible to show that the gains of an optimal PID controller for the plant can be expressed as

$$\begin{bmatrix} K_i & K_p & K_d \end{bmatrix} = \mathbf{R}_0^{-1}\mathbf{B}_0^{\mathrm{T}}\mathbf{P} \tag{2.49}$$

where $\mathbf{P} = \mathbf{P}^{\mathrm{T}} > \mathbf{0}$ is the solution of an ARE

$$\mathbf{A}_0{}^{\mathrm{T}}\mathbf{P} + \mathbf{P}\mathbf{A}_0 - \mathbf{P}\mathbf{B}_0\mathbf{R}_0{}^{-1}\mathbf{B}_0{}^{\mathrm{T}}\mathbf{P} + \mathbf{Q}_0 = \mathbf{0} \tag{2.50}$$

with the cost function defined as

$$J = \frac{1}{2}\int_0^{\infty}\left[\mathbf{x}^{\mathrm{T}}(t)\mathbf{Q}\mathbf{x}(t) + u^{\mathrm{T}}(t)\mathbf{R}u(t)\right]\mathrm{d}t \tag{2.51}$$

The system state vector for (2.19) is assumed to be augmented as

$$\mathbf{x}(t) = \left[\int y(t) \quad y(t) \quad \dot{y}(t)\right] \tag{2.52}$$

and accordingly the matrices $\mathbf{A}_0$, $\mathbf{B}_0$ become

$$\mathbf{A}_0 = \begin{bmatrix} 0 & 1 & 0 \\ 0 & 0 & 1 \\ 0 & -b_0 & -a_0 \end{bmatrix};\ \mathbf{B}_0 = \begin{bmatrix} 0 \\ 0 \\ L_0 \end{bmatrix} \tag{2.53}$$

It has been shown in [39] by He *et al.* that for

$$\mathbf{R}_0 = [r] \tag{2.54}$$

and

$$\mathbf{Q}_0 = \begin{bmatrix} \frac{r}{L_0{}^2}\left[\sigma_0^2\omega_0^4\right] & 0 & 0 \\ 0 & \frac{r}{L_0{}^2}\begin{bmatrix}\left(4\xi_0^2 - 2\right)\sigma_0^2\omega_0^2 \\ +\omega_0^4 - b_0{}^2\end{bmatrix} & 0 \\ 0 & 0 & \frac{r}{L_0{}^2}\begin{bmatrix}\left\{\sigma_0^2 + \left(4\xi_0^2 - 2\right)\omega_0^2\right\} \\ -a_0{}^2 + 2b_0\end{bmatrix} \end{bmatrix} \geq 0 \tag{2.55}$$

the poles of the closed-loop system with the optimal PID controller are at $\left(-\sigma_0, -\xi_0\omega_0 \pm \omega_0\sqrt{1-\xi_0^2}\right)$.

The controller (2.49) is the termed the nominal PID controller in this chapter. It is an optimal controller because the control law $\mathbf{u}(t) = -\begin{bmatrix} K_i & K_p & K_d \end{bmatrix}\mathbf{x}(t)$ minimizes the cost function (2.51). Now if $G_0(s)$ is replaced by an interval plant $G(s,\mathbf{p})$ and the controller (2.49) is used, then the poles of the closed-loop system shall shift and the controller may or may not remain an optimal controller any more. Thus, if a condition can be established, which is sufficient to ensure that the nominal controller (2.49) designed for the nominal plant (2.19) remains an optimal PID controller for the corresponding interval system (2.18) and produces an interval plant (2.48) in closed-loop, then acceptable closed-loop response of the interval plant (2.18) with the nominal PID controller can be guaranteed. The acceptable response is specified by acceptable bounds of the interval variables $[\alpha, \zeta, \omega]$. The implicit assumption is that the plant (2.18) remains controllable over the convex box of $[L, a, b]$. In order to establish the condition, the following Theorem is first put forward.

Theorem 2.5.1: *Let* $\dot{\mathbf{x}}(t) = \mathbf{A}_0\mathbf{x}(t) + \mathbf{B}_0\mathbf{u}(t)$ *be the state space representation of the nominal plant* $G_0(s) = \dfrac{L_0}{s^2 + a_0 s + b_0}$, *and* $\begin{bmatrix} K_i & K_p & K_d \end{bmatrix} = \mathbf{R}_0^{-1}\mathbf{B}_0^{\mathrm{T}}\mathbf{P}$ *be the corresponding nominal PID controller for* $G_0(s)$ *where* $\mathbf{P} = \mathbf{P}^{\mathrm{T}} > 0$ *is the unique solution of the ARE* $\mathbf{A}_0^{\mathrm{T}}\mathbf{P} + \mathbf{P}\mathbf{A}_0 - \mathbf{P}\mathbf{B}_0\mathbf{R}_0^{-1}\mathbf{B}_0^{\mathrm{T}}\mathbf{P} + \mathbf{Q}_0 = 0$ *with the weight matrices defined as* $\mathbf{R}_0 = [r]$ *and*

$$\mathbf{Q}_0 = \begin{bmatrix} \frac{r}{L_0^{\,2}}\left[\sigma_0^2\omega_0^4\right] & 0 & 0 \\ 0 & \frac{r}{L_0^{\,2}}\left[\omega_0^4 + \left(4\xi_0^2 - 2\right)\sigma_0^2\omega_0^2 - b_0^{\,2}\right] & 0 \\ 0 & 0 & \frac{r}{L_0^{\,2}}\left[\left\{\sigma_0^2 + \left(4\xi_0^2 - 2\right)\omega_0^2\right\} - a_0^{\,2} + 2b_0\right] \end{bmatrix} \geq 0$$

where ζ_0, ω_0 *and* σ_0 *are the desired closed-loop damping frequency and position of the real pole. Then the nominal controller remains an optimal PID controller for the corresponding interval system expressed in augmented state-space as* $\dot{\mathbf{x}}(t) = \mathbf{A}\mathbf{x}(t) + \mathbf{B}\mathbf{u}(t)$ *provided there exists an interval matrix*

$$\tilde{\mathbf{Q}} = \begin{bmatrix} \frac{r}{L_0^{\,2}}\left[\sigma_0^2\omega_0^4\right] & 0 & 0 \\ 0 & \begin{matrix}\frac{r}{L_0^{\,2}}\left[\omega_0^4 + \left\{4\xi_0^2 - 2\right\}\sigma_0^2\omega_0^2 - b_0^{\,2}\right] \\ + \frac{2r}{\gamma L_0^2}\left\{\begin{matrix}\left(\omega^2 + 2\zeta\omega\sigma - b\right)\left(\frac{b}{\gamma} - b_0\right) \\ + \sigma\omega^2\left(a_0 - \frac{a}{\gamma}\right)\end{matrix}\right\}\end{matrix} & 0 \\ 0 & 0 & \begin{matrix}\frac{r}{L_0^{\,2}}\left[\begin{matrix}\left\{\sigma_0^2 \\ + \left(4\xi_0^2 - 2\right)\omega_0^2\right\} \\ - a_0^{\,2} + 2b_0\end{matrix}\right] \\ + \frac{2r}{\gamma L_0^2}\left\{\begin{matrix}\left(2\varsigma\omega + \sigma - a\right)\left(\frac{a}{\gamma} - a_0\right) \\ - \left(\frac{1}{\gamma} - 1\right)\left(\omega^2 + 2\zeta\omega\sigma - b\right)\end{matrix}\right\}\end{matrix} \end{bmatrix} \geq 0$$

for same $\mathbf{R}_0$, *where* a, b, L, σ, ζ, *are the interval variables around* a_0, b_0, L_0, σ_0, ζ_0, ω_0 *and* $L = \gamma L_0$.

Proof:

For the plant (2.19) defining the augmented state vector as

$$\mathbf{x}(t) = \begin{bmatrix} \int y(t) & y(t) & \dot{y}(t) \end{bmatrix} \tag{2.56}$$

yields the matrices $\begin{bmatrix} \mathbf{A}_0 & \mathbf{B}_0 \end{bmatrix}$ defined as

$$\mathbf{A}_0 = \begin{bmatrix} 0 & 1 & 0 \\ 0 & 0 & 1 \\ 0 & -b_0 & -a_0 \end{bmatrix};\ \mathbf{B}_0 = \begin{bmatrix} 0 \\ 0 \\ L_0 \end{bmatrix} \tag{2.57}$$

Let the corresponding interval matrices for the interval plant (2.6) be $\mathbf{A} = \mathbf{A}_0 + \Delta\mathbf{A}$ and $\mathbf{B} = \mathbf{B}_0 + \Delta\mathbf{B}$ where

$$\Delta\mathbf{A} = \begin{bmatrix} 0 & 1 & 0 \\ 0 & 0 & 1 \\ 0 & -\Delta b & -\Delta a \end{bmatrix};\ \Delta a \in \left[\Delta\underline{a},\ \Delta\overline{a}\right],\ \Delta b \in \left[\Delta\underline{b},\ \Delta\overline{b}\right] \tag{2.58}$$

$$\Delta\mathbf{B} = \begin{bmatrix} 0 & 0 & (\gamma - 1)L_0 \end{bmatrix}^{\mathrm{T}};\quad \gamma \in \left[\underline{\gamma},\ \overline{\gamma}\right] \tag{2.59}$$

Let $\mathbf{P} = \begin{bmatrix} P_{11} & P_{12} & P_{13} \\ P_{12} & P_{22} & P_{23} \\ P_{13} & P_{23} & P_{33} \end{bmatrix}$ be the solution of the ARE (2.50), then

$$\mathbf{P} = \begin{bmatrix} P_{11} & P_{12} & \dfrac{rK_i}{L_0} \\ P_{12} & P_{22} & \dfrac{rK_p}{L_0} \\ \dfrac{rK_i}{L_0} & \dfrac{rK_p}{L_0} & \dfrac{rK_d}{L_0} \end{bmatrix} \tag{2.60}$$

Now if $\tilde{\mathbf{P}} = \mathbf{P} + \Delta\mathbf{P}$ be the solution of the ARE

$$\mathbf{A}^{\mathrm{T}}\tilde{\mathbf{P}} + \tilde{\mathbf{P}}\mathbf{A} - \tilde{\mathbf{P}}\mathbf{B}\mathbf{R}^{-1}\mathbf{B}^{\mathrm{T}}\tilde{\mathbf{P}} + \tilde{\mathbf{Q}} = 0 \tag{2.61}$$

then in order that the controller for $(\mathbf{A}, \mathbf{B})$ remains the same as that obtained for $(\mathbf{A}_0, \mathbf{B}_0)$

$$\tilde{\mathbf{P}} = \begin{bmatrix} P_{11} + \Delta P_{11} & P_{12} + \Delta P_{12} & \dfrac{rK_i}{\gamma L_0} \\ P_{12} + \Delta P_{12} & P_{22} + \Delta P_{22} & \dfrac{rK_p}{\gamma L_0} \\ \dfrac{rK_i}{\gamma L_0} & \dfrac{rK_p}{\gamma L_0} & \dfrac{rK_d}{\gamma L_0} \end{bmatrix} \tag{2.62}$$

Expanding the ARE (2.61) as

$$\begin{aligned} &(\mathbf{A}_0 + \Delta\mathbf{A})^{\mathrm{T}}(\mathbf{P} + \Delta\mathbf{P}) + (\mathbf{P} + \Delta\mathbf{P})(\mathbf{A}_0 + \Delta\mathbf{A}) \\ &-(\mathbf{P} + \Delta\mathbf{P})(\mathbf{B}_0 + \Delta\mathbf{B})\mathbf{R}_0^{-1}(\mathbf{B}_0 + \Delta\mathbf{B})^{\mathrm{T}}(\mathbf{P} + \Delta\mathbf{P}) + \tilde{\mathbf{Q}} = \mathbf{0} \end{aligned} \tag{2.63}$$

and solving yields a diagonal matrix $\tilde{\mathbf{Q}}$ and the corresponding matrix $\tilde{\mathbf{P}} = \tilde{\mathbf{P}}^{\mathrm{T}}$ that satisfies (2.63) defined as

$$\tilde{\mathbf{Q}} = \begin{bmatrix} \dfrac{r}{L_0^{\,2}}\left[\sigma_0^2\omega_0^4\right] & 0 & 0 \\ 0 & \begin{array}{l}\dfrac{r}{L_0^{\,2}}\left[\omega_0^4 + \left(4\xi_0^2 - 2\right)\sigma_0^2\omega_0^2 - b_0^{\,2}\right] \\ +2\left\{\dfrac{bP_{23}}{\gamma} - b_0P_{23} + a_0P_{13} - \dfrac{aP_{13}}{\gamma}\right\}\end{array} & 0 \\ 0 & 0 & \begin{array}{l}\dfrac{r}{L_0^{\,2}}\left[\left\{\sigma_0^2 + (4\xi_0^2 - 2)\omega_0^2\right\} - a_0^{\,2} + 2b_0\right] \\ +2\left\{\dfrac{aP_{33}}{\gamma} - a_0P_{33} - P_{23}\left(\dfrac{1}{\gamma} - 1\right)\right\}\end{array} \end{bmatrix} \tag{2.64}$$

and

$$\tilde{\mathbf{P}} = \begin{bmatrix} P_{11} + b\frac{P_{13}}{\gamma} - b_0 P_{13} & P_{12} + a\frac{P_{13}}{\gamma} - a_0 P_{13} & \frac{P_{13}}{\gamma} \\ P_{12} + a\frac{P_{13}}{\gamma} - a_0 P_{13} & P_{22} + a\frac{P_{23}}{\gamma} - a_0 P_{23} - P_{13}\left(\frac{1}{\gamma} - 1\right) + b\frac{P_{33}}{\gamma} - b_0 P_{33} & \frac{P_{23}}{\gamma} \\ \frac{P_{13}}{\gamma} & \frac{P_{23}}{\gamma} & \frac{P_{33}}{\gamma} \end{bmatrix} \tag{2.65}$$

Since the interval system $(\mathbf{A}, \mathbf{B})$ remains controllable, and $\mathbf{R}_0 = r > 0$, the condition $\tilde{\mathbf{Q}} \geq 0$ over the convex box of $[L, a, \sigma, \zeta, \omega]$ is sufficient to ensure [56] that the ARE (2.61) shall be satisfied only by an interval matrix $\tilde{\mathbf{P}} = \tilde{\mathbf{P}}^{\mathrm{T}} \geq \mathbf{0}$. This implies that $\begin{bmatrix} K_i & K_p & K_d \end{bmatrix} = \mathbf{R}_0^{-1}\mathbf{B}^{\mathrm{T}}\tilde{\mathbf{P}}$ yields an invariable set of controller gains $\begin{bmatrix} K_i & K_p & K_d \end{bmatrix}$ with the substitution $\mathbf{B} = \gamma\mathbf{L}$. □

Again, for a second order system $G(s, \mathbf{p})$ represented (2.19) and controlled by a PID controller (2.49), the following set of equations hold

$$\left.\begin{aligned} K_i &= \frac{\sigma\omega^2}{L} \\ K_p &= \frac{\left(\omega^2 + 2\zeta\sigma\omega\right) - b}{L} \\ K_d &= \frac{\left(2\zeta\omega + \sigma\right) - a}{L} \end{aligned}\right\} \tag{2.66}$$

Substituting these values in the expression for $\tilde{\mathbf{Q}}$ in (2.64) produces

$$\tilde{\mathbf{Q}} = \begin{bmatrix} \frac{r}{L_0^{\,2}}\left[\sigma_0^2\omega_0^4\right] & 0 & 0 \\ 0 & \begin{matrix}\frac{r}{L_0^{\,2}}[\omega_0^4+\left[4\xi_0^2-2\right]\sigma_0^2\omega_0^2-b_0^{\,2}] \\ +\frac{2r}{\gamma L_0^2}\{(\omega^2+2\zeta\omega\sigma-b)\left(\frac{b}{\gamma}-b_0\right) \\ +\sigma\omega^2\left(a_0-\frac{a}{\gamma}\right)\}\end{matrix} & 0 \\ 0 & 0 & \begin{matrix}\frac{r}{L_0^{\,2}}[\left\{\sigma_0^2+(4\xi_0^2-2)\omega_0^2\right\}-a_0^{\,2}+2b_0] \\ +\frac{2r}{\gamma L_0^2}\{(2\zeta\omega+\sigma-a)\left(\frac{a}{\gamma}-a_0\right) \\ -\left(\frac{1}{\gamma}-1\right)(\omega^2+2\zeta\omega\sigma-b)\}\end{matrix} \end{bmatrix} \tag{2.67}$$

It follows from Theorem 2.5.1 and (2.67) that the nominal PID controller (2.49) designed for a nominal plant $G_o(s)$ (2.19) remains an optimal controller for the interval plant $G(s, \mathbf{p})$ (2.18) and it produces a closed-loop system $G_c(s, \mathbf{q})$ defined by (2.48) with poles in regions of the complex plane specified by $[\alpha, \zeta, \omega]$ if the condition $\tilde{\mathbf{Q}} \geq 0$ is satisfied over the convex box of $[L, a, b, \sigma, \zeta, \omega]$.

The positive semi-definiteness of the matrix $\tilde{\mathbf{Q}}$ over the entire convex box of $[L, a, b, \sigma, \zeta, \omega]$ can be tested using the results presented in [50]. It has been established in [50] that for a symmetric interval matrix such as $\tilde{\mathbf{Q}}$, if

$$\tilde{\mathbf{Q}}_c = \frac{1}{2}\left(\underline{\tilde{\mathbf{Q}}} + \overline{\tilde{\mathbf{Q}}}\right) \tag{2.68}$$

and

$$\tilde{\mathbf{Q}}^{\Delta} = \frac{1}{2}\left(\bar{\tilde{\mathbf{Q}}} - \underline{\tilde{\mathbf{Q}}}\right) \tag{2.69}$$

then $\tilde{\mathbf{Q}}$ is positive semi-definite for the entire interval $\left[\underline{\tilde{\mathbf{Q}}}, \bar{\tilde{\mathbf{Q}}}\right]$ if

$$\lambda_{\min}\left(\tilde{\mathbf{Q}}_c\right) \geq \rho\left(\tilde{\mathbf{Q}}^{\Delta}\right) \tag{2.70}$$

For a given $\tilde{\mathbf{Q}}$ the matrices $\underline{\tilde{\mathbf{Q}}}$ and $\bar{\tilde{\mathbf{Q}}}$ are computed using the functions $inf\left(\tilde{\mathbf{Q}}\right)$ and $sup\left(\tilde{\mathbf{Q}}\right)$ respectively included in INTLAB using (2.67).

If the initial state for both nominal system $\left(\mathbf{A}_0, \mathbf{B}_0\right)$ and the interval system $\left(\mathbf{A}, \mathbf{B}\right)$ be $\mathbf{x}(0)$, then the incremental cost of control when the nominal PID controller is used to control the interval plant is

$$\Delta J = \mathbf{x}^{\mathrm{T}}(0)\Delta\mathbf{P}\mathbf{x}(0) \tag{2.71}$$

where

$$\Delta\mathbf{P} = \begin{bmatrix} rK_i\left(\frac{b}{L} - \frac{b_0}{L_0}\right) & rK_i\left(\frac{a}{L} - \frac{a_0}{L_0}\right) & rK_i\left(\frac{1}{L} - \frac{1}{L_0}\right) \\ rK_i\left(\frac{a}{L} - \frac{a_0}{L_0}\right) & rK_p\left(\frac{a}{L} - \frac{a_0}{L_0}\right) + rK_d\left(\frac{b}{L} - \frac{b_0}{L_0}\right) - rK_i\left(\frac{1}{L} - \frac{1}{L_0}\right) & rK_p\left(\frac{1}{L} - \frac{1}{L_0}\right) \\ rK_i\left(\frac{1}{L} - \frac{1}{L_0}\right) & rK_p\left(\frac{1}{L} - \frac{1}{L_0}\right) & rK_d\left(\frac{1}{L} - \frac{1}{L_0}\right) \end{bmatrix} \tag{2.72}$$

As in [42] it is seen that the incremental cost is bounded and the bound can be expressed as a function of the bound of parametric uncertainties.

Thus the steps involved in controller design, therefore are as follows:

Step1: For a given nominal plant (2.19) obtains the augmented state system $(\mathbf{A}_0, \mathbf{B}_0)$, choose the position of the closed-loop real pole $-\sigma_0$, closed-loop damping ζ_0 and closed-loop frequency ω_0 and value of scalar r to obtain of the matrix $\mathbf{Q}_0$ using equation (2.55).

Step2: Obtain the nominal PID controller $\begin{bmatrix} K_i & K_p & K_d \end{bmatrix}$ for $(\mathbf{A}_0, \mathbf{B}_0, \mathbf{Q}_0, \mathbf{R}_0)$ and the value of the $\mathbf{P}$ by solving the ARE (2.50).

Step3: Set suitable intervals $[\underline{\sigma}, \bar{\sigma}]$, $[\underline{\zeta}, \bar{\zeta}]$, $[\underline{\omega}, \bar{\omega}]$ and check if (2.70) holds for the entire convex box of $[L, a, \sigma, \zeta, \omega]$. If this is satisfied, then the controller $\begin{bmatrix} K_i & K_p & K_d \end{bmatrix}$ obtained in *Step1* is the desired controller, else modify $r, \sigma_0, \zeta_0, \omega_0$ and/or the intervals $[\underline{\sigma}, \bar{\sigma}]$, $[\underline{\zeta}, \bar{\zeta}]$, $[\underline{\omega}, \bar{\omega}]$ and go to *Step1*

The methodology presented in this sub-section is used to design robust PID controllers for each zone of the ZCC of a PHWR. The corresponding simulation results accompanied by thorough discussions are presented in *Chapter 4.*

This page is intentionally left blank

Chapter 3

Stability, Control and Operation of 700MWe PHWR

3.1. Introduction

Research during the last few decades has shown that it might be possible to extract more power from the core of a 540MWe PHWR by altering the thermal-hydraulic parameters of the reactor and this has resulted in a new variant viz. the 700MWe PHWRs. In this Chapter, it is attempted to analyze the open-loop behavior of a 700MWe PHWR based on the data available from available literature [12] and apply interval methodology presented in *Chapter 2* with relevant augmentation to design a single robust controller that capable of controlling the reactor under power maneuvering even in presence of limited core voiding. At the same time, the controller needs to be optimal, so as to satisfy the reactivity constraints. As a major challenge for operation and control engineers to run a 700MWe PHWR at 100%FP is to tackle the fuel burn-up which may exceed the limit of fuel-to-coolant heat flux ratio. Therefore, the coolant, in such a situation, will extract more heat from the fuel channel which may ultimately lead to the occurrence of boiling in the coolant channel. Such a circumstance of boiling in coolant transport channel is also known as *voiding*, which leads to instability of the reactor system due to a positive reactivity defect. To run a 700MWe PHWR at 100%FP, a limited voiding of up to 3%

has been considered in the design of 700MWe Indian PHWR [12]. A limited voiding under nucleate voiding condition ensures better cooling of fuel element due to substantial enhancement of heat transfer coefficient [56], owing to phase change. It is also a well-known fact that voiding in a coolant channel introduces a positive reactivity in the reactor [57] and in case of full core voiding; the estimated reactivity introduced is 6.8mk for an Indian PHWR. However, this reactivity introduction margin will vary from reactor-to-reactor. Modeling of void fraction in transient time as a function of reactor power is also a significant contribution of this dissertation, presented in detail in this chapter.

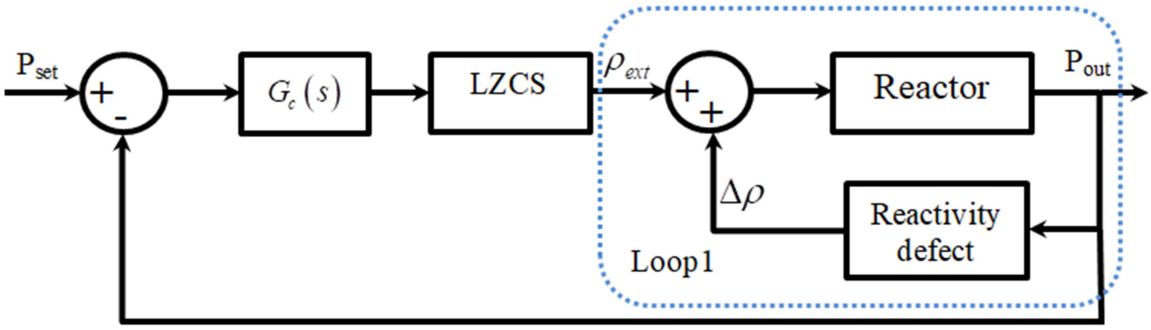

Fig. 3.1 Schematic diagram of power control of PHWR

The general schematic of power control is presented in Fig. 3.1. The inner loop in Fig. 3.1 consists of a block relating reactor power to net reactivity $(\rho_{net}$ in mk$)$ input where $\rho_{net} = \rho_{ext} + \Delta\rho$ and $\Delta\rho$ is the reactivity defect expressible as

$$\Delta\rho = \alpha_f \left(T_f - T_{f_{ss}}\right) + \alpha_c \left(T_c - T_{c_{ss}}\right) + \alpha_v \delta_v \qquad (3.1)$$

where δ_v denotes the void fraction, T_f and T_c are the fuel and average coolant temperatures while α_v, α_f and α_c represent the reactivity coefficients for the void , fuel temperature and

coolant temperatures respectively. In (3.1), ρ_{ext} is the external reactivity induced into the core by the LZCS and movements of the control rod banks.

Since $\Delta\rho$ changes with reactor power, it is clear that the inner loop transfer function changes and it can be expressed as an interval system as.

$$\left.\begin{aligned} &G(s,\mathbf{p}) = \frac{L}{s^2 + as + b} \\ &\mathbf{p} = [L,\ a,\ b] \\ &L \in [\underline{L},\ \overline{L}];\ a \in [\underline{a},\ \overline{a}];\ b \in [\underline{b},\ \overline{b}] \end{aligned}\right\} \tag{3.2}$$

However, since α_v has a sign opposite to that of α_c and α_f, with voiding, the rate of change of $\Delta\rho$ with power, changes. For a 700MWe Indian PHWR considered here, voiding in coolant channel begins at around 92.3%FP. Therefore, up-to 92.3%FP, the variation of ρ_{net} with power, is polytopic in nature. Above 92.3%FP, as soon as the voiding starts, the variation of with power is no longer polytopic as the void coefficient starts introducing positive reactivity in the core as opposed to fuel and coolant coefficients. The system defined in (3.2) considers the internal reactivity defects and therefore after 92.3%FP variation, the parametric variation of the system also does not remain polytopic. As seen from (3.1) the positive α_v introduces a positive reactivity once voiding starts, reducing the net reactivity defect and this implies lesser resistance to a power change. This means that a controller designed with nominal conditions is likely to produce a larger rate of rise of reactor power and power overshoot once voiding starts. It is therefore clear that an optimal PID controller designed by the methodology presented in *Chapter 2* where the nominal system corresponds to about 80%FP cannot produce satisfactory results when applied to a 700MWe PHWR as the methodology does not consider voiding.

Thus, if the controller design methodology prescribed in *Chapter 2* is extended to achieve satisfactory control of a 700MWe PHWR with reactor power varying between say [60%FP, 100%FP], voiding poses a major hurdle as the variation of parameter with reactor power is no longer polytopic. One way of limiting the voiding in coolant channel is by altering the coolant flow rate but as per the industry standard, this is not very advisable thing to do as it may lead to flow instability [58]. Therefore the only way to control voiding in the coolant channel is by altering the pressure of the pressurizer in Primary Heat Transport (PHT) system. This could mean a variation in the channel pressure by using the pressurizer. In this chapter the interval approach presented in *Chapter 2* for a 540MWe PHWR is extended for controlling a 700MWe PHWR between in the interval [60%FP, 100%FP] by varying the pressurizer pressure in a tight interval [9.8MPa, 10MPa]. The pressurizer is operated at 9.8MPa before voiding but as soon as the voiding starts, the pressurizer pressure is ramped up to 10MPa using the controller presented in this chapter. Therefore, the objective here is to accomplish pressurizer pressure control by optimally controlling the spray flow and heating element of the pressurizer.

3.2. Modeling of Void Fraction in Transient time for 700MWe PHWR

As discussed earlier, voiding in a coolant channel leads to the occurrence of a two-phase flow in the coolant channel. The mixture of vapor and coolant i.e., two phase flow in a nuclear reactor poses a difficult challenge in the safe and optimal operation of the plant. Generation and transport of discrete bubbles in the coolant channels cause fluctuation in the local steam content. These fluctuations in steam content affect the moderator density and hence the nuclear parameters, which in turn induce variations in the local neutron flux [59]. Therefore the net reactivity is changed. Many contemporary researchers have established the characteristic of

voiding and attempted to estimate the void fraction in two phase flow in the coolant channels [43], [60]. Lu has proposed an analytical method of the two phase flow for a Boiling Water Reactors using neutron noise analysis [43]. Ramajo *et al*. has discussed the two phase modeling of a large PHWR by finite volume method [44], however, in both cases it is difficult for a control engineer to choose a proper control strategy as these estimations are computationally intensive. Moreover, these methods do not provide any information in the transient time, i.e. during power maneuvering. Literature survey [43], [44] reveals that the operational analysis of a nuclear power plant in transient time during the occurrence of voiding in a coolant channel is limited. Also, majority of the existing literature related to void analysis, does not provide void modeling in the transient time though this is an important analysis that is required to be carried out for large modular PHWRs and is essential for design of controllers. Motivated by the need to bridge this gap, this section puts forward the details of void fraction modeling in transient time.

The void fraction (δ_v) could be defined as [61]

$$\delta_v = \frac{1}{1+\frac{\rho_v}{\rho_l} S \frac{1-x}{x}} \tag{3.3}$$

where, the subscripts v and l indicate the vapor and liquid phase respectively, symbol ρ represents density, S represents slip ratio and x represents flow quality. Slip ratio (S) of two-phase flow can be defined as

$$S = \frac{u_v}{u_l} \tag{3.4}$$

where, u_v is the velocity of the vapor and u_l is the velocity of the liquid in the coolant channel. Flow quality (x) may be defined as:

$$x = \frac{\dot{m}_v}{\dot{m}_v + \dot{m}_l} \tag{3.5}$$

where $\dot{m}$ is the mass flow rate of coolant channel in kg/sec. It is well known that the mass flow rate may be defined as the product of velocity (u) in m/sec, density of coolant (ρ) in kg/m^3 and active heat transfer area (A) in m^2. Therefore (3.3) can be rewritten as:

$$x = \frac{u_v A_v \rho_v}{u_v A_v \rho_v + u_l A_l \rho_l} \tag{3.6}$$

It is evident that the void fraction depends upon coolant temperature and hence the reactor power. So from the energy balance equation it could be written as:

$$\frac{d}{dt}(V\rho e) = \dot{q}l + \dot{m}h_i - \dot{m}h_o \tag{3.7}$$

where $\dot{q}$ is the linear heat rate in watt/m, l is the total length of coolant channel in m, h_i and h_o are the input and output enthalpy of the coolant channel in J/kg, V is the volume of coolant in m^3 and e is the specific internal energy in J/kg. The product of linear heat rate and length of the coolant channel represents the power level (P) of the reactor and thus (3.7) may be modified as

$$\frac{d}{dt}(V\rho e) = P + \dot{m}h_i - \dot{m}h_o \tag{3.8}$$

Also specific enthalpy (h) may be defined as:

$$h = e + \frac{p}{\rho} \tag{3.9}$$

where p pressure of coolant in the coolant channel in MPa. With the consideration that the coolant volume (V) in the coolant channel remains constant and putting (3.9) in (3.8), the following may be obtained:

$$V\left\{\left(h-\frac{p}{\rho}\right)\frac{d\rho}{dt}+\rho\frac{dh}{dt}-\rho\frac{d}{dt}\left(\frac{p}{\rho}\right)\right\}=P+\dot{m}h_i-\dot{m}h_o \tag{3.10}$$

Expanding (3.10), yields

$$V\left\{h\frac{d\rho}{dt}-\frac{p}{\rho}\frac{d\rho}{dt}+\rho\frac{dh}{dt}-\frac{dp}{dt}+\frac{p}{\rho}\frac{d\rho}{dt}\right\}=P+\dot{m}h_i-\dot{m}h_o \tag{3.11}$$

Now, considering constant pressure of coolant in the coolant channel, (3.11) may be re-written as

$$V\left\{h\frac{d\rho}{dt}+\rho\frac{dh}{dt}\right\}=P+\dot{m}h_i-\dot{m}h_o \tag{3.12}$$

The reason behind neglecting $\frac{dp}{dt}$ in (3.12) has been demonstrated in detail in Appendix II. The relation between (δ_v) and (ρ) may be expressed as

$$\rho=\rho_l\delta_v+(1-\delta_v)\rho_v \tag{3.13}$$

where, ρ_l and ρ_v are density of liquid and vapor respectively in two-phase flow. Here total specific enthalpy (h) is the average of input and output enthalpy and can be expressed as:

$$h=\frac{h_i+h_o}{2} \tag{3.14}$$

Similarly, the relation between total specific enthalpy (h) and quality can be represented as

$$h=h_l+x(h_v-h_l) \tag{3.15}$$

where h_l and h_v are the corresponding specific enthalpies of liquid and vapor of a two-phase flow. Substituting (3.13), (3.14) and (3.15) in (3.12) yields

$$V\begin{bmatrix}(h_l+xh_{lv})\left(-\rho_l\frac{d\delta_v}{dt}+\rho_v\frac{d\delta_v}{dt}\right)\\+\left\{\rho_l\delta_v+(1-\delta_v)\rho_v\right\}\left(-h_l\frac{dx}{dt}+h_v\frac{dx}{dt}\right)\end{bmatrix}=P+\dot{m}h_i-\dot{m}\left[2(h_l+xh_{lv})-h_i\right] \tag{3.16}$$

where

$$h_{lv} = h_v - h_l \tag{3.17}$$

The relation between (x) and (δ_v) may be represented as:

$$x = \frac{\delta_v u_v \rho_v}{\delta_v u_v \rho_v + (1-\delta_v) u_l \rho_l} \tag{3.18}$$

Substituting (3.18) in (3.16) yields

$$V\begin{bmatrix} (h_l + x h_{lv})(\rho_v - \rho_l)\dfrac{d\delta_v}{dt} \\ +\left\{\rho_l \delta_v + (1-\delta_v)\rho_v\right\} h_{lv} \dfrac{d}{dt} \\ \left\{\dfrac{\delta_v u_v \rho_v}{\delta_v u_v \rho_v + (1-\delta_v) u_l \rho_l}\right\} \end{bmatrix} = \begin{bmatrix} P + 2\dot{m} h_i \\ -2\dot{m} h_l - 2\dot{m} h_{lv} \end{bmatrix} \left\{\frac{\delta_v u_v \rho_v}{\delta_v u_v \rho_v + (1-\delta_v) u_l \rho_l}\right\} \tag{3.19}$$

Equation (3.19) has been modified to be represented as:

$$V\begin{bmatrix} \left(h_l + \dfrac{\delta_v u_v \rho_v h_{lv}}{\delta_v u_v \rho_v + (1-\delta_v) u_l \rho_l}\right)(\rho_v - \rho_l)\dfrac{d\delta_v}{dt} \\ +\left\{\left[\rho_l \delta_v + (1-\delta_v)\rho_v\right] h_{lv}\right\} \times \\ \left\{\dfrac{\left\{\delta_v u_v \rho_v + (1-\delta_v) u_l \rho_l\right\}\left\{u_v \rho_v \dfrac{d\delta_v}{dt} - \delta_v u_v \rho_v \left(u_v \rho_v \dfrac{d\delta_v}{dt} - u_l \rho_l \dfrac{d\delta_v}{dt}\right)\right\}}{\left(\delta_v u_v \rho_v + (1-\delta_v) u_l \rho_l\right)^2}\right\} \end{bmatrix} \tag{3.20}$$

$$= P + 2\dot{m} h_i - 2\dot{m} h_l - 2\dot{m} h_{lv} \left\{\frac{\delta_v u_v \rho_v}{\delta_v u_v \rho_v + (1-\delta_v) u_l \rho_l}\right\}$$

From (3.20) the rate of change of void fraction $\dfrac{d\delta_v}{dt}$ can be obtained as

$$\frac{d\delta_v}{dt}=\frac{\left[\left(P+2\dot{m}h_i-2\dot{m}h_l\right)\left\{\delta_v\left(u_v\rho_v-u_l\rho_l\right)+V\rho_l\right\}-\delta_v\dot{m}h_{lv}u_v\rho_v\right]}{\left[\frac{\left\{\rho_l\delta_v+\left(1-\delta_v\right)\rho_v\right\}h_l}{\delta_v u_v\rho_v+\left(1-\delta_v\right)u_l\rho_l}\right]\left[\begin{array}{l}\delta_v{}^2\left\{\begin{array}{l}\left(u_v\rho_v\right)^2u_l\rho_l-\left(u_l\rho_l\right)^2\\u_v\rho_v-\left(u_v\rho_v\right)^3\end{array}\right\}\\+\delta_v\left\{\begin{array}{l}\left(u_v\rho_v\right)^2+u_v\rho_v\left(u_l\rho_l\right)^2-\\\left(u_l\rho_l\right)\left(u_v\rho_v\right)^2-u_l\rho_lu_v\rho_v\end{array}\right\}\\+u_l\rho_lu_v\rho_v\end{array}\right]} \tag{3.21}$$

From (3.21) it is evident that the change of void fraction is directly proportional to the change of reactor power level. The complete thermal hydraulic and neutronic model of PHWR is assumed to be same as (2.18)-(2.25) and the analysis presented in this section is used to estimate the void fraction as power is changed.

3.3. Modeling of Pressurizer for 700MWe PHWR

The PHT system of a 540MWe PHWR consists of primary coolant loops along with Primary Coolant Pump (PCP), pumping primary coolant into the reactor core [10]. The PHT system of a 540MWe PHWR is fitted with a pressurizer to keep the PHT pressure constant [10]. PHT pressure control in such reactors essentially employs a Feed and Bleed Control Mechanism [10]. A schematic is shown in Fig. 3.2. For a 540MWe PHWR PCPs help to maintain the pressure of the PHT at a steady state operating level of 9MPa and hence additionally activating the pressurizer is not required. However, for a 700MWe PHWR, where the range of coolant saturation temperature is higher and scope of voiding exists in full load condition, additional activation and control of the pressurizer is necessary. This section therefore puts forward the details of pressurizer modeling for a 700MWe PHWR. The methodology presented in this sub-section is adopted from Xu *et al.* [62].

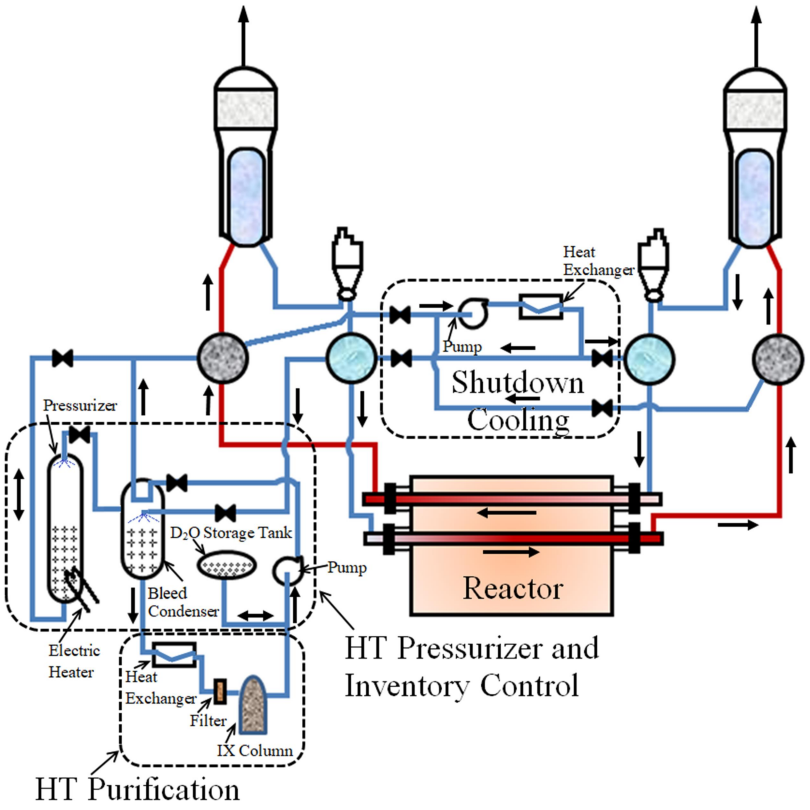

Fig. 3.2 Schematic model of PHWR with primary coolant and pressurizer [10]

The pressurizer is a subsystem of the PHT that is attached to the primary coolant channel. It is a sealed, vertical cylinder whose top and bottom sides are elliptical in nature as shown in Fig. 3.3.

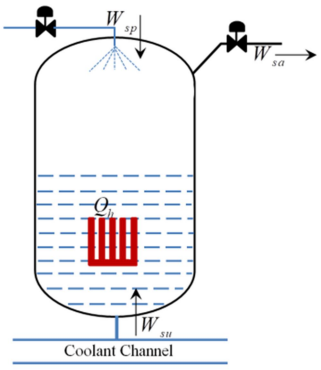

Fig. 3.3 Schematic diagram of pressurizer [63]

Out of the various components, the three main components of a pressurizer are--an electric heater, a spray valve and a pressure relief valve. The electric heater heats the water inside the pressurizer with a power output Q_h (in KW). Therefore, an increase in electrical heater power increases the enthalpy of water at saturation pressure. This leads to more steam production inside the circuit thus increasing the pressure output. On the contrary, the spray valve opening introduces jet of water droplets into the pressurizer which condenses the steam resulting in rapid drop of output pressure. Therefore, the output pressure P_R (in MPa) of the pressurizer can be maintained at a particular saturation point by the co-ordinated control of electrical heater power Q_h and mass flow-rate of water droplet jet through the spray valve W_{sp} (in kg/s). The accumulation of excessive pressure inside the pressurizer cylinder results in the opening of the safety relief valve which bleeds out the excess pressure restoring balance of the operation inside the pressurizer. The mass flow-rate of the safety valve flow is denoted as W_{sa} (in kg/s). Thus, the control of output pressure of pressurizer is an important and complex task for the control system engineer. Xu *et al.* has established a pressure equation at saturation pressure level in [62]. The three conservation equations have been obtained from Double-District Equilibrium model and can be represented as follows:

The equation for conservation of mass can be represented as:

$$\frac{dm_{P_R l}}{dt} + \frac{dm_{P_R v}}{dt} = W_{sp} + W_{su} - W_{sa} \tag{3.22}$$

where, $m_{P_R l}$ and $m_{P_R g}$ represents mass of coolant and mass of steam of the pressurizer (in kg) respectively and W_{su} is the surge flow (in kg/sec) of the coolant into the pressurizer.

The equation for energy conservation can be represented as:

$$m_{P_Rl}\frac{dh_{P_Rl}}{dt}+m_{P_Rv}\frac{dh_{P_Rv}}{dt}+h_{P_Rl}\frac{dm_{P_Rl}}{dt}+h_{P_Rv}\frac{dm_{P_Rv}}{dt}-V_{P_R}\frac{dP_R}{dt}=W_{su}h_{P_Rl}+W_{sp}h_{P_Rx1}-W_{sa}h_{P_Rv}+Q_h \quad (3.23)$$

where h_{P_Rl}, h_{P_Rv}, h_{P_Rx1} represents the specific enthalpy of saturated water, saturated steam and fluctuation water in kJ/kg, respectively and V_{P_R} represents the total volume of pressurizer in m^3.

The equation for conservation of volume can be represented as:

$$m_{P_Rl}\frac{dv_{P_Rl}}{dt}+m_{P_Rg}\frac{dv_{P_Rv}}{dt}+v_{P_Rl}\frac{dm_{P_Rl}}{dt}+v_{P_Rv}\frac{dm_{P_Rv}}{dt}=0 \quad (3.24)$$

where v_{P_Rl} and v_{P_Rv} represents the specific volume in m^3/kg of the water and steam inside the pressurizer tube respectively.

Now (3.22) can be re-written as

$$\frac{dm_{P_Rl}}{dt}=W_{sp}+W_{su}-W_{sa}-\frac{dm_{P_Rv}}{dt} \quad (3.25)$$

Again (3.23) can be expressed as

$$M_{P_Rh}\frac{dP_R}{dt}+h_{P_Rl}\frac{dm_{P_Rl}}{dt}+h_{P_Rv}\frac{dm_{P_Rv}}{dt}=W_{su}h_{P_Rl}+W_{sp}h_{P_Rx1}-W_{sa}h_{P_Rv}+Q_h \quad (3.26)$$

where,

$$M_{P_Rh}=m_{P_Rl}\frac{dh_{P_Rl}}{dP_R}+m_{P_Rv}\frac{dh_{P_Rv}}{dP_R}-V_{P_R} \quad (3.27)$$

and (3.24) can be expressed as:

$$M_{P_Rv}\frac{dP_R}{dt}+v_{P_Rl}\frac{dm_{P_Rl}}{dt}+v_{P_Rv}\frac{dm_{P_Rv}}{dt}=0 \quad (3.28)$$

where,

$$M_{P_Rv}=m_{P_Rl}\frac{dv_{P_Rl}}{dP_R}+m_{P_Rv}\frac{dv_{P_Rv}}{dP_R} \quad (3.29)$$

Substituting (3.25) in (3.26) ultimately yields

$$M_{P_R h}\frac{dP_R}{dt}+h_{P_R \mathrm{lv}}\frac{dm_{P_R v}}{dt}=W_{sp}h_{P_R x1}-\left(W_{sp}-W_{sa}\right)h_{P_R l}+W_{su}h_{P_R v}+Q_h \tag{3.30}$$

where,

$$h_{P_R \mathrm{lv}}=h_{P_R v}-h_{P_R l} \tag{3.31}$$

Again substituting (3.25) in (3.28) ultimately yields

$$M_{P_R v}\frac{dP_R}{dt}+v_{P_R lv}\frac{dm_{P_R v}}{dt}=-\left(W_{su}+W_{sp}-W_{sa}\right)v_{P_R l} \tag{3.32}$$

where,

$$v_{P_R \mathrm{lv}}=v_{P_R v}-v_{P_R l} \tag{3.33}$$

From (3.30) and (3.32), the final expression for the rate of change of pressure can be obtained as:

$$\frac{dP_R}{dt}=\frac{\left\{W_{su}\left[v_{P_R lv}\left(h_{P_R x1}-h_{P_R l}\right)+h_{P_R lv}v_{P_R l}\right]-W_{sp}\left[v_{P_R lv}\left(h_{P_R v}+h_{P_R l}\right)+h_{P_R lv}v_{P_R lv}\right]+W_{su}h_{P_R lv}v_{P_R l}+v_{P_R lv}Q_h\right\}}{\left(v_{P_R lv}M_h-h_{P_R lv}M_v\right)} \tag{3.34}$$

From (3.34) it is evident that $\frac{dP_R}{dt}$ increases with increase in Q_h and decreases with increase in W_{sp}. Equation (3.34) has been modeled in MATLAB Simulink for simulating the pressurizer dynamics. For simulating the pressurizer model along with the reactor model, (3.34) has been considered and the piece-wise variation of various reactor's thermal hydraulics parameters occurring due to the variation of pressurizer pressure, are listed below in Table 3.1.

Table 3.1

Variation of Thermal Hydraulics Parameters of Reactor with Variation of Pressure

P_R (MPa)	v_l (m^3/kg)	v_v (m^3/kg)	h_l (kJ/kg.^{0}C)	h_v (kJ/kg.^{0}C)	T_{co} (^{0}C)
9.8	0.0014456	0.0184844	1399.39	2729.12	309.516
9.82	0.00144629	0.0184382	1400.26	2728.76	309.665
9.84	0.00144699	0.0183921	1401.13	2728.4	309.814
9.86	0.00144769	0.0183463	1402	2728.04	309.962
9.88	0.00144839	0.0183006	1402.87	2728.68	310.111
9.9	0.00144909	0.0182551	1403.73	2727.31	310.259
9.92	0.00144979	0.0182097	1404.6	2726.95	310.407
9.94	0.00145049	0.0181645	1405.05	2726.59	310.555
9.96	0.00145119	0.0181195	1406.3	2726.22	310.703
9.98	0.00145189	0.0180747	1407.2	2725.86	310.85
10	0.00145259	0.01803	1408.6	2725.49	310.997

Using MATLAB System Identification Toolbox [64] [65], two transfer functions have been identified- one considering pressure as output and electric heater power as input and another considering pressure as output and spray flow-rate as input [66]. Both the transfer functions are integrating systems with reverse open loop gains and may be written as

$$\left.\begin{aligned} G_{P_R 1}(s) &= \frac{\triangle P_R}{\triangle Q_h} = \frac{k_{P_R 1}}{s} \\ G_{P_R 2}(s) &= \frac{\triangle P_R}{\triangle W_{sp}} = \frac{-k_{P_R 2}}{s} \end{aligned}\right\} \tag{3.35}$$

This matches with the result presented in [66].

Next, it is attempted to design a control scheme for control of the pressurizer using the transfer function represented by (3.35). The control scheme adopted in this chapter is similar to that proposed in [66] and represented by Fig. 3.4, where $G_{c1}(s)$ represents the controller transfer function associated with controller for the electric heater and $G_{c2}(s)$ represents the controller associated with control of spray flow. Both the gains k_{P_R1} and k_{P_R2} relate the changes in process variables Q_h and W_{sp} to change in a pressure reference P_{Rref}. The pressure reference is assumed to be ramped at a fixed pre-determined rate and the both $G_{c1}(s)$ and $G_{c2}(s)$ are PI controllers even though the plants $G_{c1}(s)$ and $G_{c2}(s)$ are both integrator plants. This ensures tracking with a ramped reference.

Optimized control of pressurizer by modulating the heating and spray flow is a challenging problem for a Multiple Input Single Output (MISO) plant representing a pressurizer as shown in Fig. 3.4. While optimal PI controller design, using the standard LQR approach, for example, has been attempted by some contemporary researchers e.g. [39], the methodology works for a Multiple Input Multiple Output (MIMO) plants with equal number of inputs and outputs i.e. for a balanced system. Schroeck *et al.* in [67] has presented controller design methodology for a MISO plant by reducing it into two individual Single Input Single Output (SISO) loops. In another work [68], quantitative feedback theory has been used for designing controllers for a MISO system. However, in both these cases, the designed controllers do not guarantee optimality. The present case mandates the design of an optimal controllers for a MISO system and this optimization has been performed using a GA. GA is an well-established robust technique that can solve complex optimization problems and produce a globally optimal solution when applied to various multi-modal problems [69], and this has been applied to the present

problem which has been formulated as an optimization problem in a continuous search space of controller gains.

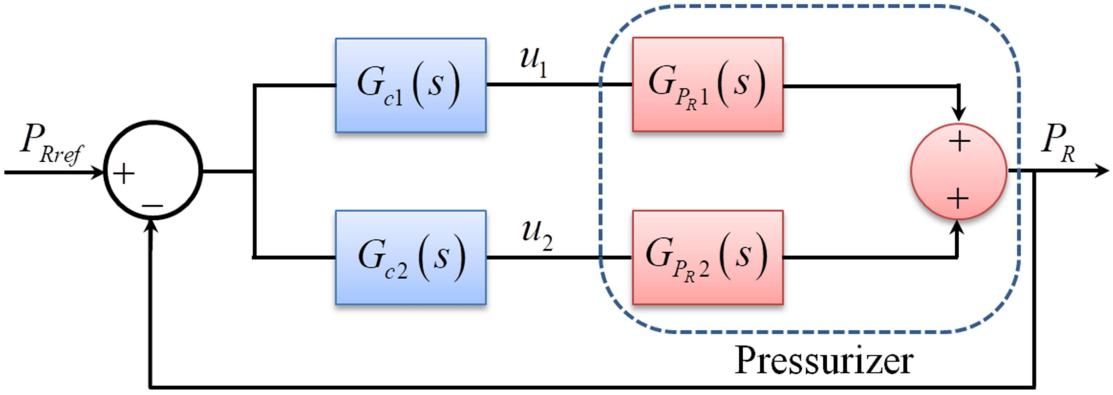

Fig. 3.4 Schematic diagram of pressurizer control loop

The pressure controller design has been elaborated in the next section.

3.4. Controller Design for a 700MWe PHWR

The control of the proposed PHWR is assumed to be achieved by two de-coupled control loops viz. the demand power control loop and the pressurizer control loop. The robust power controller design methodology presented in *Chapter 2* and adopted in this chapter and in conjunction with the pressurizer control mechanism allows the 700MWe PHWR to be controlled at any power level between 60% and 100%FP.

This section discusses in details, the controller design and control strategy for 700MWe PHWR in presence of coolant channel voiding considered during a power maneuver exceeding 93%FP. This section is divided into two sub-sections-

3.4.1 Controller design for zonal power level control

The PHWR is assumed to be composed of 14 zones and the control loop for each zone is presented in Fig. 3.1 where the zonal power demand is divided from the global demand. The corresponding open loop transfer functions with varying reactor power for zone 1, as a representative case, is presented in Table 3.2, along with estimated void fraction using the model presented in Section 3.2. As seen from Table 3.2, it is seen that voiding starts from 94%FP (approx.) and zooming in the simulation in this regime 92%-94%FP reveals that voiding start about 92.3%FP which is taken as the threshold for activating the pressurizer.

A thorough examination of Table 3.2 suggests that voiding in coolant channel starts from 92.3%FP and voiding exceeds it maximum allowable limit of 3% between 96-98%FP (approx.). Table 3.2 and Fig. 3.5 also suggest that as the power level of the reactor is raised from 60%FP, the open loop poles of the system start shifting towards the left-hand side, i.e., towards a more stable region. This matches with the nature of the PHWR reported in [49]. As soon as the voiding starts, the open loop poles starts shifting again towards the imaginary axis rapidly. This is because of positive reactivity due to voiding. Therefore, the movement of open-loop poles for 60%FP-100%FP power variation is non-polytopic in nature and thus the system cannot be represented as an interval system with parameter values corresponding to 60%FP as the *infimum* of the system and parameter values corresponding to 100%FP as the *supremum* of the system. This is in contrary to the 540MWe PHWR described in *Chapter 2* where the variation of open-loop poles is polytopic in nature. However, with a pressurizer, if the pressure of the system can be increased to control voiding, the deviation from a polytopic variation of interval parameters can be minimized.

Table 3.2

2nd Order Identified Model of 700mwe PHWR (Zone 1) At Various Operating Power

% Power	Transfer Function	% Voiding(without pressure controller)
60	$\frac{0.0063412}{s^2+1.53871s}$	0
70	$\frac{0.0058942}{s^2+1.54967s}$	0
80	$\frac{0.0054124}{s^2+1.55287s}$	0
85	$\frac{0.0052036}{s^2+1.55698s}$	0
90	$\frac{0.0051084}{s^2+1.56087s}$	0
92	$\frac{0.0050037}{s^2+1.56105s}$	0
94	$\frac{0.0129}{s^2+0.9647s}$	1.2
96	$\frac{0.01985}{s^2+0.9362s}$	2.6
98	$\frac{0.02097}{s^2+0.9047s}$	3.9
100	$\frac{0.0276}{s^2+0.89545s}$	4.5

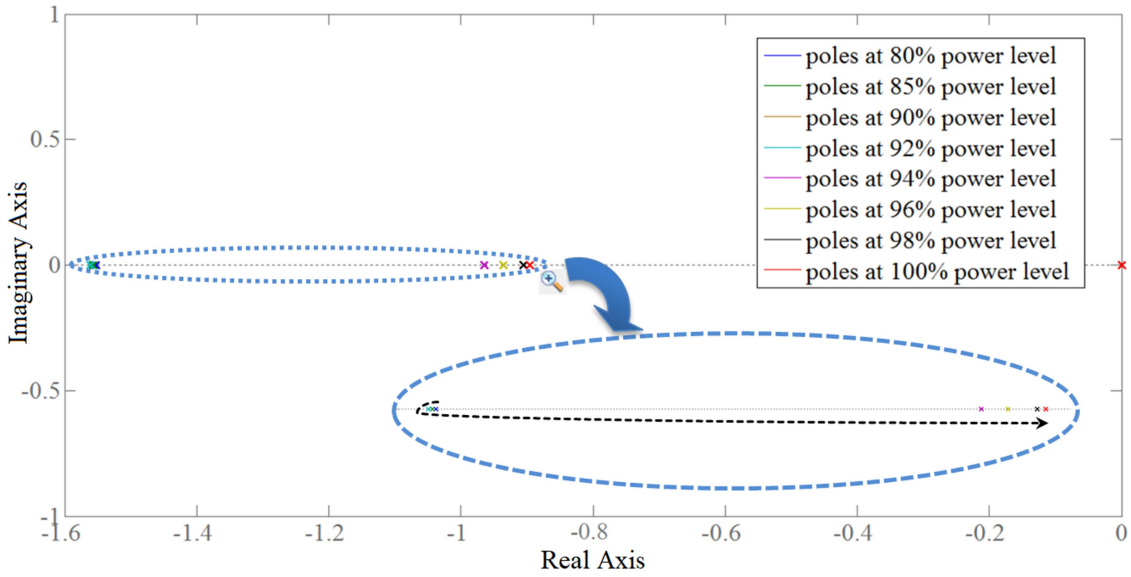

Fig. 3.5 Open-loop poles variation during power maneuvering.

Core voiding of 3% is usually allowed in 700MWe PHWR design [12] to allow enhanced heat transfer to the coolant and thus achieving lower fuel temperature. As seen in Table 3.3the reversal direction of dominant poles of the transfer function starts from about 92.3%FP. Thus the LZCS controller is designed using the methodology presented in *Chapter 2* for the interval system.

Thus, for the present case of 700MWe PHWR, the system can be identified as an interval system as:

$$G(s)=\frac{\left[\underline{L},\,\overline{L}\right]}{s^2+\left[\underline{a},\,\overline{a}\right]s} \tag{3.36}$$

where

$$\left[\underline{L},\,\overline{L}\right]=\begin{bmatrix}\min\left(60\%\text{FP-}100\%\text{FP}\right),\\ \max\left(60\%\text{FP-}100\%\text{FP}\right)\end{bmatrix} \tag{3.37}$$

and

$$[\underline{a}, \overline{a}] = \begin{bmatrix} \min(60\%\text{FP} - 100\%\text{FP}), \\ \max(60\%\text{FP} - 100\%\text{FP}) \end{bmatrix} \tag{3.38}$$

From (3.36), the nominal plant in this case can be represented as:

$$G_0(s) = \frac{L_0}{s^2 + a_0 s} \tag{3.39}$$

where $L_0 = (\underline{L} + \overline{L})/2$ and $a_0 = (\underline{a} + \overline{a})/2$.

Therefore, the new interval system for 700MWe PHWR plant can be represented as:

$$G(s) = \frac{[0.0050037, 0.0276]}{s^2 + [0.89545, 1.56105]s} \tag{3.40}$$

and the nominal system as

$$G_0(s) = \frac{0.01630185}{s^2 + 1.22825s} \tag{3.41}$$

Now using (3.41) as the nominal plant and using the controller design technique illustrated in *Chapter 2*, the new set of PID controller gain has been obtained for the 700MWe PHWR and can be represented as:

$$G_c(s) = K_p + \frac{K_i}{s} + K_d s \tag{3.42}$$

It is to be noted that the controller (3.42) has to be designed in such a way that the bound of $\tilde{\mathbf{Q}}$ as per (2.65) for (3.42) has to remain positive semi-definite. This bound may be different from that of the controller (2.47) designed for 540MWe but the condition of remaining positive semi-definite throughout the interval has to be satisfied.

3.4.2 Controller design for Pressurizer pressure control

The proposed pressurizer pressure control scheme is represented in Fig. 3.4. From Fig. 3.4, the overall closed loop pressurizer dynamics can be represented as:

$$G_{P_Rcl} = \frac{G_{P_Rc1}(s)G_{P_R1}(s) + \eta G_{P_Rc1}(s)G_{P_R2}(s)}{1 + G_{P_Rc1}(s)G_{P_R1}(s) + \eta G_{P_Rc1}(s)G_{P_R2}(s)} \tag{3.43}$$

where $G_{P_Rc2}(s) = \eta G_{P_Rc1}(s)$ and $\eta = -\frac{k_{P_R2}}{k_{P_R1}}$

Substituting (3.35) and using a standard PI controller $k_p + \frac{k_i}{s}$ in (3.43) yields

$$G_{P_Rcl} = \frac{\left(k_{P_R1} + \eta k_{P_R2}\right)k_p s + \left(k_{P_R1} + \eta k_{P_R2}\right)k_i}{s^2 + \left(k_{P_R1} + \eta k_{P_R2}\right)k_p s + \left(k_{P_R1} + \eta k_{P_R2}\right)k_i} \tag{3.44}$$

Comparing (3.44) with characteristics equation of a standard 2nd order system, closed loop frequency (ω_{cl}) and closed loop damping (ξ_{cl}) can be obtained as:

$$\left.\begin{aligned} \omega_{cl} &= \sqrt{\left(k_{P_R1} + \eta k_{P_R2}\right)k_i} \\ \xi_{cl} &= \frac{\sqrt{\left(k_{P_R1} + \eta k_{P_R2}\right)}k_p}{2\sqrt{k_i}} \end{aligned}\right\} \tag{3.45}$$

For the purpose of designing an optimal controller for optimally controlling the heater element and spray valve of the pressurizer, an objective function needs to be defined. The objective function f is assumed be the weighted sum of three individual functions namely-

1. Function for error minimization of the closed loop plant i.e. G_{P_Rcl} . It is a well-known fact that for tracking, Integrated Time Absolute Error (ITAE) function produces the most

satisfactory results [70]. Thus for the error minimization ITAE function has been chosen. The ITAE function can be written as:

$$f_1 = \int_0^t t\left|e(t)\right| dt = 0 \tag{3.46}$$

$$\text{where } e(t) = \left[1 - \mathcal{L}^{-1}\left(G_{P_R cl}\frac{1}{s}\right)\right] \tag{3.47}$$

2. Minimization of electric heater power. From Fig. 3.4, the controller output u_1, referred to as electric heater output, needs to be minimized and hence a function can be chosen as:

$$f_2 = u_1 = e(t)\left\{k_p e(t) + k_i \int_0^t e(t)dt\right\} \tag{3.48}$$

3. Function for minimization of the spray flow. From Fig. 3.4, the controller output u_2, referred to as spray flow, needs to be minimized and hence a function can be chosen as:

$$f_3 = u_2 = e(t)\left\{\eta k_p e(t) + \eta k_i \int_0^t e(t)dt\right\} \tag{3.49}$$

Therefore the objective function $f(t)$ can be defined as:

$$f = w_1 f_1 + w_2 f_2 + w_3 f_3 \tag{3.50}$$

where w_1, w_2 and w_3 are the weights assigned to the corresponding functions and they can be obtained as:

$$\left.\begin{aligned} w_i &= \frac{\Pi_{r=1}^{3}(R_r)}{R_i},\ i \in \{1,2,3\} \\ R_r &= (\max f_r - \min f_r),\ \forall r \end{aligned}\right\} \tag{3.51}$$

Now, in order to minimize the objective function f, the following constraints need to be satisfied:

1. Poles of the $G_{P_R cl}$ should lie in the left-half of the *s*-plane.
2. The range of variation of ω_{cl} should lie in between $0.1 < \omega_{cl} < 0.3$.
3. The range of variation of ξ_{cl} should lie in between $0.7 < \xi_{cl} < 0.9$.

The task of finding gains of the optimal controller that minimizes the cost function (3.50) with the constraints (3.1)-(3.2) mentioned above is cast as a search problem in the continuous space of controller gains and solved using GA. First, the GA [45] is initialized with a random *population*, where population represents a possible set of controller gains and the string representing the binary value of each controller gain is known as the *chromosome.* In this case, two chromosomes (one k_p chromosome and one k_i chromosome) form a *community* and a number of such communities form a population. The next step involves selection of *parent* population from amongst the existing population to form a *mating pool* which consists of some superior communities. Communities of the mating pool result in offspring generation through *reproduction* that occurs in two stages viz. *cross-over* and *mutation* [71]. Within the set of parents and off-springs, only the superiors survive and the rest are discarded. The iteration continues and the population evolves as a better population (i.e. a set of more optimal controller gains) through the iterations of GA process. Different steps of GA application for the present problem are enumerated as follows:

i. Random population initialization

The initial population can be represented as $\mathbf{K}_{cj}^{0}$, where $j \in (1, 2)$ represents the chromosome of the population, $\mathbf{K}_{c_n 1} = k_{p_{c_n}}$, $\mathbf{K}_{c_n 2} = k_{i_{c_n}}$ and $c \in (c_1, \ldots, c_n, \ldots, c_N)$ where, N is the number of community. $\mathbf{K}_{c1}$ and $\mathbf{K}_{c2}$ correspond to the arbitrarily initialized controller gains.

Now, population size can be chosen as a function of the string span [45] and this can be expressed as:

$$\mathbf{K}_{c_n j}^{0} \approx UNF\left(\mathbf{K}_{j}^{min}, \mathbf{K}_{j}^{max}\right) \tag{3.52}$$

where, $\mathbf{K}_{c_n j}^{0}$ is the initial population corresponding to j^{th} chromosome of the n^{th} community and $UNF\left(\mathbf{K}_{j}^{min}, \mathbf{K}_{j}^{max}\right)$ (Universal Normalized-distribution Function) is a statistical operator acting over $\left(\mathbf{K}_{j}^{min}, \mathbf{K}_{j}^{max}\right)$ in an uniform manner where $\mathbf{K}_{j}^{min}$ and $\mathbf{K}_{j}^{\max}$ represent the minimum and the maximum values of the corresponding controller gains respectively.

ii. Selection of parent populations

For selection of parental population for a mating pool, binary tournament selection method [71] has been adopted. Two parental chromosomes are randomly selected from the existing population and amongst them the one with the lower value of objective function f of (3.50) is set as the *winner* and is separately kept in the mating pool. Likewise the iteration continues until the mating pool gets filled up with the winner chromosomes.

iii. Simulated Binary Crossover (SBC)

The SBC operator searches for the global optimum by combining the substructures of the parental chromosomes and thereby results in the generation of a new offspring. A stochastic parameter φ, which determines the position of the pivot point in the chromosome where the crossover is done, is computed with the help of a multinomial type probability allocation as in (3.53).

$$\varphi = \begin{cases} (\mathbb{N}\theta)^{1/(\eta_v+1)} & ; \mathbb{N} \le \dfrac{1}{\theta} \\ \dfrac{1}{(2-\mathbb{N}\theta)^{1/(\eta_v+1)}} & ; \mathbb{N} > \dfrac{1}{\theta} \end{cases} \tag{3.53}$$

where, $\mathbb{N}$ is a random binary number between [0,1] and

$$\theta = 2 - \frac{1}{B^{(\eta_v+1)}} \tag{3.54}$$

$$B = 1 + \frac{2}{\left(\mathbf{K}_{c_2} - \mathbf{K}_{c_1}\right)} min\left[\left(\mathbf{K}_{c_1} - \mathbf{K}_c^{min}\right), \left(\mathbf{K}_c^{max} - \mathbf{K}_{c_2}\right)\right] \tag{3.55}$$

Here, η_v denotes allocation index corresponding to the SBC. Offspring community generation depends upon the value assigned to η_v which is essentially a positive integer. Value assigned to η_v indicates how close the generated offspring is to its parents. In between parents and offspring, the intermediate controller gains can be calculates as:

$$\mathbf{K}_{c_1} = \frac{1}{2}\left[\left(\mathbf{K}_{c_1} + \mathbf{K}_{c_2}\right) - \varphi\left(\left|\mathbf{K}_{c_2} - \mathbf{K}_{c_1}\right|\right)\right] \tag{3.56}$$

$$\mathbf{K}_{c_2} = \frac{1}{2}\left[\left(\mathbf{K}_{c_1} + \mathbf{K}_{c_2}\right) + \varphi\left(\left|\mathbf{K}_{c_2} - \mathbf{K}_{c_1}\right|\right)\right] \tag{3.57}$$

iv. Operation of multinomial mutation

A stochastic parameter χ has been calculated as (3.58) to generate an offspring closest possible to the parent population through mutation. This parameter determines the intensity of mutation. It depends on another random binary number $\mathbb{N}'$ ranging between [0, 1].

$$\left.\begin{array}{l}\text{if } \mathbb{N}' \le \dfrac{1}{2}, \\ \chi = \left[2\mathbb{N}' + (1-2\mathbb{N}')(1-\lambda)^{(\eta_m+1)}\right]^{\frac{1}{(\eta_m+1)}} - 1 \\ \text{else,} \\ \chi = 1 - \left[2\mathbb{N}' + (1-2\mathbb{N}')(1-\lambda)^{(\eta_m+1)}\right]^{\frac{1}{(\eta_m+1)}}\end{array}\right\} \quad (3.58)$$

$$\text{where, } \lambda = \frac{min\left[\left(\mathbf{K}_{c_n} - \mathbf{K}_c^{min}\right), \left(\mathbf{K}_c^{max} - \mathbf{K}_{c_n}\right)\right]}{\left(\mathbf{K}_c^{max} - \mathbf{K}_c^{min}\right)} \quad (3.59)$$

c. Equations for generating mutated offspring can be represented as

$$\mathbf{K}'_{c_1} = \mathbf{K}_{c_1} + \chi\left(\mathbf{K}_c^{max} - \mathbf{K}_c^{min}\right) \quad (3.60)$$

$$\mathbf{K}'_{c_2} = \mathbf{K}_{c_2} + \chi\left(\mathbf{K}_c^{max} - \mathbf{K}_c^{min}\right) \quad (3.61)$$

The allocation index η_m corresponding to mutation can be represented as

$$\eta_m = \eta_{m,min} + i_n \quad (3.62)$$

where $\eta_{n,\min} = \min\left(\eta_m\right)$ and η_m is updated with corresponding iterations $\left(i_n\right)$ and with the ongoing iteration, the objective function f is computed.

v. Selection between a parent and an offspring

The value of f of each parent $\mathbf{K}_{c_n j}$ is compared with that of matching offspring $\mathbf{K}'_{c_n j}$. The population that has lower value of f gets selected in order to operate in the following iteration as in equation (3.63).

$$\left.\begin{array}{l}\mathbf{K}_{c_n j} = \mathbf{K}'_{c_n j}, \text{ if } f\left(\mathbf{K}'_{c_n j}\right) \le f\left(\mathbf{K}_{c_n j}\right) \\ \mathbf{K}_{c_n j} = \mathbf{K}_{c_n j}, \text{ otherwise}\end{array}\right\} \quad (3.63)$$

The flowchart of the GA and the schematic of GA-based PI controller design for pressurizer are presented as Fig. 3.6 and Fig. 3.7 respectively.

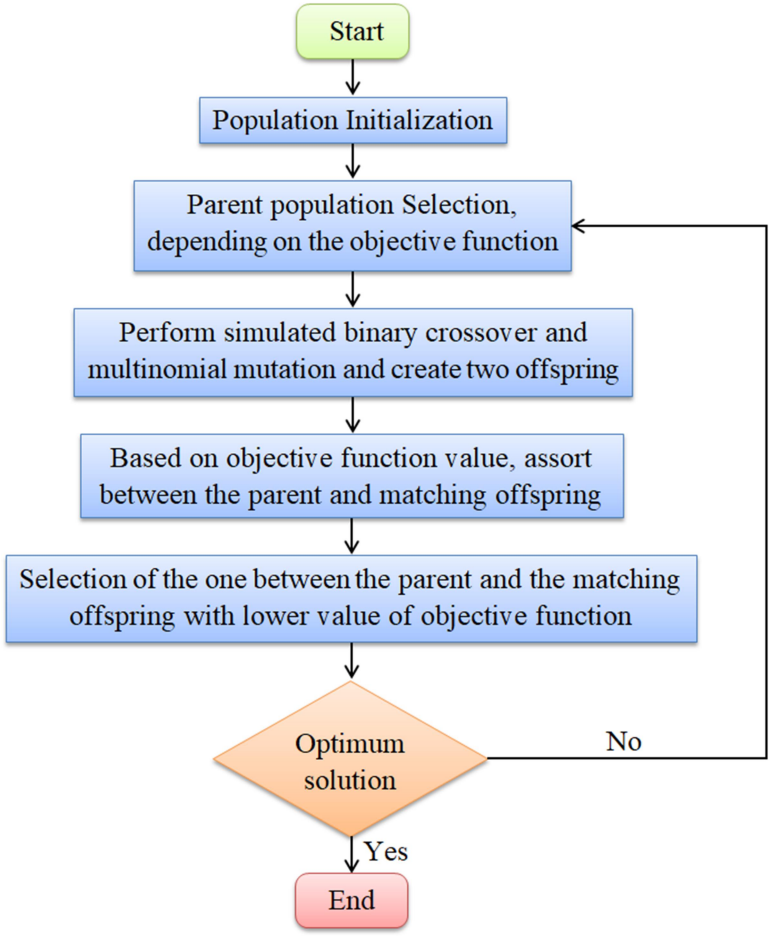

Fig. 3.6 Flowchart of the GA

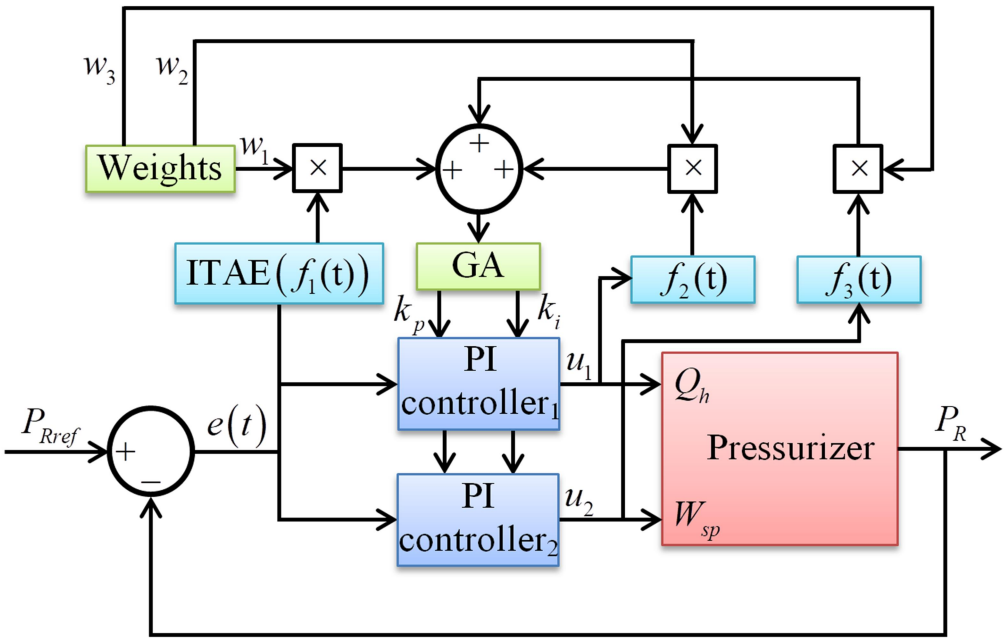

Fig. 3.7 GA-based PI controller design for pressurizer [70]

The methodology presented in this chapter has been validated using credible simulation-based studies and the corresponding results are presented in *Chapter 4*.

This page is intentionally left blank

This page is intentionally left blank

Chapter 4

Simulation and Results

4.1 Introduction

The controller design methodologies and the related stability studies for both 540MWe and 700MWe PHWRs presented in the last two chapters are established in this chapter using credible real-time (online) and offline (MATLAB/Simulink) simulations as and where applicable.

This chapter is organized as follows. Section 4.2 represents the details of the real-time simulation test-bench that has been used in this dissertation. The set-up comprises of the real-time simulator OPAL-RT (OP4500) which simulates the plant (reactor in this case) and a separate controller PC simulating the controller. Next, the performance of the PID controller, designed using the methodology presented in *Chapter 2* for controlling a 540MWe PHWR, is established in Section 4.3 using both offline and online simulations. The related stability study for the closed-loop system with the designed controller has been analyzed at different power levels. Lastly, Section 4.4 presents the online simulations results related to the control and stable operation of 700MWe PHWR using the controller design methodologies presented in *Chapter 3*.

4.2 The Real-time simulation test-bench

The controller design methodology is tested using Hardware in Loop (HiL) simulation over an OPAL RT (OP4500) module [72]. The OP4500 is a compact simulator capable of performing high speed simulation with sub-microseconds step size. It is fully integrable with MATLAB/Simulink through the RT LAB 11 software and consists of 16 fast input and output channels. The non-linear simulation model of the 540MWe PHWR is developed using MATLAB/Simulink installed in a host computer using the set of equations (2.18)-(2.25). The model is made compatible to run in the real time simulator OPAL RT (OP4500) [73] using the prescribed OPAL RT block sets. The host computer hosting this RT LAB 11[73] software generates C code from the Simulink model and downloads the generated code to the simulator. The complex non-linear plant module running in real-time on the OP4500 therefore forms a virtual plant whose dynamics and behavior under various operating scenarios need to be studied

The controller derived for the purpose of achieving desired system performance is simulated in MATLAB/Simulink installed in a separate computer named as *Controller PC*. This computer uses the MATLAB Real Time Workshop (RTW) [74] which automatically generates the corresponding C code from the Simulink model resulting in an executable file that can be run in real-time by the Real Time Windows Target (RTWT) [75] installed the Controller PC. An ADVANTEC PCI 1711 I/O card [76] is installed in the Controller PC to communicate the real-time data to the *plant* simulated by the OP4500 module. This 12 bit A/D converter with a sampling rate of up to 100 KHz consists of 16 analog input channels and 2 analog output channels. When running models in real time, RTWT captures a sample of data from one or more input channels through the PCI card, uses the data as inputs to the executable file generated by

the RTW, immediately processes the data, and sends it back to the outside world via an output channel through the PCI card. Figure 4.1 gives the block diagram of the entire process.

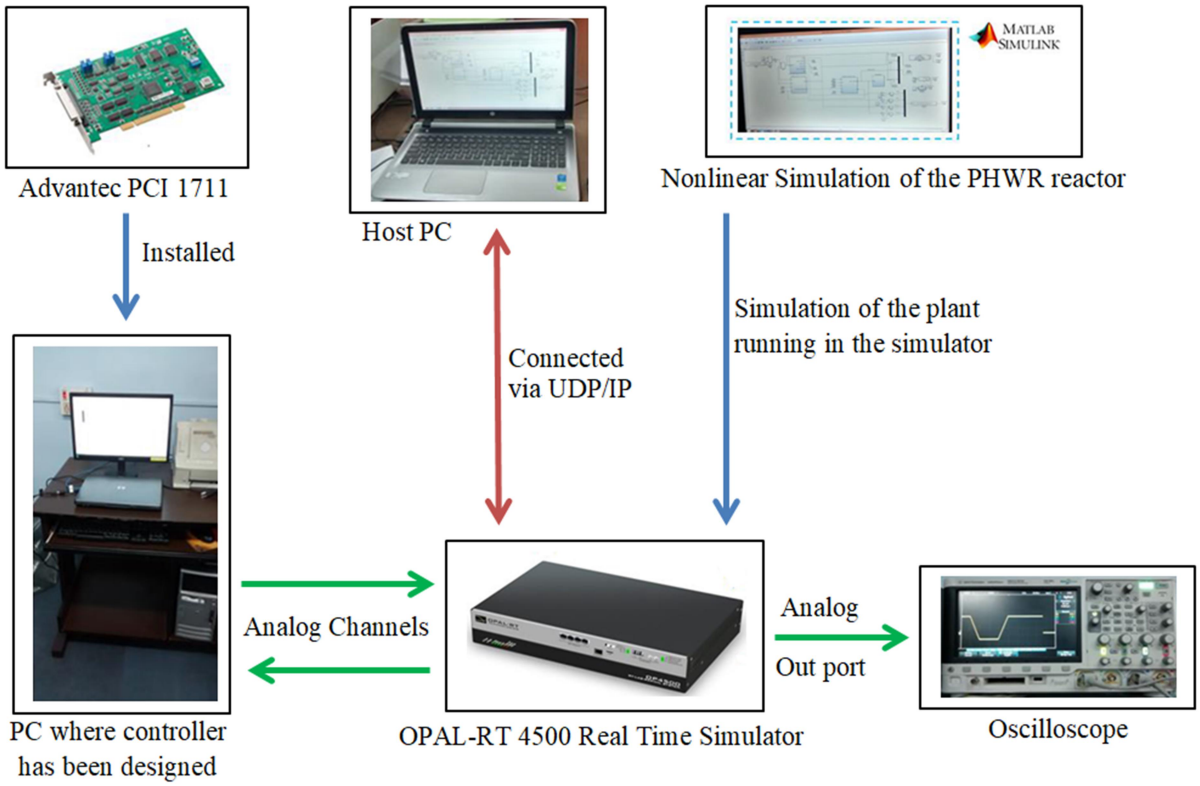

Fig. 4.1 Schematic of HiL test-bench

The real-time simulation results presented in the subsequent sections therefore represent scenarios where the actual non-linear plant is controlled by the controllers designed by the methodologies presented in *Chapters 2* and *3*.

4.3 Simulation Results of 540MWe PHWR

The LQR based PID controller has been demonstrated by contemporary researchers e.g. [15], [29] and forms the basis of controller design detailed in *Chapter 2*. As mentioned before, the methodology presented in *Chapter 2* is used to design robust PID controllers for each zone of the ZCC of a 540MWe PHWR to achieve the following:

i. To produce satisfactory time response with an uncertainty $\Delta P_{ss} = \pm 20\%$FP where ΔP_{ss} is defined as $\Delta P_{ss} = P_{ss} - P_{ss_0}$, P_{ss_o} being the reactor power corresponding to the nominal system.

ii. To produce satisfactory time response with injected uncertainties into the tune of ±5% in each element of the set of parameters $\mathbf{p} = \left[P_{ss}, \alpha_c, \alpha_f, \Omega\right]$ representing zonal reactor power P_{ss}, reactivity coefficients α_c and α_f, the parameter Ω.

The satisfaction of requirement (i) ensures the robustness of the PID controller in terms of its ability to control the 540MWe PHWR under a possible power variation scenario when the demand power set-point is changed within a $\pm 20\%$FP band and the requirement (ii) ensures that the controller performance remains satisfactory under uncertainties in the measurement of power, reactivity of coolant and fuel and in estimation of heat transfer parameters.

In order that a robust PID controller achieves both (i) and (ii), the intervals $\left[\underline{L}, \overline{L}\right]$ and $\left[\underline{a}, \overline{a}\right]$ computed using (tns22)-(tns23) should be able to accommodate the corresponding intervals of $\left[P_{ss}, \alpha_c, \alpha_f, \Omega\right]$. A study of the data presented in Tables 2.3 and 2.4 show that the interval $\left[\underline{L}, \overline{L}\right]$ for each zone of the PHWR in Table 2.4 (with injected uncertainties of $\pm 10\%$ in $P_{ss}, \alpha_f, \alpha_c, \Omega$) includes the corresponding interval $\left[\underline{L}, \overline{L}\right]$ computed from Table 2.3 (with $\Delta P_{ss} = \pm 20\%$FP) and the reverse is true for the intervals $\left[\underline{a}, \overline{a}\right]$. In order that the nominal PID controllers are capable of achieving both (i) and (ii) the larger of the two intervals are selected from Tables 2.3 and 2.4 for both $\left[\underline{L}, \overline{L}\right]$ and $\left[\underline{a}, \overline{a}\right]$ to define interval plant for each zone of the

PHWR and subsequent design of robust PID controllers. Table 4.1 summarizes the transfer functions of the nominal plants and corresponding intervals $\left[\underline{L}, \overline{L}\right]$ and $\left[\underline{a}, \overline{a}\right]$.

Table 4.1

Nominal Plants and Interval Parameters for Controller Design

Zone	$G_0(s)$	$\left[\underline{L}, \overline{L}\right]$	$\left[\underline{a}, \overline{a}\right]$
1,8	$\frac{0.0064626}{s^2+1.55496s}$	$[0.0051034, 0.0084124]$	$[1.3287, 1.7793]$
2,9	$\frac{0.0062857}{s^2+1.54870s}$	$[0.0050102, 0.0062857]$	$[1.3235, 1.7725]$
3,10	$\frac{0.0071854}{s^2+1.524855s}$	$[0.0052687, 0.0071854]$	$[1.3030, 1, 7450]$
4,11	$\frac{0.0088249876}{s^2+1.54933s}$	$[0.0068255, 0.0114929]$	$[1.3247, 1.7740]$
5,12	$\frac{0.0071854}{s^2+1.524855s}$	$[0.0052687, 0.0071854]$	$[1.3030, 1.7450]$
6,13	$\frac{0.0064626}{s^2+1.55496s}$	$[0.0051034, 0.0084124]$	$[1.3287, 1.7793]$
7,14	$\frac{0.0062857}{s^2+1.54870s}$	$[0.0050102, 0.0062857]$	$[1.3235, 1.7725]$

For nominal controller, design the nominal values of closed-loop system parameters are specified as $\sigma_0 = 1.55,\ \zeta_0 = 0.9,\ \omega_0 = 0.1$ rad/sec for the closed-loop template (2.43)

With these specifications, an acceptable time-response is specified as one which produces a $\pm 10\%$ uncertainty bound in $[\sigma, \zeta, \omega]$ around $\alpha_0, \zeta_0, \omega_0$. Thus,

$$\sigma \in [1.39, 1.70];\ \zeta \in [0.81, 0.99];\ \omega \in [0.09, 0.11]; \qquad (4.1)$$

Table 4.2 presents the nominal PID controller parameters for all the 14 zones of a PHWR obtained with these considerations following the methodology presented in *Chapter 2*.

Table 4.2

Nominal PID Controller Parameters

Zone	K_p	K_i	K_d
1,8	44.7188	2.3984	27.0851
2,9	44.9774	2.8432	28.8432
3,10	40.2204	2.1572	28.5503
4,11	32.7482	1.7564	20.4728
5,12	40.2204	2.1572	28.5503
6,13	44.7188	2.3984	27.0851
7,14	44.9774	2.8432	28.8432

With the nominal plants and the corresponding nominal controllers designed, it is next attempted to study the robustness of the closed-loop plants using MATLAB simulation. Fig. 4.2 shows the general schematic used for MATLAB simulation. Simulink blocks for ZCC models reported in [36] have been used for developing the Simulink model for Fig. 4.2 and the PID controller blocks listed in Table 4.2 are included in the LZC Controller block. The Zonal Demand Power block shown in Fig. 4.2 generates the zonal power demand set-points and zonal power errors for each zone of the PHWR.

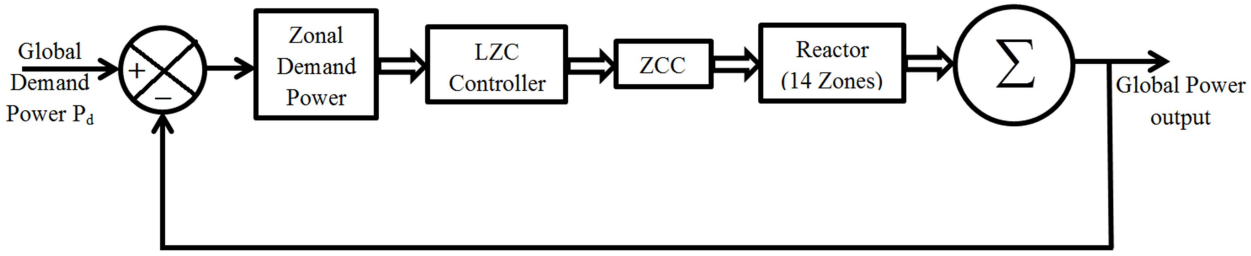

Fig 4.2 Schematic diagram of MATLAB SIMULINK model

To test the fulfillment of the first requirement, the demand power set-point is ramped at -0.5%FP/sec for 20sec with the reactor operating at 80%FP (nominal plant), at 100%FP (i.e. ΔP_{ss} = +20%FP) and at 60%FP(i.e. ΔP_{ss} = -20%FP) and the PID controllers, as described by Table 4.2, in loop. The simulated variations of the global reactor power (sum of individual zonal powers) with time in each case are presented in a single graph represented by Fig. 4.3.

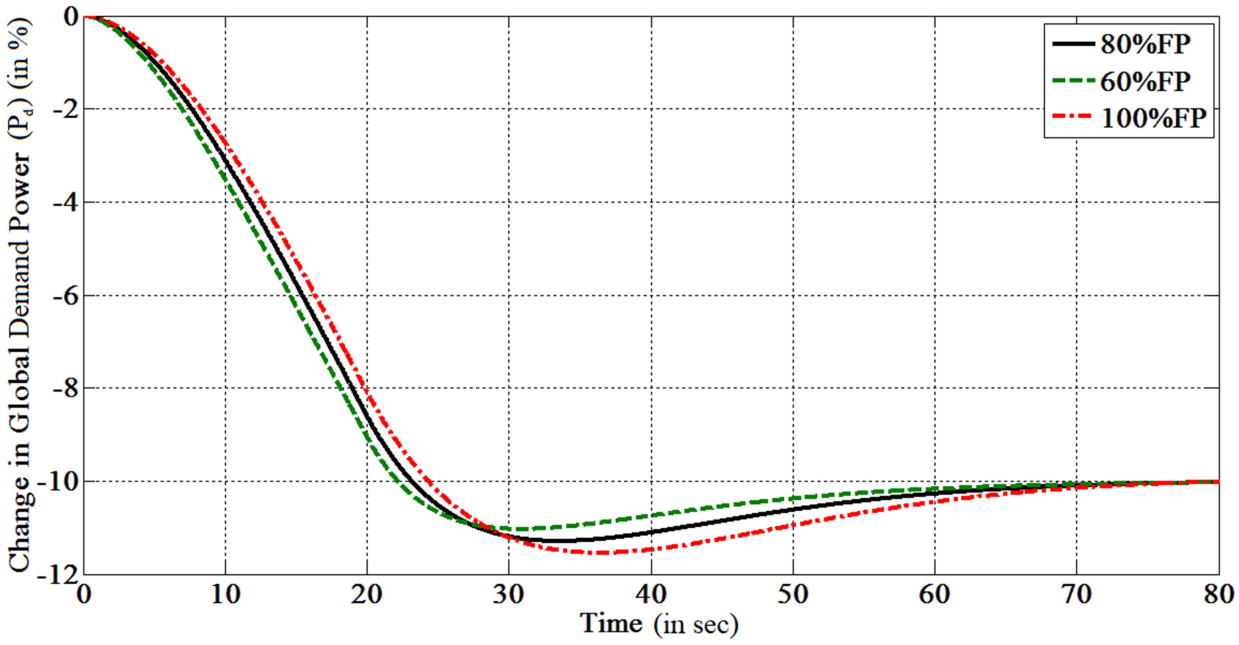

Fig. 4.3 Global Power Variation due to Demand Power Set-point Ramping at 100%FP, 80%FP and 60%FP with nominal PID controller

As seen from Fig. 4.3, the PID controllers are capable of achieving effective control of reactor power over a range of $\pm 20\%$ FP around the power level associated with the nominal plant i.e. from 60%FP to 100%FP. In the case of a 540MWe Indian PHWR it means that the same controller can be used to control reactor power between 324MWe to 540MWe. In Fig. 4.3, for each case, the peak overshoot is a little more than the value corresponding to $\zeta = 0.9$ mainly because of the zeroes introduced by the PID controller in closed-loop. A study of Fig. 4.3 also shows that the peak overshoot in global reactor power with nominal PID controllers in loop reduces from 1.12 to 1.10 when the power is reduced to 60% FP from 80%FP and increases to 1.15 when the power is increased to 100%FP. Figure 4.3 shows that the bulk power settles within 2% of its steady-state value within 60sec with marginal decrease when power is reduced to 60%FP and marginal increase at 100%FP. Assuming that the real root at $s = -\sigma_0$ in the template (2.44) not influence the time response since $\sigma_0 >> \bar{\zeta}\,\bar{\omega}$, as evident from (4.1), and the settling time remains constant, the variation in closed-loop damping $|\Delta\zeta|$ is less than 10% as envisaged.

Next, in order to test the robustness of the control system, i.e., requirement (ii), an uncertainty bound of $\pm 5\%$ is considered in the parameters $[P_{ss}, \alpha_c, \alpha_f, \Omega]$ and the corresponding zonal transfer functions are obtained for cases corresponding to the 4 vertices of the resultant convex box of $[L, a]$ computed using rule-set (2.2) and (2.39)-(2.40). These plants are controlled using the controllers described by Table 4.2. The global demand power set-point is again ramped at -0.5%FP/sec. While the global power variation represents the variation of cumulative zonal powers, study of robustness requires study of individual zonal powers as well, since the robust controllers are designed for each zone. Fig. 4.4 depicts a representative variation of zonal powers (Zone 4) under this condition, for four cases each corresponding to a vertex of the convex box of

$[L, a]$. Figure 4.5 represents the corresponding controller outputs for the same zone and Fig. 4.6 presents the frequency response for each case.

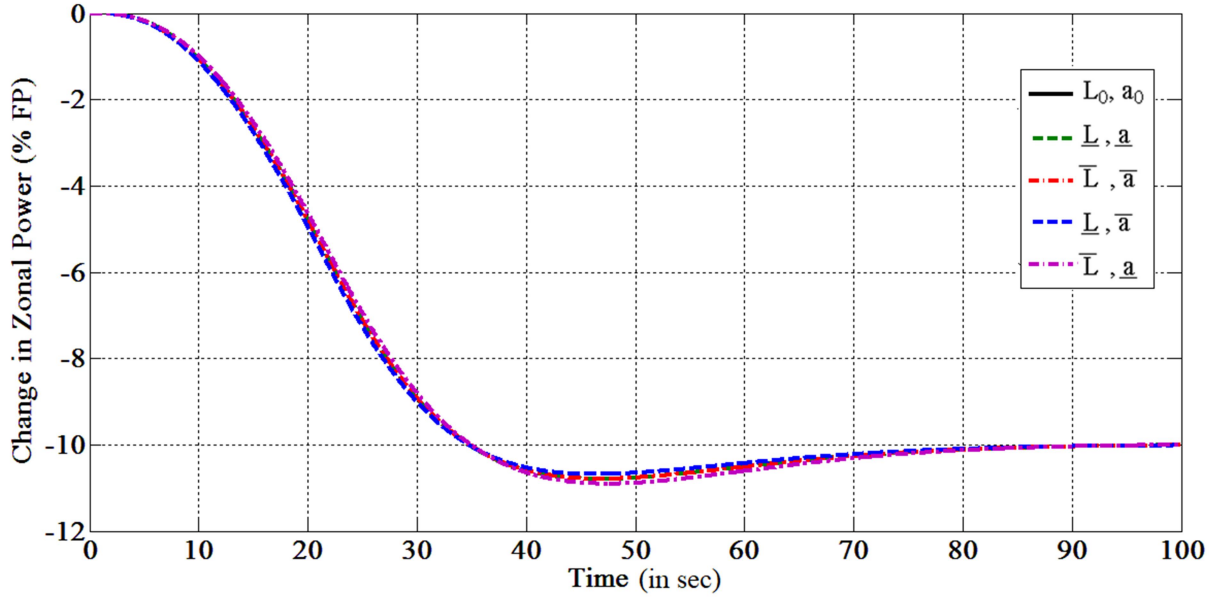

Fig 4.4 Representative Zonal Reactor Power variation due to Demand Power Set-point Ramping for 4 different cases arising out of parametric uncertainties

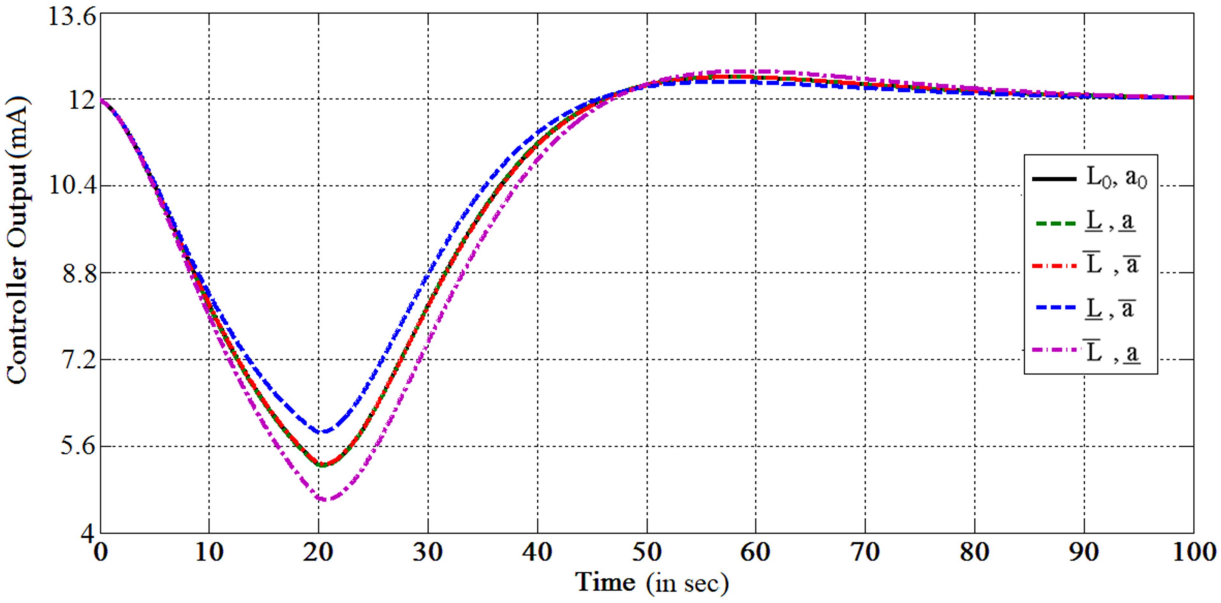

Fig 4.5 Representative controller output due to Demand Power Set-point Ramping for 4 different cases arising out of parametric uncertainties

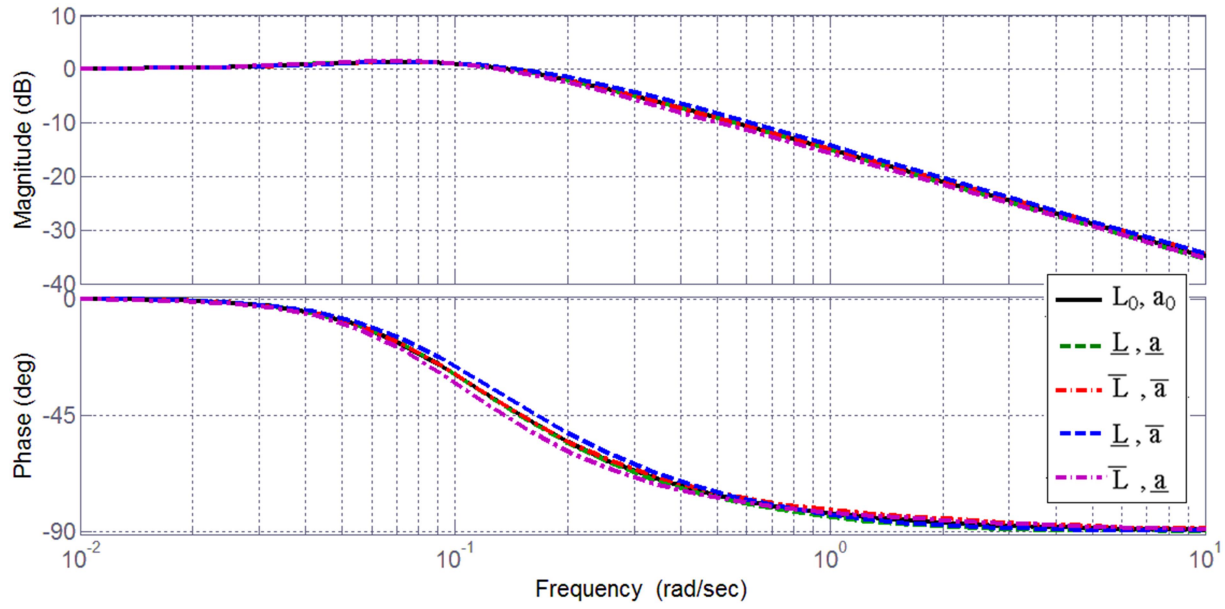

Fig 4.6 Representative Frequency Response for a Zone 4 with nominal PID controller for 4 different cases arising out of parametric uncertainties

As seen from the Fig. 4.4 and Fig. 4.6 , the time response and frequency response for the zone considered (zone 4) with the corresponding robust PID controller in loop remain almost unaltered with of ±5% uncertainty bound in the parameters $[P_{ss}, \alpha_c, \alpha_f, \Omega]$. The time response of the other zones exhibit similar behavior with peak overshoots varying between 1.12 and 1.14 and settling time between 59.7sec and 62.7sec for the same ramp-down of demand power set-point and have not been presented for the sake of brevity. Figure 4.4 may thus be taken as the representative time variation of the global power of the PHWR which is the sum of the powers produced by the individual zones. Similarity is also exhibited by the variations in controller outputs and frequency responses for the other zones.

Further, Fig. 4.5 reveals that the controller output is minimum when the gain term L is minimum and the pole at $s = -a$ is farthest from the origin for the plant (2.17) representing the

reactor zone considered. Similarly, the controller output is maximum when the term L is maximum and the pole at $s=-a$ is nearest to the origin. Uncertainties which cause L and a to shift in the same direction keep the controller output almost unaltered with respect to the nominal system. This can be explained with equations (2.39)-(2.40) and the representative values of the parameters presented in Table 2.3. It is seen that for a particular power level, the parameters L, a are most sensitive to changes in two parameters viz. P_{ss} and Ω. This has also been reported by [49] where robustness in presence of bounded parametric uncertainties have been examined by injecting uncertainties in these two parameters viz. P_{ss} and Ω only. An examination of (2.39)-(2.40) shows that L, a reduce in presence of positive uncertainties in P_{ss}, Ω and increase in presence of negative uncertainties in both of these parameters. But uncertainties of opposite signs in P_{ss}, Ω keep L, a constant. Again, it is seen that the value of the matrix $\Delta\mathbf{P}$ defined by (2.70) is negative implying decrease in cost of control for the condition $(L < L_0)$ and vice-versa. This explains the variation in controller output depicted in Fig. 4.5. The output of the controller is converted to a 4-20mA signal that is used to control the opening or closing of a control valve, to alter the level of light water in a ZCC. The steady-state value is 12mA.

The ramping rate of $\pm 0.5\%\,\mathrm{FP/sec}$ for demand power comes from the constraints associated with a 540MWe PHWR and has been kept unaltered as in the existing design of the present LZCS for Indian PHWRS. Though studies on uncertainties associated with heat transfer related parameters for a large PHWR are not available in published literature, Kazeminejad [77] reports an uncertainty bound of 1% in P_{ss} an 2.1% in Ω for a 2MW reactor. From this point of view, an uncertainty of $\pm 5\%$ in these parameters seems to be justified.

Next, the time response of the 540MWe PHWR with the designed PID controllers is studied on the real-time test bench described in Section 4.2. In this case, as mentioned before, the 540MWe reactor model represented as a 6^{th} non-linear order plant by equations (2.18)-(2.25) is simulated on the OP4500 platform and the controller set on the Controller PC. The reactor's demand power is now ramped-up from 60%FP to 100%FP at the rate of 0.5%FP/sec for 80sec. The PID controller output from the Controller PC is fed as an analog input to the OP4500 module is assumed to control the height of the water level in LZCS based upon which the reactivity introduced by the LZCS $\Delta\rho_{ext}$ is controlled computed using the LZCS gain mentioned in *Chapter 2*. The simulation results presented in Fig. 4.7 through Fig. 4.10 representing variations in P_{th}, T_f, $T_{c_{outlet}}$ and ρ_{ext} respectively due to variation in global demand power set-point P_d obtained as analog outputs from the OP4500 module and traced on a Mixed Signal Oscilloscope (MSO). For real-time simulation, different zone viz. zone 1 of the PHWR is now selected with a full power of 132.3MWth and the results are presented in Fig. 4.7 through Fig. 4.10.

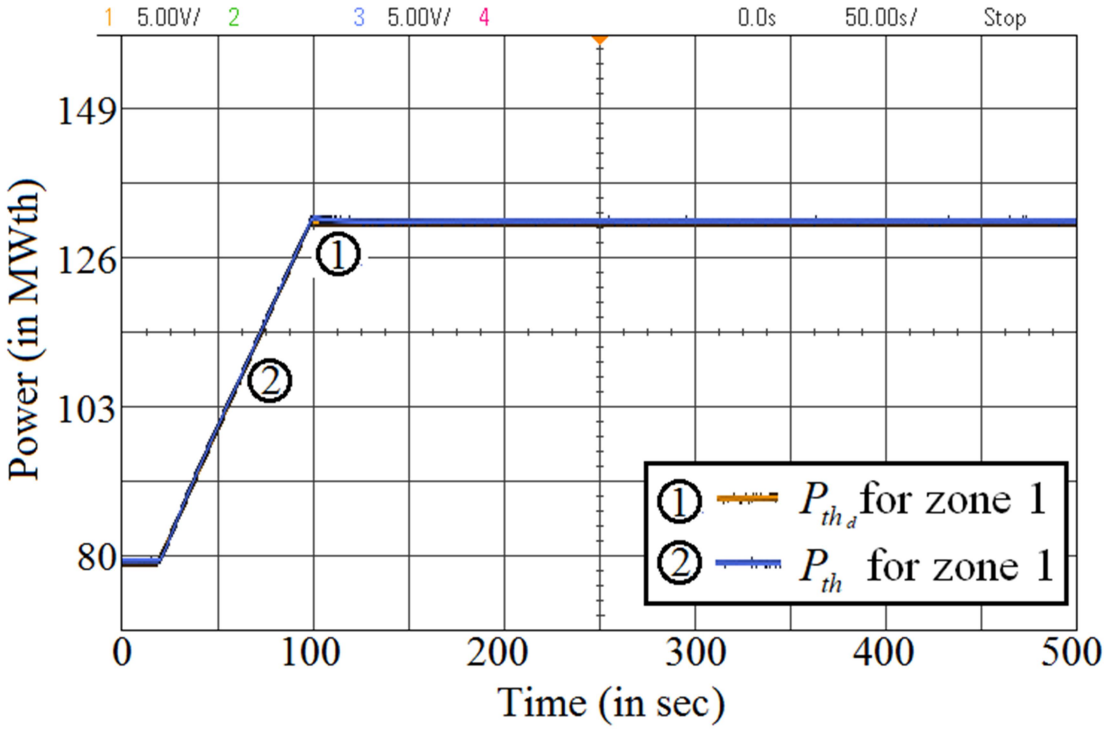

Fig. 4.7 Zonal demand power and actual power tracking of zone 1 during 60%-100%FP power maneuvering of 540MWe PHWR

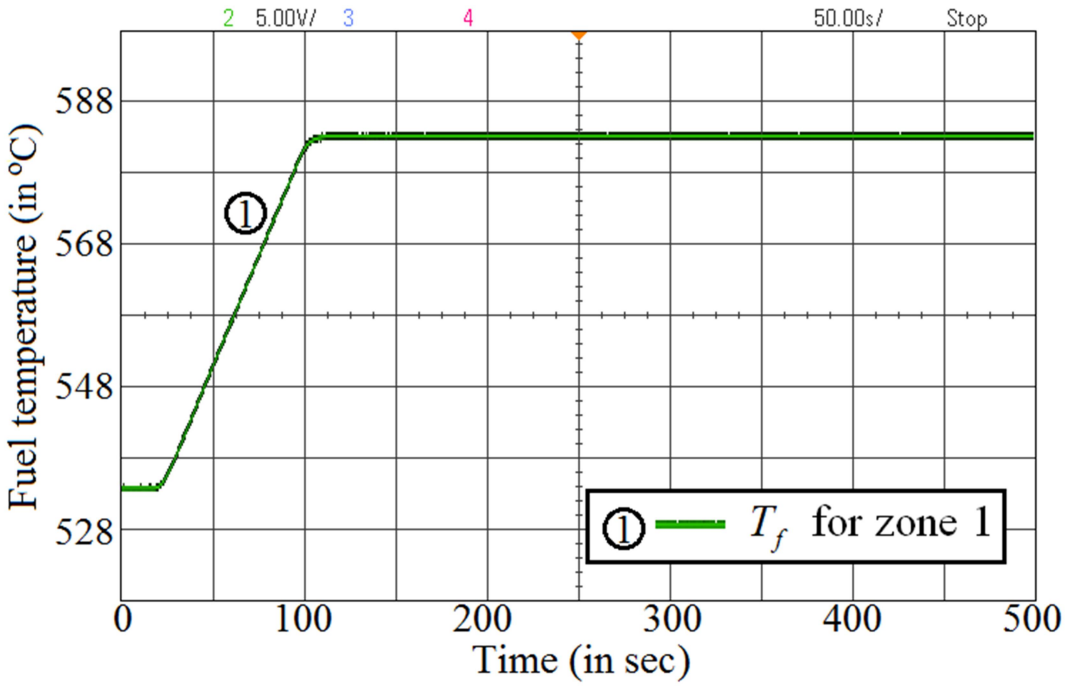

Fig. 4.8 Fuel temperature response during 60%-100%FP power maneuvering of 540MWe PHWR

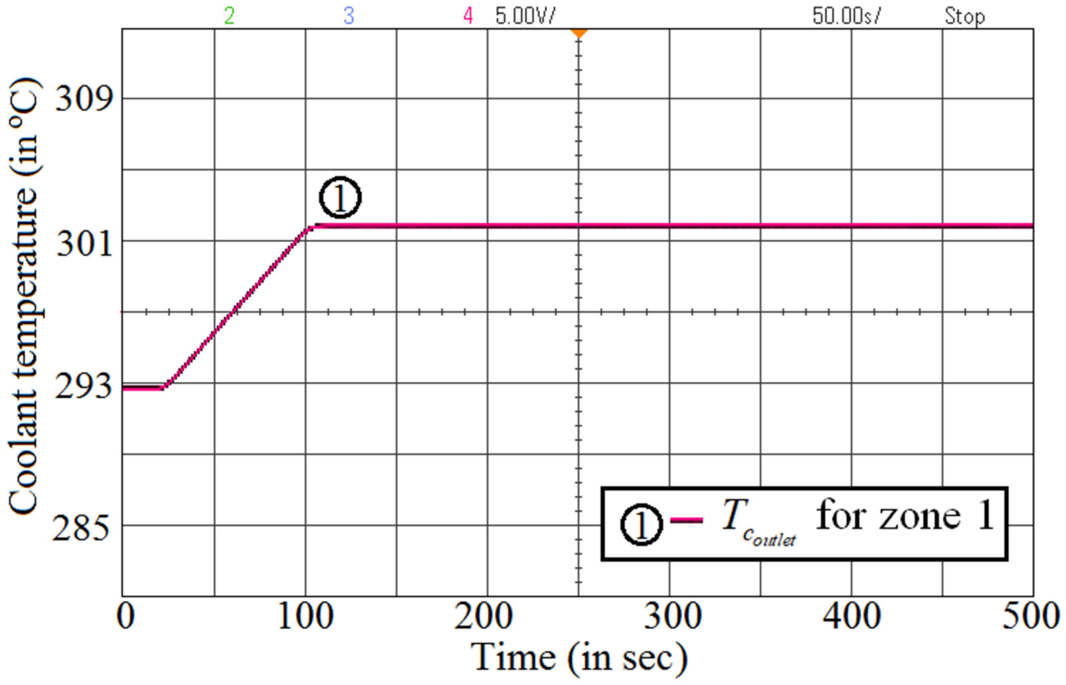

Fig. 4.9 Coolant temperature response during 60%-100%FP power maneuvering of 540MWe PHWR

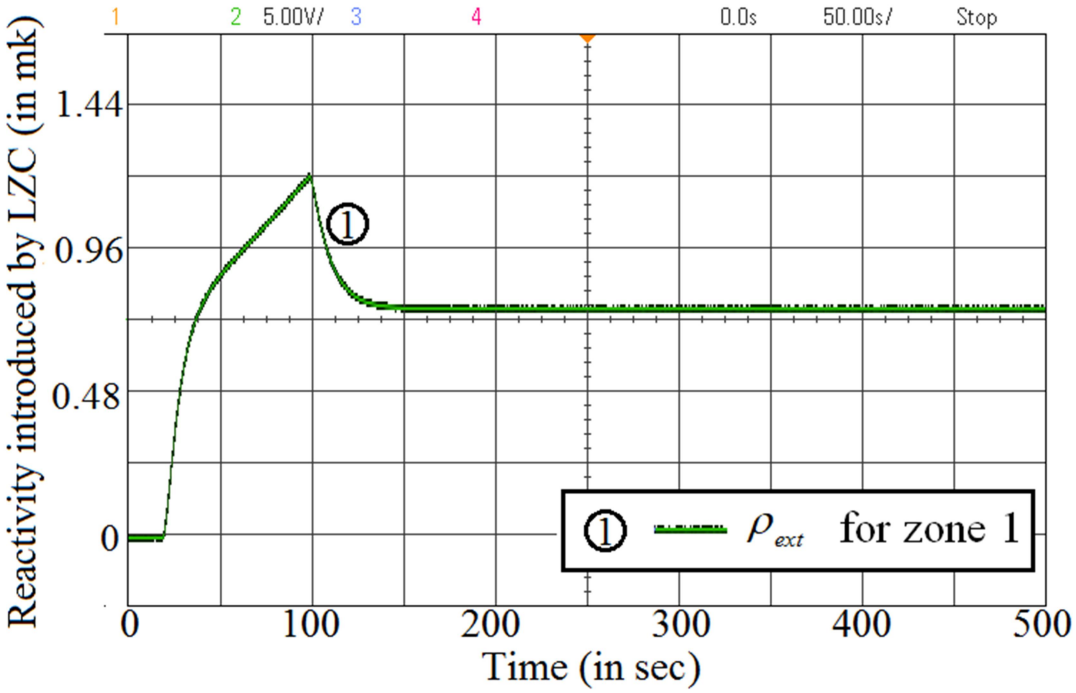

Fig. 4.10 Reactivity introduced by LZC of zone 1 during 60%-100%FP power maneuvering of 540MWe PHWR

Figure 4.7 suggests that the actual reactor power efficiently tracks the demand power set-point with the designed PID controllers. With the increase of reactor power, the fuel temperature and the coolant outlet temperature should increase and these are evident from Fig. 4.8 and Fig. 4.9 respectively. The primary side pressure for 540MWe PHWR is 9MPa corresponding to which the saturation coolant temperature is 303.345^0C. Figure 4.9 suggests that the outlet coolant temperature has not exceeded this saturation temperature limit. Finally Fig. 4.10 represents the reactivity introduced by the LZCS in the reactor core.

The simulation results presented in this sub-section establish the effectiveness of the robust control methodology presented in *Chapter 2* for a 540MWe PHWR with standard PID controllers when applied to the actual non-linear plant.

4.3 Simulation Results for a 700MWe plant

The methodologies presented in *Chapter 3*, have been used to derive optimal controllers for

i. A 700MWe PHWR with constraint on fuel, coolant temperatures and reactivity satisfied in the regime 60%-100%FP.

ii. Controlling the pressurizer pressure output to keep voiding within 3% in the regime 92.3%-100%FP.

Again, the methodology is validated using credible real-time simulation with the following two cases enumerated below:

Case (i): This presents a scenario where the demand power of the reactor is maneuvered from 60%FP to 100%FP at a rate of 0.5%FP/sec. First, the reactor is considered to be operating at a steady state of 60%FP. Then, the power maneuvering starts at $t = 20\,\text{sec}$ and with the given ramping rate, the power maneuvering continues up-to $t = 100\,\text{sec}$ and thereafter it is kept constant

at 100%FP. This case has been simulated to depict the occurrence of voiding in coolant channel in a high power regime (92.3%FP-100%FP) when the pressurizer remains un-activated. The reactor's zone 1 is chosen as a representative case for simulation. For this case, an optimal PID controller has been designed using the methodology described in *Chapter 2*. The PID controller gain has been obtained, for zone 1, corresponding to nominal system defined by (3.41), as:

$$G_c(s) = 45.6296 + \frac{2.3281}{s} + 28.7684s \qquad (4.2)$$

In this case, the simulation results on the real-time test bench with the actual non-linear plant are only presented for the sake of brevity.

The oscilloscope traces of power-tracking response, fuel temperature response, coolant temperature response, void fraction and LZC output corresponding to Zone 1 of 700MWe PHWR, are presented in Fig. 4.11-Fig. 4.14.

A thorough examination of Fig. 4.11 reveals that actual reactor power has tracked the demand power variation. As the power varies, so do the fuel and the coolant temperatures and these variations are depicted in Fig. 4.12 and Fig. 4.13 respectively. As the pressurizer remains un-activated in this case, a constant pressure of 9.8MPa is maintained corresponding to which the coolant saturation temperature is 309.561^0C. With the increase in demand power, the coolant temperature starts increasing from 301.6^0C and as soon as it reaches its saturation point, the coolant temperature becomes constant and the coolant enters into a mixture phase of liquid-vapor. From Fig. 4.13, it is seen that the coolant enters into its mixture phase at $t = 65\,\text{sec}$ and this corresponds to 92.3%FP for zone 1. As soon as the coolant temperature reaches its saturation value, voiding starts to occur and this is depicted in Fig. 4.14. Void fraction, which was initially 0 at $t = 65\,\text{sec}$, starts rising and settles at a final value of 4.5% in $t = 456\,\text{sec}$. It is to be noted that

the maximum allowable limit of void fraction is 3% [12]. Voiding of 4.5% in coolant channels introduces positive reactivity of 0.3mk in the reactor core [57]. The reactivity introduced by the LZC level variation is shown in Fig. 4.15.

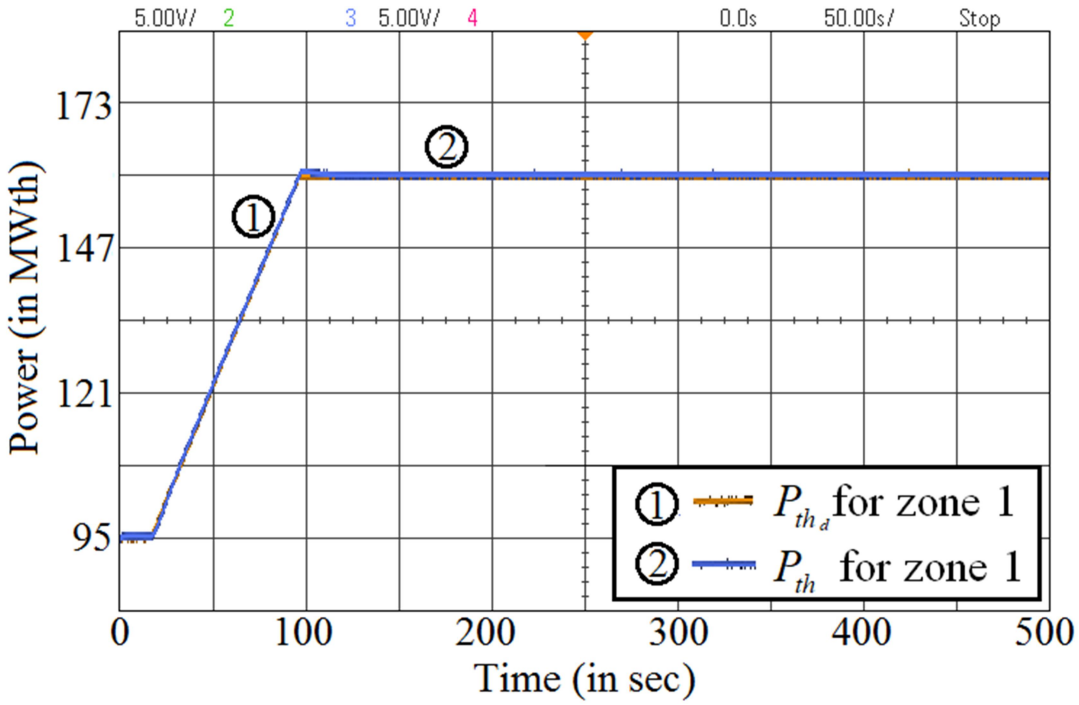

Fig. 4.11 Demand power and actual power tracking of zone 1 during 60%-100%FP power maneuvering without activating the pressurizer

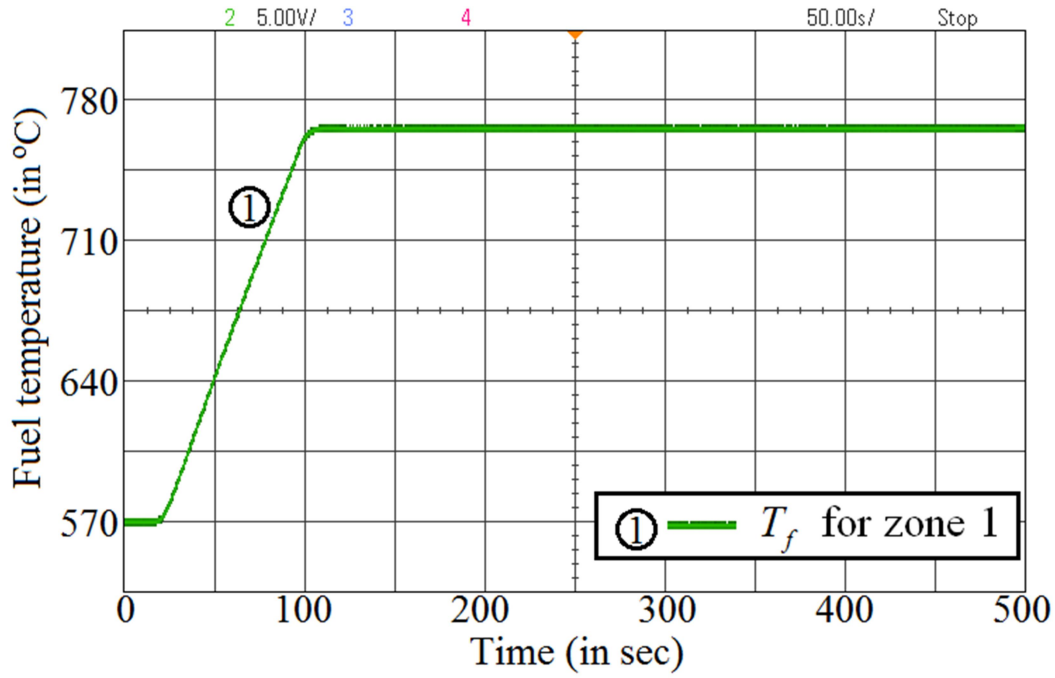

Fig. 4.12 Fuel temperature response during 60%-100%FP power maneuvering without activating the pressurizer

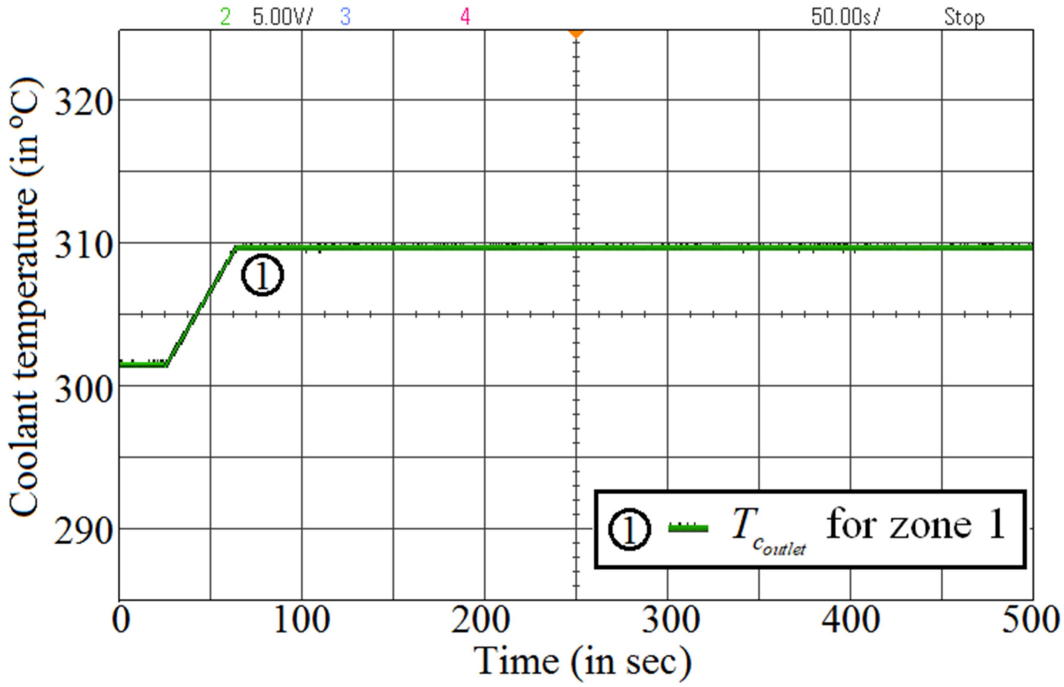

Fig. 4.13 Coolant temperature response during 60%-100%FP power maneuvering without activating the pressurizer

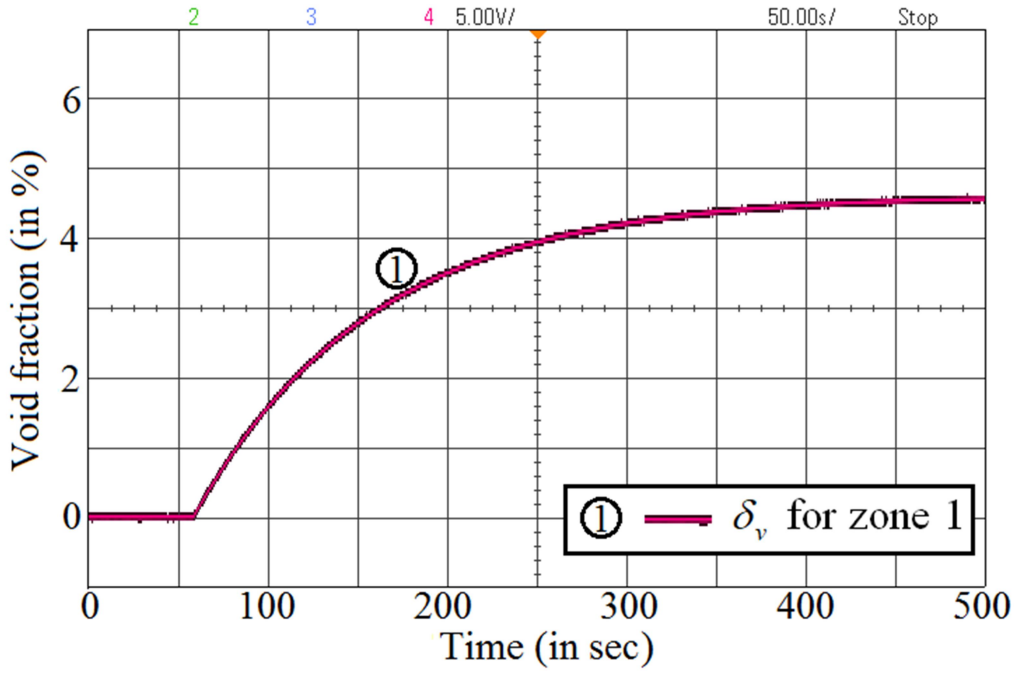

Fig. 4.14 Void fraction response during 60%-100%FP power maneuvering without activating the pressurizer

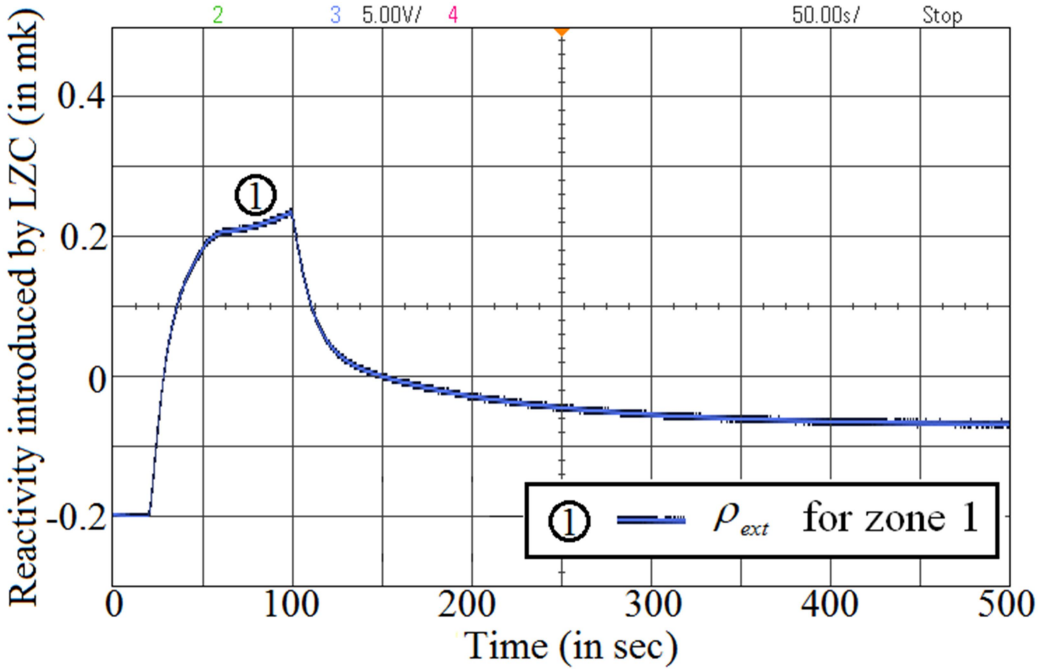

Fig. 4.15 Reactivity introduced by LZC of zone 1 during 60%-100%FP power maneuvering without activating the pressurizer

Case (ii) represents the case where the pressurizer is activated. For simulating case (ii), the conditions related to demand power set-point variation is the considered in case (i) remain unaltered except the fact that the pressurizer is now activated. The important parameters related to the pressurizer pressure control are listed in Table 4.3.

Table 4.3

Parameters Related To the Pressurizer Pressure Control

k_{P_R1}	k_{P_R2}	η	k_p	k_i	w_1	w_2	w_3
0.0038	-0.0017	-0.447	431.372	682.352	$1.2\text{x}10^5$	1.000011	$3.00001\text{x}10^5$

For pressurizer pressure control, the pressure set-point of the pressurizer is ramped-up from the 9.8MPa to 10MPa as soon as the temperature of the coolant reaches its saturation point i.e. at $t = 65\,\text{sec}$. The objective of the PI controllers for the pressurizer is to ensure that the actual pressure perfectly tracks the set-point with minimum control effort i.e. by minimizing the electrical heater power and spray flow. Thus, the two PI controllers are optimally designed using the methodologies presented in the *Chapter 3* and the corresponding controller gains obtained along with the weights considered in (3.51) are listed in Table 4.3. Figure 4.16- Fig. 4.20 depict the oscilloscope traces of power-tracking response, fuel temperature response, coolant temperature response, computed void fraction and LZC output respectively, corresponding to Zone 1 of 700MWe PHWR with the pressurizer activated to restrict voiding. The power tracking response and the fuel temperature response remain unaltered as compared to Fig. 4.11 and Fig. 4.12 respectively. However, comparing Fig. 4.18 to Fig. 4.13 suggests that the coolant output saturation temperature which was 309.516^0C at 9.8MPa has changed to 310.997^0C corresponding to 10MPa. Due to the activation of the pressurizer, the void fraction has however drastically reduced to 2.2% (which is within the maximum allowable limit of 3%) and has

remained there for the rest of the time. This is clearly evident from Fig. 4.19. As the void fraction reduces, so does the amount of positive reactivity addition in to the core due to coolant voiding and thus the LZC output variation also reduces as evident from Fig. 4.20 when compared to Fig. 4.15. The oscilloscope traces of pressure tracking response, electric heater power and spray flow are presented through Fig. 4.21-4.23. An examination of Fig. 4.21 suggests that the optimal PI controllers are able to accomplish perfect pressure tracking response with optimal variation of electric heater power which increases and spray flow which decreases with increase in pressure.

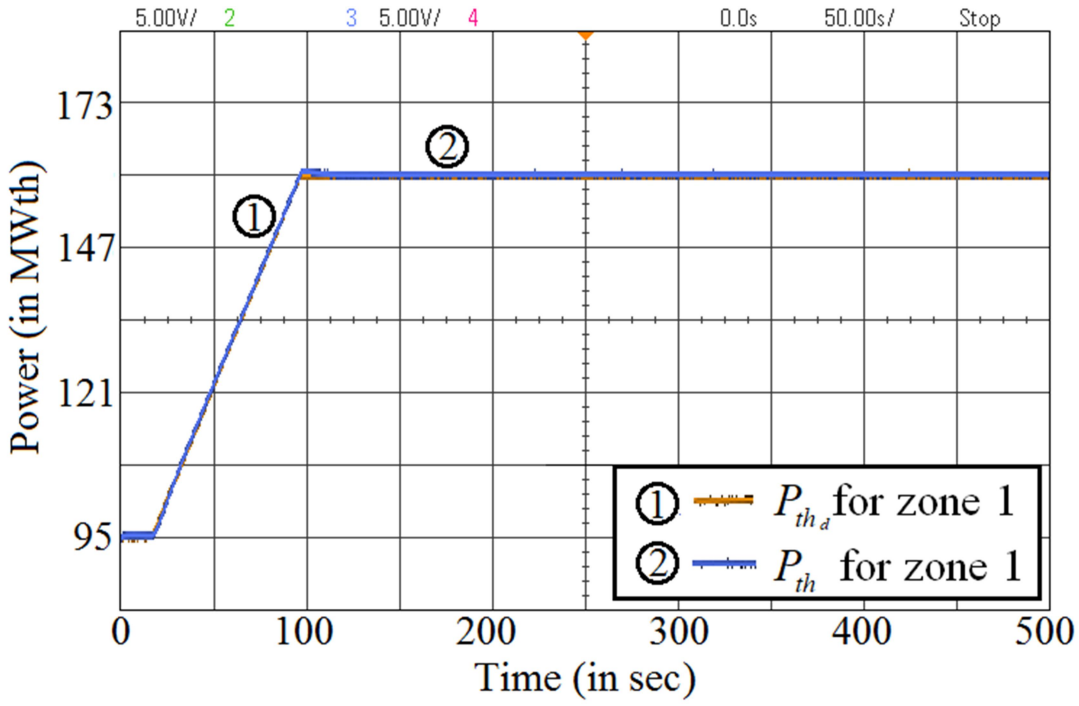

Fig. 4.16 Demand power and actual power tracking of zone 1 during 60%-100%FP power maneuvering with pressurizer activated during void fraction occurrence

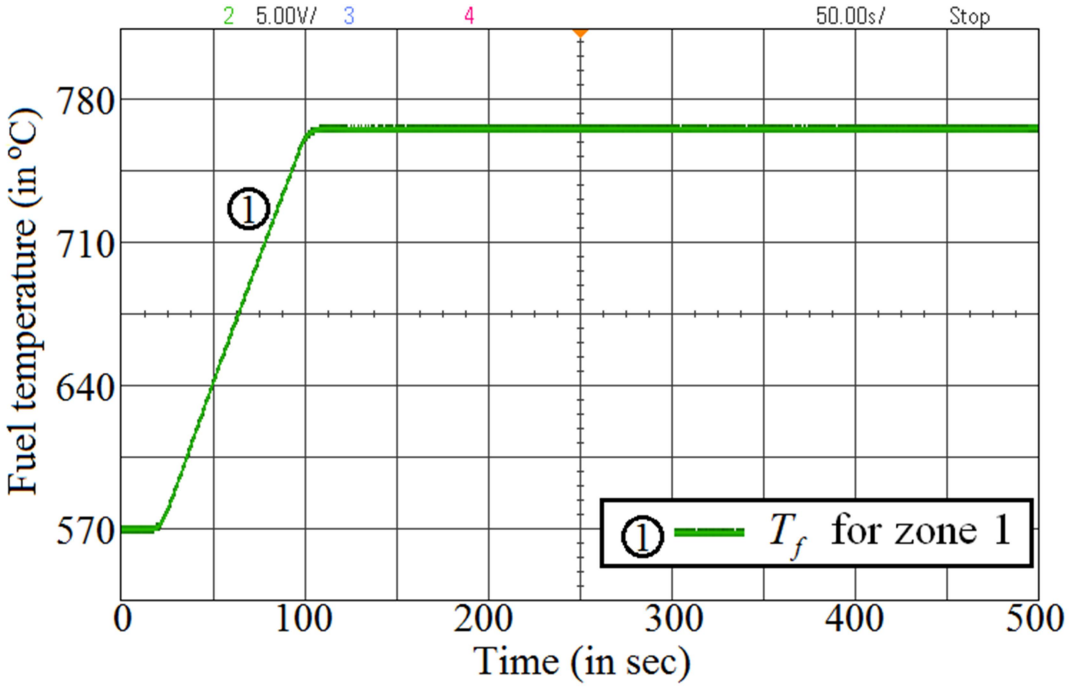

Fig. 4.17 Fuel temperature response during 60%-100%FP power maneuvering with pressurizer activated during void fraction occurrence

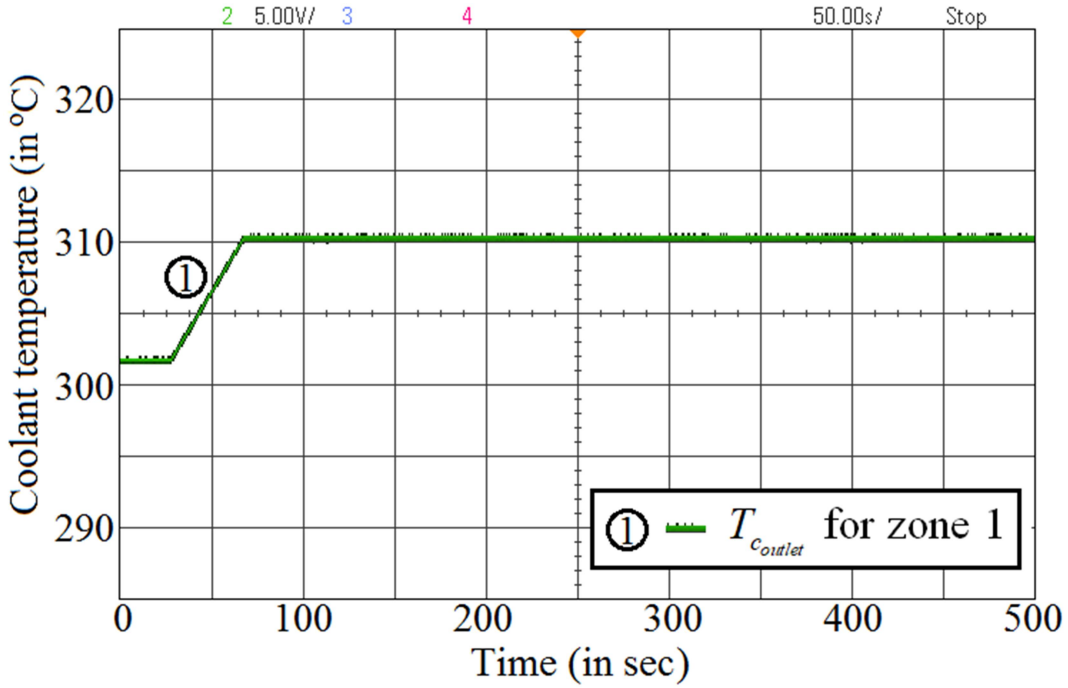

Fig. 4.18 Coolant temperature response during 60%-100%FP power maneuvering with pressurizer activated during void fraction occurrence

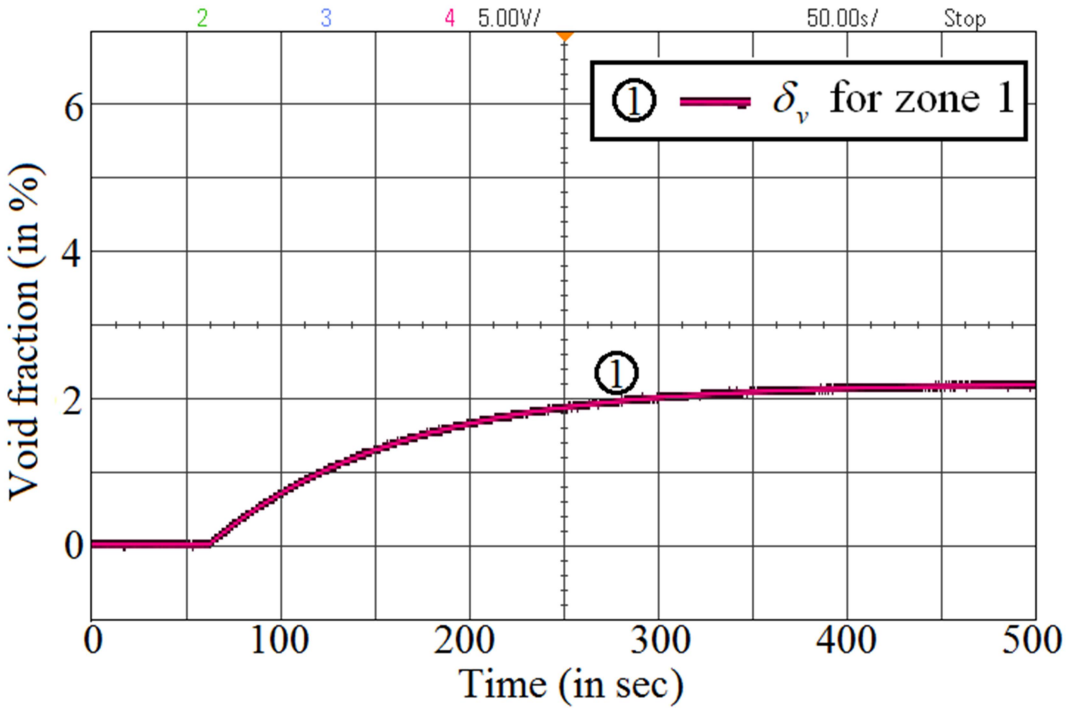

Fig. 4.19 Void fraction response during 60%-100%FP power maneuvering with pressurizer activated during void fraction occurrence

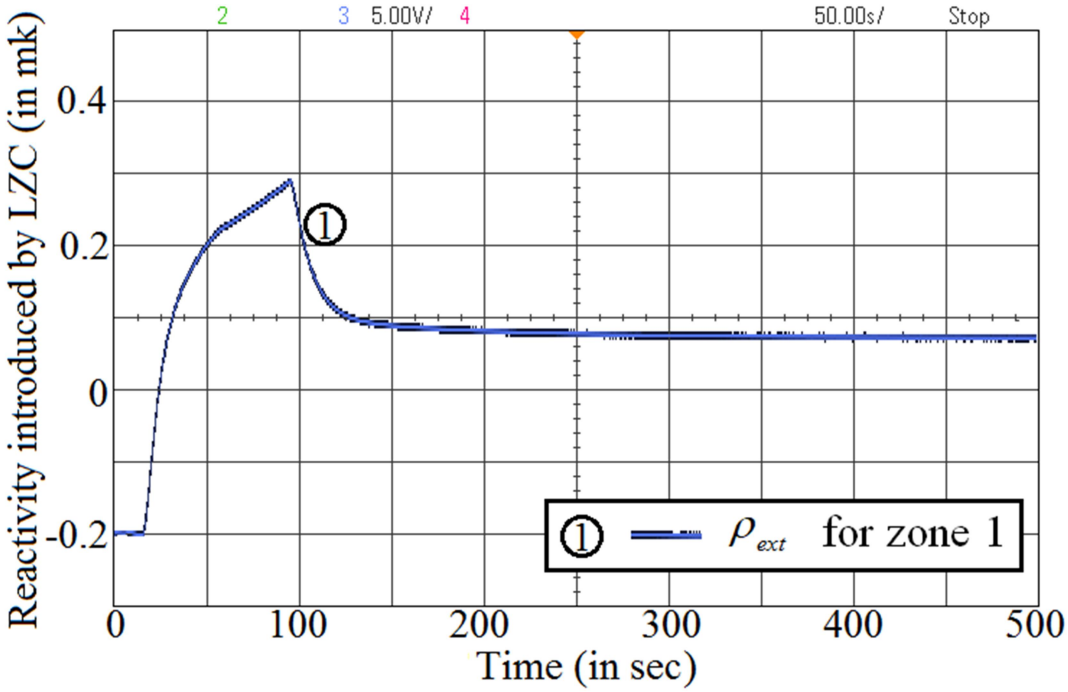

Fig. 4.20 Reactivity introduced by LZC of zone 1 during 60%-100%FP power maneuvering with pressurizer activated during void fraction occurrence

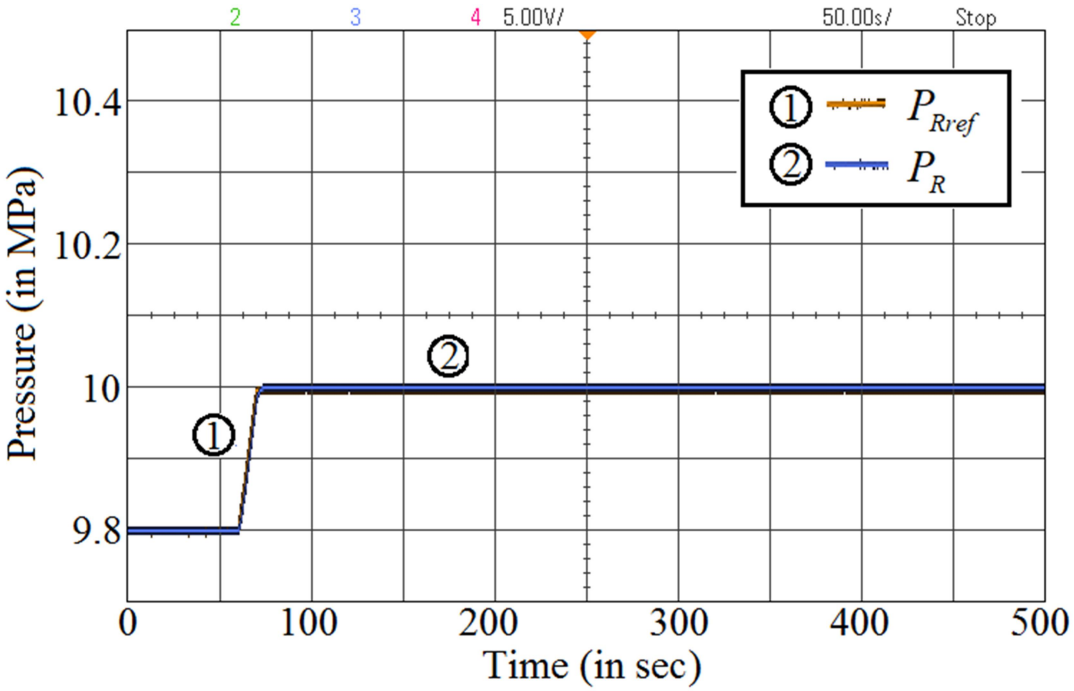

Fig. 4.21 Actual pressure and pressure set-point variations during 60%-100%FP power maneuvering with pressurizer activated during void fraction occurrence

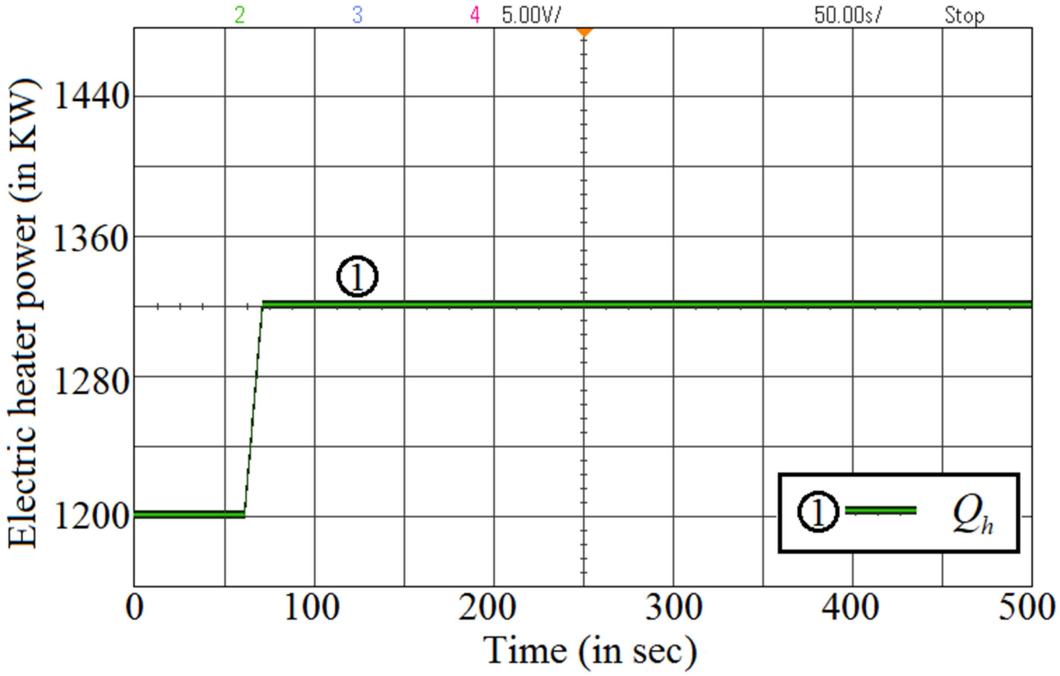

Fig. 4.22 Output of electrical heater power of pressurizer during 60%-100%FP power maneuvering with pressurizer activated during void fraction occurrence

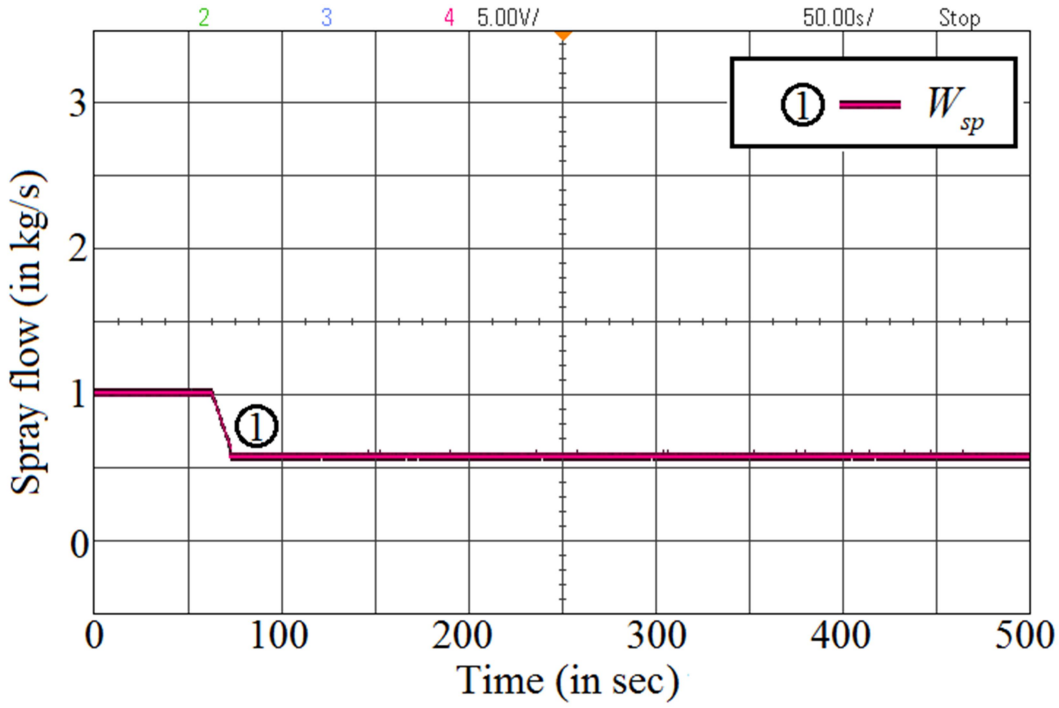

Fig. 4.23 Spray flow of the pressurizer during 60%-100%FP power maneuvering with pressurizer activated during void fraction occurrence

It is to be noted that the pressurizer is not kept activated since the beginning of the power maneuver because such a case would require much more heater power and hence the overall process would not be cost effective. Therefore the pressurizer is activated only on occurrence of voiding in coolant channel and in this case heater power and spray flow has been optimally controlled so that the desired pressure can be accomplished by a combination of minimum heater power and minimum spray flow. This justifies the optimal design of PI controllers for pressurizer pressure control.

The simulation results presented in this chapter, therefore, establish the effectiveness of the controller design methodologies for both 540MWe and 700MWe PHWRS and produce stable reactor operation under a variable demand power regime. In both the cases, the controllers designed for a linearized non-linear plant produce desired stable closed loop response when applied to the non-linear plant within the interval of demand power variation considered.

This page is intentionally left blank

Chapter 5

Conclusion and Scope of Future Work

5.1 Conclusion

At first, this dissertation puts forward the details of modeling a nuclear reactor as an interval system with bounded parametric uncertainties during the scenario of demand power variation. Further, the stability analysis of such an interval system suggests that even though the system is marginally stable in nature, the system is fully controllable over a prescribed operating interval of reactor power. This dissertation puts forward a methodology to achieve robust control of a 540MWe PHWR under changes in demand power set-point and uncertainties in measurement of reactor power, reactivity coefficients and heat transfer related parameters. The methodology uses an interval approach and can be used to tune conventional PID controllers to achieve robust control of PHWR. The controller obtained by this methodology is an optimal controller and the acceptable bounds in closed-loop time response parameters can also be directly specified. The robustness of the controllers has been established using credible real-time and offline simulations of 540MWe PHWR with representative data.

The next objective of the dissertation is to extend the controller design methodology for 540MWe towards the control of 700MWe PHWRs. The 700MWe PHWRs are prone to voiding occurrences in coolant channel at higher power regime (93.2%FP onwards). This dissertation puts forward the details of modeling void fraction in transient time. Stability analysis of such a

700MWe PHWR in presence of voiding, suggests that the system tends to become unstable as soon as the voiding starts due to the introduction of positive reactivity. Therefore, this dissertation presents a credible technique by which a robust control of a 700MWe PHWR can be achieved over an operating regime spanning 60%-100%FP. The void fraction can be estimated as a function of reactor power and this has been established in this dissertation. For keeping the void fraction within the prescribed limit, a pressurizer needs to be activated which uses an electric heater power and spray flow. For pressurizer pressure control, PI controllers are optimally designed using GA such that the desired pressure can be achieved by minimum controller effort i.e. by minimum heater power and spray flow requirement. Pressurizer PI controllers together with reactor power level PID controllers can r achieve power maneuvering at desired rate keeping void fraction constrained to its specified limit. Real-time simulation results validate the controller performance.

5.2 Scope of Future work

Drawing conclusions to the dissertation has further given rise to many challenging and interesting notions in the domain of reactor control which need to be explored in future as an extension of this dissertation. This dissertation puts forward the void fraction modeling in transient time but does not take into consideration the location of void occurrence in the coolant channel. Also, the reactivity feedback due to void is dependent upon the nature of bubbles occurring in coolant channel. Therefore, for more precise and detailed analysis of void fraction, these factors need to be considered and such study would be a highly challenging research domain. The interval approach based modeling and robust optimal controller design for system

with bounded parametric uncertainties, may be directly applied towards the design of appropriate controller for the next generation reactors.

Secondly, the methodology presented in this dissertation does not take into consideration the coupling between the different zones of a PHWR . Considering this would lead to a larger system comprising sub-systems constituted by neighboring zones and pose a challenge to controller design for such a system with extension of the interval based methodology presented in this dissertation. Similarly the effects arising out of flux asymmetry in a coupled reactor e.g. Xenon Oscillations also need to be considered in the controller design and is left as a future work- as a matter of fact interval approach has already been applied for control of Xenon oscillations in a Pressurized Water Reactor (PWR) as in [27].

This page is intentionally left blank

References

[1]. Wallner, A., and G. Mraz. A Report on "The true costs of nuclear power." (2013).

[2]. Bajaj, S. S., and A. R. Gore. "The Indian PHWR." Nuclear Engineering and Design 236, no. 7-8 (2006): 701-722.

[3]. Jha, K. K., Y. K. Budhiraja, A. K. Vijaya, and Rajee Guptan. "Level-1 PSA of RAPS-2: Review of the safety of the first Indian PHWR by probabilistic method." In Reliability, Safety and Hazard (ICRESH), 2010 2nd International Conference on, pp. 230-233. IEEE, 2010.

[4]. Banerjee, S., and H. P. Gupta. "Development of Technologies and Safety Systems for Pressurized Heavy Water Reactors in India." Journal of Nuclear Engineering and Radiation Science 3, no. 2 (2017): 020902.

[5]. CANDU Heavy Water Nuclear Reactors [online] Available: https://www.thebalance.com/candu-nuclear-reactor-is-moderated-with-heavy-water-1182652 How Canada's CANDU Heavy Water Nuclear Reactors Work WENDY LYONS SUNSHINE

[6]. Status report 105 - Indian 700 MWe PHWR (IPHWR-700)[online] Available: https://aris.iaea.org/PDF/IPHWR-700.pdf

[7]. Prasad, Sumit V., and A. K. Nayak. "In-Calandria Retention of Corium in PHWR: Experimental Investigation and Remaining Issues." Journal of Nuclear Engineering and Radiation Science 3, no. 2 (2017): 020909.

[8]. Grande, Lisa, Wargha Peiman, Sally Mikhael, Bryan Villamere, Adrianexy Rodriguez-Prado, Leyland Allison, and Igor Pioro. "Thermal Aspects of Using Uranium Nitride in Supercritical Water-Cooled Nuclear Reactors." In 18th International Conference on Nuclear Engineering, pp. 705-712. American Society of Mechanical Engineers, 2010.

[9]. Talange, D. B., B. Bandyopadhyay, and A. P. Tiwari. "Spatial control of a large PHWR by decentralized periodic output feedback and model reduction techniques." IEEE Transactions on Nuclear Science 53, no. 4 (2006): 2308-2317.

[10]. Bereznai, George. "Nuclear Power Plant Systems and Operation." Univ. of Ontario Institute of Technology, Oshawa, ON, Canada (2005).

[11]. https://www.iaea.org/NuclearPower/Downloads/Technology/meetings/2011-Jul-4-8-ANRT-WS/2_INDIA_PHWR_NPCIL_Muktibodh.pdf

[12]. INTERIM REPORT ON Safety Evaluation of 700 MWe Indian PHWRs at KAPP-3,4 and RAPP-7,8 POST FUKUSHIMA EVENT
[online] Available: http://www.npcil.nic.in/WriteReadData/userfiles/file/Safety_ A6.pdf

[13]. Reddy, G. Datatreya, B. Bandyopadhyay, and A. P. Tiwari. "Spatial control of a large PHWR by multirate output feedback based sliding mode control." In Industrial Technology, 2006. ICIT 2006. IEEE International Conference on, pp. 1925-1930. IEEE, 2006.

[14]. Bhatt, T.U., K. C. Madala, S.R. Shimjith, & A.P. Tiwari. "Application of fuzzy logic control system for regulation of differential pressure in liquid zone control system." Annals of Nuclear Energy, 36: 1412-1423 (2009).

[15]. Saha, S.; Das, S.; Ghosh, R.; Goswami, B.; Balasubramanian, R.; Chandra, AK.; Das, S.; Gupta, A, "Design of a Fractional Order Phase Shaper for Iso-Damped Control of a PHWR Under Step-Back Condition," Nuclear Science, IEEE Transactions on , vol.57, no.3, pp.1602,1612, June 2010.

[16]. Y. J. Lee, "H Robust Controller Design of Reactor Power Control System," J. of KNS, Vol. 29(4), pp. 280-290 (1997).

[17]. K. Suzuki., Shimazaki J., Shinohara Y., "Application of H-infinity Control-Theory To Power-Control of A Nonlinear Reactor Model", Nuclear science and engineering, 115(2), 1993, pp. 142-151.

[18]. X. Jin, A. Ray, and R. M. Edwards, "Integrated robust and resilient control of nuclear power plants for operational safety and high performance", IEEE Transactions on Nuclear Science, vol. 57, no. 2, pp. 807-817, April 2010.

[19]. S. S. Shyu and R. M. Edwards, "A robust multivariable feedforward/feedback controller design for integrated power control of boiling water reactor power plants", Nucl. Technol., vol. 140, no. 2, pp. 129-140, Nov. 2002.

[20]. Edwards, R.M., Lee, K.Y., and Ray A., "Robust Optimal Control of Nuclear Reactors and Power Plants", Nuclear Technology, Vol.98 May 1992, pp. 137-148.

[21]. Hisch, Florian, Andrea Giusti, and Matthias Althoff. "Robust control of continuum robots using interval arithmetic." IFAC-PapersOnLine 50, no. 1 (2017): 5660-5665.

[22]. Hiroshi Ito, Thach Ngoc Dinh, Interval observers for global feedback control of nonlinear systems with robustness with respect to disturbances, European Journal of Control, Volume 39, 2018, Pages 68-77.

[23]. Jie Li, Yuanqing Xia, Xiaohui Qi, Pengpeng Zhao, Robust absolute stability analysis for interval nonlinear active disturbance rejection based control system, ISA Transactions, Volume 69,2017,Pages 122-130.

[24]. Bhattacharyya, Shankar P., Lee H. Keel, and Aniruddha Datta. Linear control theory: structure, robustness, and optimization. CRC press, 2009.

[25]. Y. J. Lee, M. G. Na, "Robust Controller Design of Nuclear Power Reactor by Parametric Method," J. of KNS, 34(5). pp. 436-444, Oct., 2002.

[26]. Bose, D; Banerjee; S; Kumar, M; Marathe, P. P; Mukhopadhyay, S; and Gupta; A, "An Interval Approach to Nonlinear Controller Design for Load-Following Operation of a Small Modular Pressurized Water Reactor." IEEE Transactions on Nuclear Science 64, no. 9 (2017): 2474-2488.

[27]. Yadav, Deepak Kumar, Amitava Gupta, and Prabhat Munshi. "Non linear Dynamic Inversion based controller design for load following operations in Pressurized Water Reactors with bounded Xenon oscillations." Nuclear Engineering and Design 328 (2018): 241-254.

[28]. Tiwari, A. P., B. Banyopadhyay, and G. Govindarajan. "Spatial control of a large pressurized heavy water reactor." IEEE Transactions on Nuclear Science 43, no. 4 (1996): 2440-2453.

[29]. Das, Saptarshi, Shantanu Das, and Amitava Gupta. "Fractional Order Modeling of a PHWR Under Step-Back Condition and Control of Its Global Power With a Robust $PI^{\lambda}D^{\mu}$ Controller." IEEE Transactions on Nuclear Science 58, no. 5 (2011): 2431-2441.

[30]. Perruquetti, Wilfrid, and Jean-Pierre Barbot. Sliding mode control in engineering. CRC press, 2002.

[31]. Zhihong, Man, and Xing Huo Yu. "Terminal sliding mode control of MIMO linear systems." IEEE Transactions on Circuits and Systems I: Fundamental Theory and Applications 44, no. 11 (1997): 1065-1070.

[32]. Ansarifar, Gholam Reza, and Maesam Rafiei. "Second-order sliding-mode control for a pressurized water nuclear reactor considering the xenon concentration feedback." Nuclear Engineering and Technology 47, no. 1 (2015): 94-101.

[33]. Reddy, G. Datatreya, B. Bandyopadhyay, and A. P. Tiwari. "Multirate output feedback based sliding mode spatial control for a large PHWR." IEEE Transactions on Nuclear Science 54, no. 6 (2007): 2677-2686.

[34]. Surjagade, Piyush V., Akhilanand Pati Tiwari, and Sreyas Rajagopal Shimjith. "Robust Optimal Integral Sliding Mode Controller for Total Power Control of Large PHWRs." IEEE Transactions on Nuclear Science (2018).

[35]. Liu, Xiangjie, Di Jiang, and Kwang Y. Lee. "Decentralized fuzzy MPC on spatial power control of a large PHWR." IEEE Transactions on Nuclear Science 63, no. 4 (2016): 2343-2351.

[36]. Das, Monotosh, Ratna Ghosh, Bhaswati Goswami, Amitava Gupta, A. P. Tiwari, R. Balasubrmanian, and A. K. Chandra. "Network control system applied to a large pressurized heavy water reactor." IEEE Transactions on Nuclear Science 53, no. 5 (2006): 2948-2956.

[37]. Dasgupta, Soumya, Avijit Routh, Shohan Banerjee, K. Agilageswari, R. Balasubramanian, S. G. Bhandarkar, Sujit Chattopadhyay, Manoj Kumar, and Amitava Gupta. "Networked control of a large pressurized heavy water reactor (PHWR) with discrete proportional-integral-derivative (PID) controllers." IEEE Transactions on Nuclear Science 60, no. 5 (2013): 3879-3888.

[38]. K. J. Astrom "Computer-Controlled-Systems: Theory and Design", 1997 :Prentice-Hall.

[39]. [35] J. B. He , Q.-G. Wang and T. H. Lee "PI/PID controller tuning via LQR approach", Chem. Eng. Sci., vol. 55, no. 13, pp.2429 -2439 2000.

[40]. L. Granvilliers and F. Benhamou. Algorithm 852: Realpaver: an Interval Solver using Constraint Satisfaction Techniques. ACM TOMS, 32(1):138-156, 2006.

[41]. S.M. Rump. INTLAB - INTerval LABoratory. In Tibor Csendes, editor, Developments in Reliable Computing, pages 77-104. Kluwer Academic Publishers, Dordrecht, 1999.

[42]. Marsh, Clive, and Hao Wei. "Robustness bounds for systems with parametric uncertainty." Automatica 32.10 (1996): 1447-1453.

[43]. Lu, Jerry Tong-Huei. "Detection of void fluctuations in reactor coolant channels by neutron noise analysis." (1976).

[44]. Ramajo, Damian, Santiago Corzo, and M. Nigro. "A Coupled Model for Two-Phase Simulation of a Heavy Water Pressure Vessel Reactor." World Academy of Science, Engineering and Technology, International Journal of Nuclear and Quantum Engineering 2, no. 11 (2015).

[45]. J. Holland, "Adaptation in natural and artificial systems", MIT Press, Cambridge, MA, 1992.

[46]. D. Goldberg, Genetic Algorithms in Search, Optimization & Machine Learning, Reading, Ma: Addison-Wesley Publishing Company, Inc., 1989.

[47]. Kumar, D. Kranthi, S. K. Nagar, and J. P. Tiwari. “Model order reduction of interval systems using mihailov criterion and factor division method.” Int. J. Comput. Appl. (IJCA) 28.11 (2011): 4-8.

[48]. Rump, Siegfried M. "Fast interval matrix multiplication." Numerical Algorithms 61, no. 1 (2012): 1-34.

[49]. Das, S.; Pan, I; Majumder, B.; Das, S.; Gupta, A, “Control of nuclear reactor power with thermal-hydraulic effects via fuzzy $PI^{\lambda}D^{\mu}$ controllers,” Communication and Industrial Application (ICCIA), 2011 International Conference on , vol., no., pp.1,5, 26-28 Dec. 2011.

[50]. Hladík, Milan, David Daney, and Elias Tsigaridas. “Bounds on real eigenvalues and singular values of interval matrices.” SIAM Journal on Matrix Analysis and Applications 31.4 (2010): 2116-2129.

[51]. Wang, Kaining, and Anthony N. Michel. "Necessary and sufficient conditions for the controllability and observability of a class of linear, time-invariant systems with interval plants." IEEE Transactions on Automatic Control 39, no. 7 (1994): 1443-1447.

[52]. Haynes, G. W., and H. Hermes. "Nonlinear controllability via Lie theory." SIAM Journal on Control 8, no. 4 (1970): 450-460.

[53]. B. Bandyopadhyay , H. Unbenhauen and B. M. Patre “A new algorithm for compensator design for higher-order system via reduced model”, Automatica, vol. 34, 1998.

[54]. Das. Monotosh, “Some Studies on Online Tuning And Decoupling of Multivariable Systems Using Message Passing Across Embedded Controllers,” Phd. Dissertation, March 2007, Power Engineering Dept., Jadavpur University.

[55]. Khadraoui, S.; Rakotondrabe, M.; Lutz, P., “PID-structured controller design for interval systems: Application to piezoelectric microactuators,” American Control Conference (ACC), 2011, vol., no., pp.3477, 3482, June 29 2011-July 1 2011.

[56]. Brian D. O. Anderson, John B. Moore; “Optimal Control: Linear Quadratic Methods”; Prentice-Hall International, Inc., Englewood Cliffs, NJ(1989).

[57]. Prodea, Iosif, Cristina Alice MARGEANU, Andrei RIZOIU, Ilie PRISECARU, and Nicolae DANILA. "Void Reactivity Reduction in CANDU Reactors Using Burnable Absorbers and Advanced Fuel Designs." UPB Scientific Bulletin Series C 72, no. 1 (2010): 145-152.

[58]. Board, Atomic Energy Regulatory. PRIMARY HEAT TRANSPORT SYSTEM FOR PRESSURISED HEAVY WATER REACTORS. AERB/NPP-PHWR/SG/D-8, AERB, Mumbai, India, 2003.

[59]. Saleh, Mikdam Mahmood. "Two-phase flow characterization using reactor noise techniques." (1980).

[60]. Verma, Dinkar, Manjeet Singh Kalra, and Pankaj Wahi. "Effect of nonlinear void reactivity on bifurcation characteristics of a lumped-parameter model of a BWR: A study relevant to RBMK." Nuclear Engineering and Design 315 (2017): 179-193.

[61]. Wallis, Graham B. "One-dimensional two-phase flow." (1969).

[62]. Xu, Z. B., J. Wu, Z. T. Quan, X. S. Zhang, and X. Q. Ma. "Model and Simulation Study on Pressurizer Pressure System." (2015).

[63]. Ma, Jin, Yongling Li, Yu Huang, Bingshu Wang, and Afang Chan. "Mechanism model and simulation of pressurizer in the pressurized water reactor nuclear power plant." In Control Conference (CCC), 2011 30th Chinese, pp. 1538-1543. IEEE, 2011.

[64]. Lennart Ljung, "System identification: theory for the user," Prentice Hall, Upper Saddle River, 1999.

[65]. Lennart Ljung, "System identification toolbox: user's guide", MathWorks, Inc, 2009.

[66]. Jin, Ma, Afang Chan, and Lv Lixia. "Mathematical modeling and simulation of pressuriser pressure control system." In The 2nd International Conference of Computer Application and System Modeling, pp. 362-366. 2012.

[67]. Schroeck, Steven J., William C. Messner, and Robert J. McNab. "On compensator design for linear time-invariant dual-input single-output systems." IEEE/ASME Transactions On Mechatronics 6, no. 1 (2001): 50-57.

[68]. Chait, Yossi, and Oded Yaniv. "Multi-input/single-output computer-aided control design using the quantitative feedback theory." International Journal of Robust and Nonlinear Control 3, no. 1 (1993): 47-54.

[69]. F. Herrera, M. Lozano, and J. L. Verdegay, "Tackling real-coded genetic algorithms: Operators and tools for behavioral analysis", Artif. Intell. Rev., vol.12, no. 4, pp. 265-319, 1998.

[70]. Jayachitra, A., and R. Vinodha. "Genetic algorithm based PID controller tuning approach for continuous stirred tank reactor." Advances in Artificial Intelligence 2014 (2014): 9.

[71]. K. Deb and R. B. Agrawal, "Simulated binary crossover for continuous search space", Complex Systems, vol. 9, no. 2, pp. 115-148, 1995.

[72]. OPAL RT, OP4500 RT-Lab-RCP/HIL System User Guide.[Online]. Available:https://www.opal-rt.com/wp-content/themes/enfold-opal/pdf/L00161_0436.pdf.

[73]. OPAL RT, OP4500 RT-Lab System User Guide.[Online]. Available: http://www.opalrt.com/sites/default/files/doc/OP4500%20User%20Manual.pdf.

[74]. MATLAB Real-Time Workshophttp User Guide.[Online]. Available: http//radio.feld.cvut.cz/matlab/pdf_doc/rtw/rtw_ug.pdf.

[75]. Real Time Windows Target User Guide. [Online]. Available: http://radio.feld.cvut.cz/matlab/pdf_doc/rtwin/rtwin_target_ug.pdf.

[76]. Advantec User Guide. [Online]. Available: http://eia.udg.es/~carles/ETQI/PC_1711.pdf.

[77]. Kazeminejad, H., "Uncertainty and sensitivity analyses for steady-state thermal-hydraulics of research reactors", Progress in Nuclear Energy, 49, pp. 313-322, 2007.A. Kheirkhah, D. Aschenbrenner, M. Fritscher, F. Sittner, and K. Schilling, "Networked Control Systems with Application in the Industrial Tele-Robotics", IFAC-Papers OnLine, vol. 48, no. 10, pp. 147-152, 2015.

Appendices

Appendix-I

MATLAB codes for Chapter 2 and Chapter 3

%%% Code for interval model and controller design %%%

```
%%%540MW nuclear reactor%%%%%
P=1440e6;pi=80e6;beta=7.5e-3;sigmaX1=9.024e-24; sigmaa1=2.43e-
2;lamda1=608e-3; lamdaX=2.1e-5;l=7.9e-4; alfaf=-3.2e-5; alfac=-5.59e-4;
lamdaI=2.878e-5; sigmaf1=9.4e-3; gamaX=0.006; gamaI=0.0618; sigmai=0;
X=(gamaX+gamaI)*sigmaf1*pi;I0=gamaI*sigmaf1*pi/lamdaI;klzc=(2.5e-6)/14
%%%%%thermal hydraulics%%%%%%
muf=1.233e6;muc=3.794e6;omega=2.321e5;Mc=3.844e6;
%%%%interval algorithm
x=5
d=5
Pi=infsup(P-P*d/100,P+P*d/100)
pi0=infsup(pi-pi*d/100,pi+pi*d/100)
Pi=infsup(1400e6,1800e6)
pi0=infsup(106e6,131.5e6)
omegai=infsup(omega-omega*x/100,omega+omega*x/100)
alfaci=infsup(alfac+alfac*x/100,alfac-alfac*x/100)
alfafi=infsup(alfaf+alfaf*x/100,alfaf-alfaf*x/100)
%%%%
%%%value
M=(beta+(sigmaX1*X/sigmaa1))/l
```

```
Lm=lamda1

Gs=(sigmaX1/sigmaa1)*pi0/l

Tf=-alfafi*pi0/l

Tc=-alfaci*pi0/l

Rs=beta/l

Ts=(gamaI*sigmaf1-sigmaX1*I0)

DD=-(lamdaI+sigmaX1*pi0)

V=(gamaX*sigmaf1-sigmaX1*X)

LI=lamdaI

J=(lamdaX+sigmaX1*pi0)

E=1/muf

Fs=omegai/muf

L=(2*omegai)/muc

Lc=(2*Mc+omegai)/muc

%%%interval for a and L

Li=(Pi*lamdaX*(2*Mc+2*omegai)*klzc)/(2*Mc+beta+((sigmaX1*X)/sigmaa1)-

2*Mc*beta-omegai*alfaci+2*Mc+omegai*alfafi);

L1=inf(Li)

L2=sup(Li)

%%%%

ai=(Fs+Lc+Lm+M)/(Fs*Lm*(Lc*M-L*M+L*Rs-Lc*Rs)+Lm*E*(L*Tc+Lc*Tf));

a1=inf(ai)

a2=sup(ai)

%%%%% value of parameters

L0=0.0088249;a0=1.54933;b0=0;

%%%%% system matix

A=[0 1 0;0 0 1;0 -b0 -a0]; B=[0;0;L0];

%%%%%

w_cl=0.1;z_cl=0.9;

alfa=1.55;
```

```
R=100
Q11=(R/L0^2)*(alfa^2*w_cl^4)
Q22=(R/L0^2)*(w_cl^4+(2*z_cl*w_cl*alfa)^2-2*(alfa*w_cl)^2-b0^2)
Q33=(R/L0^2)*(alfa^2+(4*z_cl^2-2)*w_cl^2-a0^2+b0)
Q=[Q11 0 0;0 Q22 0;0 0 Q33]
% %%%%%interval algorithm
i=10; x=5;
ai=infsup(a0-a0*x/100,a0+a0*x/100)
Li=infsup(L0-L0*x/100,L0+L0*x/100)
bi=infsup(b0-b0*x/100,b0+b0*x/100)
z_cli=infsup(z_cl-z_cl*i/100,z_cl+z_cl*i/100)
w_cli=infsup(w_cl-w_cl*i/100,w_cl+w_cl*i/100)
alfai=infsup(alfa-alfa*i/100,alfa+alfa*i/100)
a1=inf(ai),a2=sup(ai),L1=inf(Li),L2=sup(Li)
gama=L2/L1
%%%%interval for Q matrix
delta_q11=0
Q11nett=Q11-delta_q11
delta_q22=(2*R/gama*L0^2)*((w_cli^2+2*z_cli*w_cli*alfai-bi)*((bi/gama)-
b0)+alfai*w_cli^2*(a0-(ai/gama)))
Q22nett=Q22+delta_q22
delta_q33=(2*R/gama*L0^2)*((2*z_cli*w_cli+alfai-ai)*((ai/gama)-a0)-
(w_cli^2+2*z_cli*w_cli*alfai-bi)*((1/gama)-1))
Q33nett=Q33+delta_q33
Qi=[Q11nett 0 0;0 Q22nett 0;0 0 Q33nett]
Q1=inf(Qi)
Q2=sup(Qi)
%%%%%controller design
[p,l,kr]=care(A,B,Q,R);
kri=kr*[1 0 0]'
```

```
krp=kr*[0 1 0]'

krd=kr*[0 0 1]'

%%%%%%%%%

%%%%%%%%%for frequency domain response

%%%tf of system

numn=[0 0 L0];

denn=[1 a0 b0];

num1=[0 0 L1];

den1=[1 a1 b0];

num2=[0 0 L2];

den2=[1 a2 b0];

g0=tf(numn,denn);

g1=tf(num1,den1);

g2=tf(num2,den2);

g3=tf(num2,den1);

g4=tf(num1,den2);

nc=[krd krp kri];

dc=[0 1 0];

gc=tf(nc,dc);

sys0=series(gc,g0);

sys1=series(gc,g1);

sys2=series(gc,g2);

sys3=series(gc,g3);

sys4=series(gc,g4);

gc0=feedback(sys0,1);

gc1=feedback(sys1,1);

gc2=feedback(sys2,1);

gc3=feedback(sys3,1);

gc4=feedback(sys4,1);

bode(gc0,gc1,gc2,gc3,gc4)
```

%%% Code for model order reduction %%%

```
%%%%540MW nuclear reactor%%%%%
Pg=1800e6; pi0=132.75e6; beta=7.5e-3;sigmaX1=9.024e-24; sigmaa1=2.43e-
2;lamda1=608e-3; lamdaX=2.1e-5;l=7.9e-4; alfaf=-2.9e-5; alfac=-6.3e-4;
lamdaI=2.878e-5; sigmaf1=9.4e-3; gamaX=0.006; gamaI=0.0618; sigmai=0;
X=(gamaX+gamaI)*sigmaf1*pi0;I0=gamaI*sigmaf1*pi0/lamdaI
%%%%%thermal hydraulics%%%%%%
muf=1.69e6;muc=5.1e6;omega=2.96e5;Mc=5.3e6;
%%%%%element of 6x6matrix of nuclear reactor%%%%%
%
M=(beta+(sigmaX1*X/sigmaa1))/l
Lm=lamda1
Gs=(sigmaX1/sigmaa1)*pi0/l
Tf=-alfaf*pi0/l
Tc=-alfac*pi0/l
Rs=beta/l
Ts=(gamaI*sigmaf1-sigmaX1*I0)
DD=-(lamdaI+sigmaX1*pi0)
V=(gamaX*sigmaf1-sigmaX1*X)
LI=lamdaI
J=(lamdaX+sigmaX1*pi0)
E=1/muf
Fs=omega/muf
L=(2*omega)/muc
Lc=((2*Mc+omega)/muc)
Rp=pi0/l
%
syms real M Lm Gs Tf Tc Rs Lm Ts DD V LI J E Fs L Lc Rp s
%%%system matrix of reactor in continuous time%%%%%
A=[-M Lm 0 -Gs -Tf -Tc;Rs -Lm 0 0 0 0;Ts 0 DD 0 0 0;V 0 LI -J 0 0;E 0 0 0 -
Fs Fs;0 0 0 0 L -Lc]
e=eig(A)
B=[Rp;0; 0; 0; 0; 0]
I=eye(6)
C=[1 0 0 0 0 0]
D=zeros(1)
tf=C*inv(s*I-A)*B


%% The value of tf has been altered to obtain the various values of a and L
and the very small values have been neglected. This is how model order
reduction using aggregation method has been performed. %%

a=(Fs+Lc+Lm+M)/(Fs*Lm*(Lc*M-L*M+L*Rs-Lc*Rs)+Lm*E*(L*Tc+Lc*Tf));
%%%% putting the all character in above

a=((omega/muf)+((2*Mc+omega)/muc)+lamda1+(pi0+beta+sigmaX1*X/sigmaa1)/l)/((
omega*lamda1/muf*muc*l)*(2*Mc*pi0+beta+((sigmaX1*X)/sigmaa1)-2*Mc*beta-
omega*alfac*pi0+2*Mc+omega*alfaf*pi0))

%%%%similarly L form as:
L=(pi0*lamdaX*(2*Mc+2*omegai))/(2*Mc+beta+((sigmaX1*X)/sigmaa1)-2*Mc*beta-
omega*alfac+2*Mc+omega*alfaf);
```

%%% Code for pressurizer controller %%%

```
%%%cost function


function fit = cost_fun(L,a,b,alp)


% kp=847.0588;ki=376.4706;
kp=L(1);ki=L(2);
% a=3.085e-4;
% alp=6.481;
G=tf([(a+alp*b)*kp (a+b*alp)*ki],[(1) (a+alp*b)*kp (a+b*alp)*ki]);
t=0:100;
[y t]=step(G,t);
for i=1:101
    error(i)=1-y(i);
end
 u1=(kp.*error) + ki*sum(error)*ones(1,i);
u2=alp*u1;
 error1=error*error';
Z=abs(sum(error1));
%Z=trapz(1-y);
if (u1<abs(u2))
    Z=10e10;
end
if (Z<0)
    Z=10e10;
end


PL=pole(G);


for i=1:2
```

```
    if (PL(i)>=0)
        Z=10e10;
    end
end

Wcl=sqrt(a+(b*alp)*ki);
Zcl=((a+b*alp)*kp)/(2*Wcl);
% Wcl=(a*(1+alp)*ki)^0.5;
% Zcl=(kp*a*(1+alp))/(2*Wcl);

if (Wcl<0.2)||(Wcl>0.8)
    Z=10e10;
end

if (Zcl<0.8)||(Zcl>1)
    Z=10e10;
end

fit=Z;

%%%% for GA function
function [x_best, best,conv,T]=ga(a,b,alp,tp)

t1=cputime;

 %_____________________________________________________________
% I. Setup the GA
% ff =@test_functions; % objective function
ff =@cost_fun;
% F_index = 23; % select Fn.
```

```
% npar = 2; % number of optimization variables
% low= 0; up= 10; %low & up limit

% [low,up,npar]=test_functions_range(F_index);
low=0; up=1000; npar=2;
%_____________________________________________________________
% II. Stopping criteria
% maxit=100; % max number of iterations
maxit=tp;
mincost=-99999999999999999999999999999999; % minimum cost
%_____________________________________________________________
% III. GA parameters
popsize=50; % set population size
mutrate=0.15; % set mutation rate
selection=0.5; % fraction of population kept
nbits=8; % number of bits in each parameter
Nt=nbits*npar; % total number of bits in a chormosome
keep=floor(selection*popsize); % #population members that survive
%_____________________________________________________________________________
% Create the initial population
iga=0; % generation counter
% initialized
pop=round(rand(popsize,Nt)); % random population of 1s and 0s
par=gadecode(pop,low,up,nbits); % convert binary to continuous values
% cost=feval(ff,par,F_index); % calculates population cost using ff
for i=1:popsize
%     cost(popsize)=ff(par(popsize,:),F_index,npar);
    cost(popsize)=ff(par(popsize,:),a,b,alp);
end
[cost,ind]=sort(cost); % min cost in element 1
```

```
par=par(ind,:); pop=pop(ind,:); % sorts population with lowest cost first
minc = min(cost); % minc contains min of population
meanc = mean(cost); % meanc contains mean of population
%_____________________________________________________________
% Iterate through generations
while iga < maxit
iga=iga+1; % increments generation counter
clc;
iga
%_____________________________________________________________
% Pair and mate
M=ceil((popsize-keep)/2); % number of matings
prob=flipud([1:keep]'/sum([1:keep]));% weights
% chromosomes based
% upon position in
% list
odds=[0 cumsum(prob(1:keep))']; % probability distribution function
pick1=rand(1,M); % mate #1
pick2=rand(1,M); % mate #2
% ma and pa contain the indicies of the chromosomes
% that will mate
ic=1;
while ic<=M
for id=2:keep+1
if pick1(ic)<=odds(id) && pick1(ic)>odds(id-1)
ma(ic)=id-1;
end % if
if pick2(ic)<=odds(id) && pick2(ic)>odds(id-1)
pa(ic)=id-1;
end % if
```

```
end % id
ic=ic+1;
end % while
%_____________________________________________________________
% Performs mating using single point crossover
ix=1:2:keep; % index of mate #1
xp=ceil(rand(1,M)*(Nt-1)); % crossover point
pop(keep+ix,:)=[pop(ma,1:xp) pop(pa,xp+1:Nt)];
% first offspring
pop(keep+ix+1,:)=[pop(pa,1:xp) pop(ma,xp+1:Nt)];
% second offspring
%_____________________________________________________________
% Mutate the population
nmut=ceil((popsize-1)*Nt*mutrate); % total number
% of mutations
mrow=ceil(rand(1,nmut)*(popsize-1))+1; % row to mutate
mcol=ceil(rand(1,nmut)*Nt); % column to mutate
for ii=1:nmut
pop(mrow(ii),mcol(ii))=abs(pop(mrow(ii),mcol(ii))-1);
% toggles bits
end % ii
%_____________________________________________________________
% The population is re-evaluated for cost
par(2:popsize,:)=gadecode(pop(2:popsize,:),0,10,nbits);
% decode
%sz=size(par);
%F_id_array = ones(sz(1,1),1)*F_index;
% cost(2:popsize) = feval(ff,par(2:popsize,:),F_index);
for i=2:popsize
%     cost(popsize)=ff(par(popsize,:),F_index,npar);
```

```
    cost(popsize)=ff(par(popsize,:),a,b,alp);
end
%for flg = 2:popsize
%    cost(flg) = feval(ff,par(flg,:),F_index);
%end

% Sort the costs and associated parameters
[cost,ind]=sort(cost);
par=par(ind,:); pop=pop(ind,:);
%_____________________________________________________________
% Do statistics for a single nonaveraging run
minc(iga+1)=min(cost);
meanc(iga+1)=mean(cost);
%_____________________________________________________________
% Stopping criteria
if iga>maxit || cost(1)<mincost
break
end
% [iga cost(1)]
conv(iga) = cost(1);
end%iga
x_best=par(1,:);
best=conv(iga);
t2=cputime;
T=t2-t1;
%_____________________________________________________________
% Displays the output

clear all; clc;
a=3.0843e-06;
```

```
b= -0.0020;

alp=b/a;

tp=100;

[x_best, best,conv,T]=ga(a,b,alp,tp);

L=x_best;

kp=L(1);ki=L(2);

G=tf([(a+alp*b)*kp (a+b*alp)*ki],[(1) (a+alp*b)*kp (a+b*alp)*ki]);

step(G)
```

Appendix-II

Calculation of order of magnitude due to pressure drop

From (3.11) in Chapter 3,

$$V\left\{h\frac{d\rho}{dt}-\frac{p}{\rho}\frac{d\rho}{dt}+\rho\frac{dh}{dt}-\frac{dp}{dt}+\frac{p}{\rho}\frac{d\rho}{dt}\right\}=P+\dot{m}h_i-\dot{m}h_o$$

Dividing both sides by $h\frac{d\rho}{dt}$ yields

$$V\left\{1+\frac{\rho}{h}\frac{dh}{d\rho}-\frac{1}{h}\frac{dp}{d\rho}\right\}=\frac{\left(P+\dot{m}h_i-\dot{m}h_o\right)}{h\frac{d\rho}{dt}}$$

Now, in order to calculate sonic speed for pressure drop, the term $\frac{1}{h}\frac{dp}{d\rho}$ needs to be evaluated.

We know that

$$\frac{dp}{d\rho}=c^2$$

where c is the sonic speed in liquid at pressure of 9.8MPa considered in the dissertation.

Now, $\frac{1}{h}\frac{dp}{d\rho}$ can be expressed as $\frac{c^2}{h}$. Calculating $\frac{c^2}{h}$ at 9.8MPa pressure for the $c=855.941m/s$ and $h=1798.31KJ/kg$ yields 0.4074. Since the value of $\frac{c^2}{h}$ is less than 1, therefore it is neglected.